The Impact of Radiation on Glioblastoma Evolution

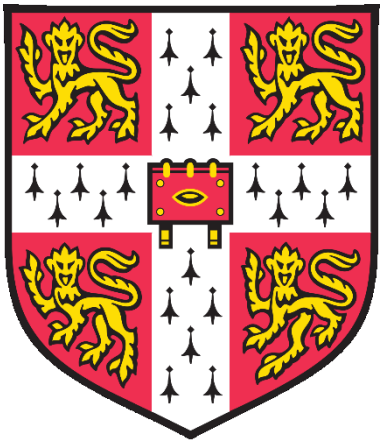

Joseph Hiram McAbee

Supervisors: Prof. Colin Watts
Prof. Stephen Price
Dr. Philip Tofilon

Department of Clinical Neurosciences
University of Cambridge
St. John's College

September 2019

This dissertation is submitted for the degree of

Doctor of Philosophy

Declaration

I hereby declare, that except where specific reference is made to the work of others, the contents of this dissertation are original and have not been submitted in whole or in part for consideration for a degree or diploma or other qualification at the University of Cambridge or any other University or similar institution.

This dissertation is the result of my own work and includes nothing which is the outcome of work done in collaboration except as declared in the Acknowledgements and specified in the text.

This dissertation contains fewer than 60,000 words excluding figures, photographs, tables, and bibliography.

Joseph Hiram McAbee

September 2019

Abstract

The Impact of Radiation on Glioblastoma Evolution

Joseph Hiram McAbee

Glioblastoma (GB) is the most common and malignant primary adult brain cancer with a median survival of 15 months despite treatment with surgical resection followed by chemo-radiotherapy. The clonal diversity and evolutionary dynamics inherent to GBs is considered a major obstacle to effective treatment response. While studies have focused on temozolomide, a role for radiotherapy as an independent driver of GB evolution has not been investigated. We addressed the impact of radiation on glioblastoma evolution and potential treatment implications by examining the influence of intratumoral heterogeneity (ITH) on intrinsic radiosensitivity, by determining the effects of radiation on glioma stem-like cell (GSC) initiated orthotopic xenografts, and by assessing radioresistance with a reirradiation protocol.

To determine the impact of ITH on intrinsic radiosensitivity, we performed whole-exome sequencing (WES) of multiple tumour fragments and corresponding patient-derived cell lines that underwent γH2AX foci analysis and limiting dilution assay analysis. Cell lines from the same tumour seem to display similar levels of intrinsic radiosensitivity despite genomic differences, suggesting that radiotherapy regimens may be effective for the whole of the tumour. To test the ability of radiation to drive GB evolution, we utilised GSC-initiated orthotopic xenograft models treated with or without fractionated radiation (3x5Gy) to examine differences in survival, morphology/histology, Viral integration site analysis (VISA), and WES. Irradiated mice experienced a survival advantage and harboured less invasive tumours compared to control mice. VISA revealed that control tumours harbour fewer clones than in vitro lines and that irradiated tumours harbour the fewest clones of all suggesting that radiation, particularly in the context of the brain microenvironment, drives GBM evolution. WES results demonstrated that variants from irradiated tumours mapped to different COSMIC mutational signatures and displayed a considerable amount of subpopulation shifting compared to control tumours, consistent with radiation-induced evolution and subpopulation selection. By adding a reirradiation protocol to this GSC-initiated orthotopic xenograft model, we sought to better understand the functional impact of radiotherapy on recurrent GB evolution and to establish an in vivo model for studying reirradiation. After initial treatment, mice were rerandomised into

control (3x5Gy-Control) and radiation therapy groups (3x5Gy-3x5Gy) and retreated once the average BLI ratio began to increase. A further survival advantage was found for mice undergoing reirradiation compared to mice receiving only one course of radiation. This survival advantage was supported by clonogenic survival and reimplantation studies of cell lines derived from control and irradiated NSC11 tumours that did not demonstrate a difference in survival after radiation regardless of the previous tumour's treatment regimen. Whereas radiation-induced evolution may not influence radioresponse, it may lead to the identification of novel targets for sensitisation which may ultimately yield more effective treatment strategies.

Our results demonstrate that radiation, a treatment component for almost all glioblastoma patients, can have wide-ranging effects on the evolution of this dynamic tumour. In particular, the pressures imposed by radiation treatment seem to lead to the selection of a reduced number of clones. This selection may have future implications for tumour evolution and the treatment of recurrent GB. In addition, we have demonstrated for the first time the utility of a GSC-initiated orthotopic xenograft model for studying retreatment protocols and recurrent GB biology. This reirradiation model may provide the opportunity to design and test more effective recurrent GB treatment strategies centered around recurrent biology.

Acknowledgements

I am incredibly grateful for so many people who not only contributed to this work but also supported me throughout my PhD journey. I would like to acknowledge a few of these individuals below.

First and foremost, I would like to thank Professor Colin Watts for providing me the opportunity to join his lab in the Department of Clinical Neurosciences to study glioblastoma at the University of Cambridge. I very much enjoyed our impromptu lab meetings in the OR and I am grateful to have worked under such an excellent example of a neurosurgeon-scientist. Likewise, I am thankful for another neurosurgeon-scientist, Professor Stephen Price, for his willingness to supervise my final PhD year and his guidance on thesis writing and submission during my final months of work.

I am particularly indebted to Dr. Philip Tofilon for allowing me to join his lab at the National Cancer Institute as part of the NIH OxCam Program. The resources and support provided by Dr. Tofilon and the Radiation Oncology Branch made my thesis research possible, for which I will be forever grateful. Dr. Tofilon's guidance and mentorship have significantly advanced my scientific research training. I feel well equipped on how to think about, approach, implement, and communicate science after having been in his lab.

I am certainly very thankful for the funding bodies that supported me financially during my PhD. The Gates Cambridge Scholarship Program provided funding during my time in the UK and provided an incredible professional and social community (along with St. John's College) which greatly enhanced my time abroad. The NIH Oxford-Cambridge Scholars Program, the International Biomedical Research Alliance, and the National Cancer Institute CRTA Program have provided much needed funding during the entirety of my PhD. It has been an incredible opportunity to be involved with such a unique program that provides graduate students with the chance to train in an internationally collaborative context. I believe the NIH OxCam and Gates Cambridge programs have prepared me well for future independent research within a global cancer research community, and for that I am very grateful.

One of the greatest benefits of an international PhD program was the incredible people with whom I had the privilege of working and collaborating. Dr. Anna Kolb trained me on how to properly derive and maintain patient-derived glioblastoma cell lines. Dr. Astrid Wendler was an incredible source of insight and scientific support during my time at Cambridge and helped make time in the BRC much more enjoyable and educational. Dr. Alexandra Vaideanu and Luca Peruzzotti-Jametti helped immensely with initiating our Cambridge in vivo work and for intracranial tumour implantation training, respectively. It was a great joy collaborating with Christopher Parkins and Professor Oren Scherman on the hydrogel work contained in this thesis. From grant writing to experimental work to publication, working on the hydrogel project with Chris has been a wonderful example of effective scientific collaboration in action. On the NIH side of the pond, I am equally thankful for many wonderful people. Dr. Barbara Rath was a tremendous resource and scientific mentor for me when I got started in the ROB by patiently training me on in vivo

techniques and providing guidance on innumerable other aspects of my work. I am grateful for Dr. Charlotte Degorre who performed limiting dilution assays and for Kristin Valdez and Dr. Uma Shankavaram who provided bioinformatic expertise for WES analysis and presentation. I am thankful for the opportunity to have participated in a small way in the career of Dejauwne Young, one of my first trainees, who assisted with several aspects of my project, particularly γH2AX analysis. If all my future collaborators, colleagues, lab members, and trainees are as kind, helpful, and engaging as the individuals mentioned above, then I am looking forward to a career filled with wonderful interactions with wonderful people.

Importantly, I would like to thank my family and friends. My parents, John and Kim McAbee, have always valued learning and encouraged me from a young age to pursue my dreams and follow my passions. They provided me with such a stable and happy home life that I felt safe and free to chase after dreams, like pursuing a PhD at Cambridge, because I knew that they would love and support me no matter what. Every day I feel blessed and proud to be your son, and I hope I live in such a way that makes you feel the same. I am equally blessed and thankful to have an extended family, including a loving grandmother, and loyal friends that provide me with love and support that follow and strengthen me wherever I go. My broader church family, which in DC also includes my CS Lewis Institute family (the Wyatts, in particular), has provided prayers and friendship for which I will always be grateful. Also, during the writing of my thesis my girlfriend, Meredith Cotton, was one of my greatest sources of encouragement. I am grateful for her continual support and the much-needed writing breaks she provided during one of the busiest times of my PhD life. There are innumerable friends, roommates, and colleagues that I cannot mention by name here, but have nonetheless enhanced and enriched my PhD experience. To all of you, I give you my thanks.

Last, but certainly not least, I would like to thank the patients with whom I have had the privilege of working over these years. The courage and fighting spirit displayed by so many patients and their families are a true source of inspiration to me. It is an honor to perform research aimed at improving our understanding of this terrible disease. Ultimately, it is my hope and prayer that together we will improve the outcomes for all future glioblastoma patients.

Table of Contents

List of Figures

Chapter 1. Introduction

1.1 The Evolution of Cancer

The cancer burden is increasing. In the United States, almost 40% of adults are expected to be diagnosed with cancer at some point during their lifetimes. While the rate of deaths attributable to cancer fell by 26% from 1991 to 2015, the international incidence of cancer cases is expected to rise from 14.1 million in 2012 to an estimated 23.6 million by 2030 (1). Certainly, this elevation in cancer incidence can be attributed in some degree to a combination of improved methods of early cancer detection, increased post-reproductive average lifespan, and continued exposure to harmful carcinogens. But the increased burden and the need for more effective treatments necessitate a better understanding of the various cancer types and the evolutionary processes which lead to their development, maintenance, progression, and resistance. This thesis will examine the radiation-induced evolution of glioblastoma, the most malignant form of brain cancer. We will first discuss some important aspects of cancer evolution, in general, before describing how glioblastoma specifically fits into an evolutionary framework.

1.1.1 Determinants of Cancer

In order for cancer cells to develop, survive, and proliferate, they must acquire several distinct capabilities which provide them a fitness advantage to generate a tumour and progress to malignancy. Hanahan and Weinberg proposed a list of such cancer hallmarks (2). As a cancer is a collection of aberrantly proliferating, mutated cells, two necessary and fundamental traits of neoplastic cells are their ability to sustain proliferative signaling and evade growth suppressors. Neoplasms sustain chronic proliferation through many redundant mechanisms such as increased production of growth factors, amplification of receptor expression, or mutation-induced structural changes in receptors leading to ligand-independent constitutive activation (3). In addition to enhancing proliferation, cancer cells must simultaneously be able to evade the normal cellular regulations against such uninhibited proliferation. The retinoblastoma (Rb) and TP53 proteins and the cell cycle progression role which they command

are two extremely important examples of tumour suppressors. Rb and TP53, or elements in their respective pathways, are often mutated in cancers and allow cancer cells to evade these critical gatekeepers regardless of high levels of extracellular or intracellular stress signals or genomic damage (4). Further to the ability to evade growth suppressors, is the ability to resist cell death through apoptosis (5). TP53 plays a major role in inducing apoptosis after extensive DNA damage but is one of the most commonly mutated tumour suppressors, resulting in the loss of apoptotic regulation. Apoptosis can also be reduced in cancer cells through a tumour-promoting imbalance of anti-apoptotic (Bcl-2, Bcl-x_L) and pro-apoptotic (Bax, Bim) factors. Other avenues of resisting cell death or capitalizing off of cell death of other cells involve autophagy which can cause cancer cells to shrink and become reversibly dormant (6) or necrosis which can recruit tumour-promoting immune cells to the tumour microenvironment through extracellular release of proinflammatory contents (7).

Longevity of cancer cells is important for providing adequate time to attain and propagate cancer attributes. While resisting cell death is an important contributory factor to this longevity, mechanisms by which cancer cells maintain replicative immortality are also important for tumour survival and progression. Telomeres, which protect the ends of chromosomes with multiple tandem hexanucleotide repeats, are maintained in many cancers allowing neoplastic cells to undergo unlimited cycles of proliferation (8). Increased expression of telomerase, which adds repeats to chromosome ends, enables cancer cells to avoid senescence and apoptosis to achieve a relatively immortalized state.

Cancer cells which have evolved to the point of replicating and proliferating without regulation may be able to grow and progress into a full tumour. Some of the extrinsic factors which can contribute to the natural evolution of a growing tumour are limitations on available space and nutrients. Angiogenesis, a normal, transient component of wound healing, is co-opted and continuously activated by cancer to produce new vessels for the provision of more nutrients and oxygen for tumour expansion as well as waste disposal (9). Vascular endothelial growth factor (VEGF) is an angiogenesis inducer that is commonly upregulated in cancer by oncogenic signaling or hypoxic environments (10). Angiogenesis represents a dynamic interaction between a tumour and its microenvironment. In addition to angiogenesis, limited space and resources may also contribute to a cancer cell's predilection for invasion and metastasis. A cellular program typically involved in development, epithelial-mesenchymal transition (EMT), has been implicated in the invasion-metastasis cascade (11). EMT-inducing transcription factors have been demonstrated in various cancer types and contribute to a variety

of functions including loss of adherens junctions, increased motility, and expression of matrix-degrading enzymes which contribute to an invasive phenotype.

Hanahan and Weinberg also describe two additional emerging hallmarks of cancer (immune evasion and metabolic reprogramming) and two characteristics of most cancers (tumour-promoting inflammation and genomic instability) which enable them to acquire many of the hallmarks discussed above (see Figure 1.1) (2). Despite a usually intact host immune response, cancer cells which grow into tumours have successfully evaded destruction. Because cancer cells are derived from a patient's own cells and undergo periods of quiescence, a certain degree of self-tolerance can be built up (12). More directly, cancer cells can downregulate its tumour-specific antigens and dysregulate antigen processing. Cancer cells may also actively suppress the immune system through cytokine secretion (TGFβ and IL10) or PD-L1 expression which can reduce the level of active T cells and increase T regulatory cell function (13). Immune cells not only fail to destroy cancer cells but can actually contribute to tumour survival as inflammation, which may originate as non-specific anti-tumour responses, may ultimately provide a source of growth factors, survival factors, and angiogenesis inducers that are necessary for cancer survival (14).

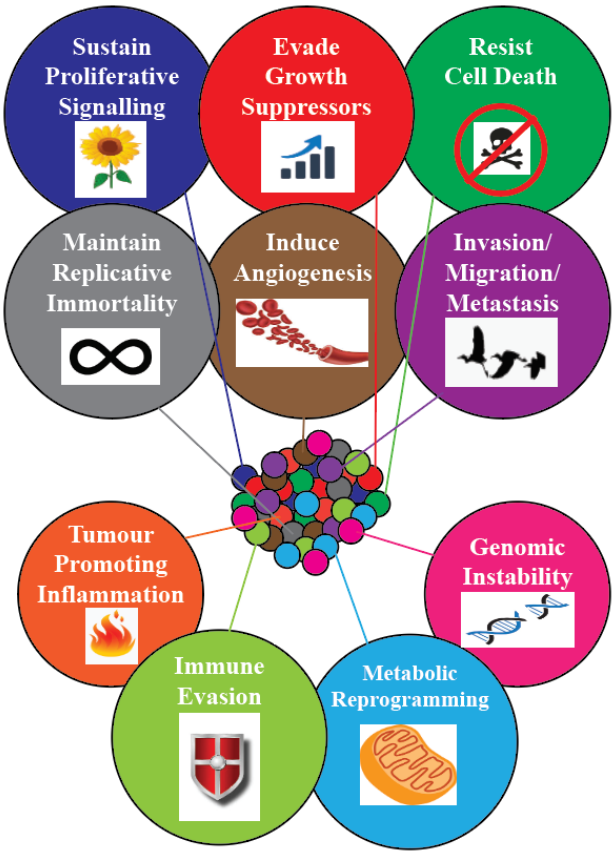

Figure 1.1 Cancer Hallmarks. Established hallmarks, emerging hallmarks, and cancer characteristics as proposed by Hanahan and Weinberg (2).

While angiogenesis manipulates the microenvironment to increase oxygen and nutrient availability, reprogramming of metabolic pathways is an intrinsic attempt to quickly obtain the energy required to undergo cell proliferation. For instance, cancer cells have been shown to obtain a large portion of their energy through aerobic glycolysis (15). While not as fruitful in ATP production as oxidative phosphorylation, aerobic glycolysis does provide a rapid source of ATP through breakdown of extracellular glucose which produces both energy and biosynthetic intermediates (16). Such reprogramming can be directed by overexpression or overactivation of Myc, HIF-1, and PI3K pathways which are commonly altered in cancers to promote proliferation. But clearly, very few of the hallmarks and characteristics listed above would be possible without underlying genomic alterations triggering cancer phenotypes. Therefore, genomic instability has emerged as an important characteristic of tumour cells (17,18). As more mutations are gained the likelihood increases of acquiring advantageous mutations which confer necessary cancer hallmarks. Increased mutation rates, dysfunctional DNA repair mechanisms, or epigenetic silencing can all contribute to genomic instability and intratumoral heterogeneity which ultimately leads to the production of cancer cells with enough advantageous mutations and acquired hallmarks to grow and populate a fully formed tumour.

1.1.2 The Cancer Stem Cell Hypothesis

Once a subset of cancer cells acquires the hallmarks mentioned above, the cancer cells must then proliferate. This requirement for extensive self-renewal is one reason why "cancer stem cells" (CSC) represent potential units of selection for cancer evolution (19-21). The cancer stem cell hypothesis originally developed through studies of leukaemia in which a cellular hierarchy emerged with CSCs at the apex (22). Other cancers, including solid tumours, have since been described as developing through this process. Essentially, CSCs are considered cancer cells which possess many of the same properties of adult somatic stem cells, i.e. replicative immortality and propagation of differentiated cells. The ability of CSCs to produce a diverse pool of differentiated cells also grants them tumourigenic potential, another important feature of cells which are thought to promote development, progression, and resistance of cancer.

An underlying prerequisite to produce a diverse cohort of progenitor and differentiated cells which encompass a heterogeneous tumour is that CSCs must themselves express a high

level of genotypic and phenotypic diversity. The diversity inherent in CSCs makes them prime units of selection, because they harbour many mutations with different relative fitness levels. Based on the specific selective pressure driving evolution or the current need of the cancer, CSCs can redirect towards the resistant or most fit clone or subclone for a given situation. The extensive self-renewal properties of CSCs allow them to then propagate whichever cell underwent positive selection. Thus, sufficient genetic diversity of CSCs allows for evolutionary selection while extensive self-renewal allows for the selected trait to be passed on to cells that can populate a tumour (23,24). CSCs have also been shown to be intrinsically resistant to therapies (25) which may be due to intrinsic diversity, stem cell niches, or periods of transient quiescence (26). In fact, CSCs in glioblastoma are able to transition between proliferative and slow cycling states by Notch signalling and upregulation of histone demethylases (27). Taken together, CSCs give rise to heterogeneous tumours capable of adaptation under evolutionary selective pressures (Figure 1.2).

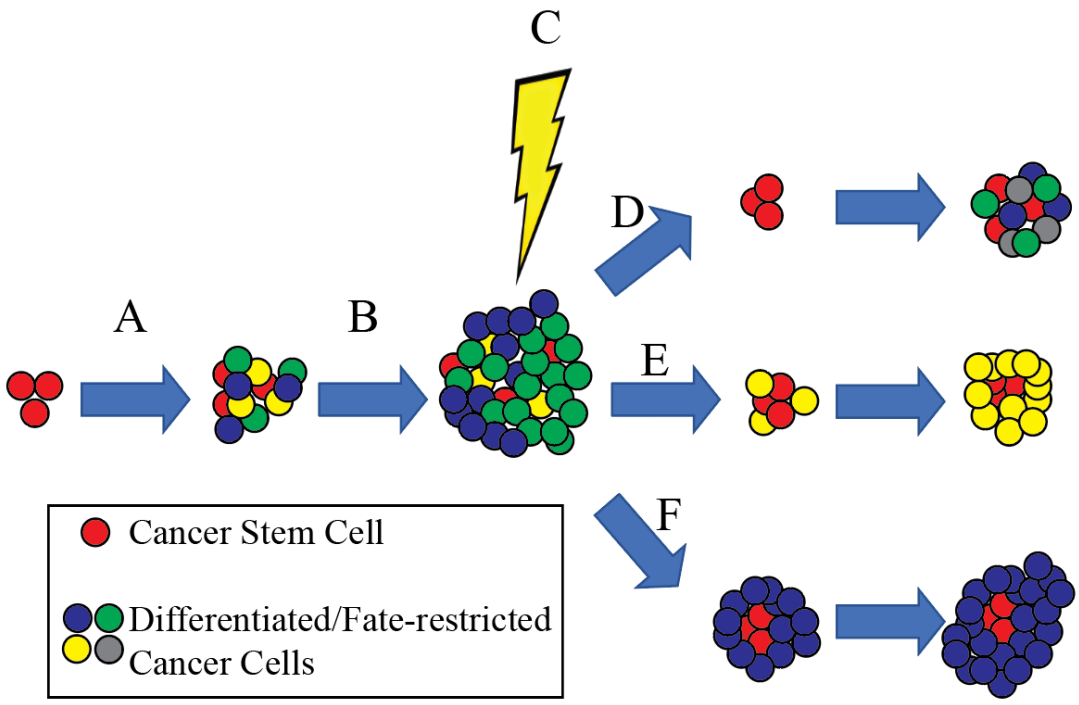

Figure 1.2 CSCs as Units of Evolution. A) Cancer stems cells propagate differentiated/fate-restricted cancer cells to produce a heterogeneous tumour. B) Cancer cells with fitness advantages are better able to compete for limited space and resources. C) Therapeutic selection pressures such as surgery, radiotherapy, and chemotherapy are applied to the tumour. D) CSCs sometimes survive to repropagate a heterogeneous recurrent tumour because of resistance to or protection from therapy. E) Competitive release can eliminate or reduce larger, therapy-sensitive populations providing the opportunity for smaller subpopulations to expand and populate a recurrent tumour. E) Intrinsic therapeutic resistance can cause a clonal population to continue to thrive during and after treatment.

1.1.3 Cancer as a Darwinian Process

Cancer can be considered a complex, Darwinian, adaptive system (28,29) in part because cancer arises through a protracted evolutionary course in which various challenges and pressures contribute to the accumulation of adapted phenotypes and genotypes (30). As discussed, heterogeneity is a requirement for Darwinian selection as the intratumoral diversity within a given cancer type allows for natural selection to drive the cancer into a more well suited, more fit state (23). Mutations with the potential to drive or enhance carcinogenesis (driver mutations) may arise through neutral evolution (large scale genomic/chromosomal instability that blindly increases rate of mutations), natural evolution (space and nutrient competition selects for clones better equipped to survive in harsh environments), or selective evolution (therapeutic pressures lead to the expansion of resistant clones) (31). The interplay of acquired intrinsic mutations with extrinsic factors which test the fitness of those mutations contributes to the development of cancer. The diversity of extrinsic factors demonstrate that cancer does not grow in a vacuum but is instead impacted by a dynamic milieu of diverse cell types, extracellular networks, and anti-cancer compounds.

The diversity between unique cancers originating in different tissue types demonstrate that local interactions with and restrictions by the tumour microenvironment can affect diversity over time. The tissue ecosystem in which a tumour resides not only provides the location for natural selection to occur, but also provides its own set of challenges to determine fitness selection and impact clonal evolution (32). The microenvironment provides many levels of mutual interactions with cancer cells ranging from immune cell infiltration with subsequent anti-tumour or even pro-tumour effects to providing protective/supportive niches for phenotypically inclined CSCs to promoting invasion/migration by the spatial heterogeneity of available resources (24,31). Like cancer cells, the tumour microenvironment can also be impacted and altered by carcinogenic exposures and chemoradiotherapy. In fact, the remodelled microenvironment post-therapy may provide new selection pressures or advantageous expansion opportunities for cancer cells that survived treatment either through intrinsic resistance or protective niches (33). An alternative to the unidirectional hierarchy of the CSCs postulates that tumours arise from common ancestors of malignant cells that exist in a limited set of cellular expression states (NPC-like, OPC-like, Astrocyte-like, Mesenchymal-like) with inherent plasticity which allows tumours to evolve and reversibly transition between states in response to various pressures (34). Such complex interactions and evolutionary

possibilities make it obvious that we cannot solely rely on the underlying mutational architecture of primary cancers to provide insight into cancer biology. We must also work to better understand the dynamic nature of cancer as an evolutionary, adaptive system.

1.1.4 Selection Pressures Drive Evolution

Maley and a panel of experts developed a consensus framework for classifying tumours and investigating the clinical implications of cancer evolution and ecology (35). The components which make up their proposed ecological index are the available resources which sustain cancer cells and the potential hazards which harm them. Certainly, cancer cells need oxygen, glucose, growth signals, and survival factors to develop and proliferate. As stated previously, the microenvironment plays a significant role in this capacity and is a major source of selection pressures which drive evolution at all stages of cancer development and progression. In addition to the microenvironment, one of the most potent sources of selective pressure with the ability to drive cancer evolution is anti-cancer therapy.

Cancer therapeutics, such as chemotherapy or radiotherapy, impose artificial selection pressures which lead to high levels of cellular death, thus providing cells with resistance mutations or cells which evade treatment through other mechanisms to proliferate with less competition. In addition to selecting cells which already possess intrinsic resistant properties, genotoxic drugs such as chemotherapies can induce novel mutations which can further enhance cancer cell fitness (24,36). Even targeted therapies which incorporate knowledge of genetic alterations in cancer to attack a clonal driver mutation can be overcome as a subclone present at low frequency prior to treatment could potentially expand after therapy to generate a resistant, recurrent tumour (37-39). Additionally, it has been postulated that another possibility for targeted therapy failure is because recurrences emerge from a persistent cellular reservoir of common ancestors which possess early truncal events not in common protein-coding variants, but in larger genetic alterations such as whole copy-loss of chromosome 10, copy gain of chromosome 7, or TERT promoter mutations (40). It is important, therefore, to examine cancer genomics both before and after treatment to obtain a more longitudinal picture of cancer evolution. In order to design more effective therapies, we must consider the dynamic interplay between the genomic architecture of cancer, the tumour microenvironment, and therapy-driven evolution. Glioblastoma is a rapidly evolving, heterogeneous brain cancer and elucidating the

impact of radiation on glioblastoma evolution could provide valuable insights for recurrent tumour biology and treatment.

1.2 Glioblastoma

Glioblastoma (GB), the most common and malignant form of adult brain cancer (41), develops de novo (primary) or from a lower grade tumour (secondary) (42). It is of neuroepithelial origin and is thought to arise from neural stem cells, glial progenitor cells (such as OPCs), or astrocytes (43,44). The incidence of GB is 3.21 per 100,000 in the United States and 4.64 per 100,000 in the United Kingdom (45,46). The highest incidence rates of GB occur after the fifth decade of life and the cancer is 1.58 times more commonly diagnosed in men than women (45). However, glioblastoma is diagnosed across all ages and is almost uniformly fatal, causing it to have one of the highest average years of life lost of any cancer (47).

According to the World Health Organisation (WHO) classification of brain tumours, GB is considered a grade 4 neoplasm due to its malignant histological/cytological features, invasive propensity, rapid disease evolution, and poor outcomes (48). Typically, glioblastoma has been presumptively diagnosed as a heterogeneously, peripherally enhancing lesion on T1-weighted MRI with gadolinium contrast and definitively diagnosed after surgical resection and histopathological analysis. In particular, evidence of nuclear atypia, increased mitotic activity, palisading necrosis and/or microvascular proliferation provide support for a diagnosis of glioblastoma (48). The most recent iteration of the WHO classification scheme also considers some molecular markers to more accurately subtype gliomas. In particular, the 2016 classification scheme divides GB into IDH-wildtype (90%), IDH-mutant (10%; secondary GB), and GB NOS (IDH evaluation not available) (49). ATRX loss and TP53 mutation are commonly identified in IDH mutant diffuse astrocytomas, whereas 1p/19q codeletion defines oligodendrogliomas, a different diffuse glioma entity not typically associated with GB (49). While the current WHO classification system is an improvement because it utilises some molecular evidence in its algorithm, the molecular and phenotypic landscape of GB is much more diverse and complicated than the few mutations mentioned in the classification scheme.

1.2.1 Intrinsic Mutational Landscape

Glioblastoma was one of the first solid tumours investigated by The Cancer Genome Atlas (TCGA). In 2008, the TCGA published its initial findings after examining the methylation, gene expression and copy number profiles of over 200 human GB samples (50). Almost half of the tumours were also subjected to genomic variant analysis. Integrating multiple types of analysis for such a large cohort allowed for the delineation of three core GB pathogenesis pathways: receptor tyrosine kinases (RTK/RAS/PI3K), retinoblastoma (Rb), and tumour suppressor p53 (TP53). Of the tumours sampled approximately 75% contained mutations in all three of the core pathways, suggesting potential targets for therapeutic intervention (50) and highlighting the need for multi-target combination therapies.

One of the most commonly mutated RTKs is epidermal growth factor receptor (EGFR). EGFR, which is encoded on chromosome 7p12, has been shown to be overexpressed or amplified in over 40% of GB (51,52) or structurally altered in others. The most common mutant structural variant (EGFRvIII) is caused by a deletion of exons 2 to 7 which results in truncation of the extracellular domain of the receptor and ultimately causes ligand-independent constitutive activation of EGFR (53). Constitutive activation of the RTK leads to activation of the PI3K downstream signaling pathway which has been implicated in proliferation through alteration of mRNA for enhanced association with polysomes for active transcription (54). While the implications of EGFR amplification and variants on clinical outcomes have not been completely determined, they have been proposed as potential indicators of poor prognosis. The prevalence of EGFR variants has made the receptor an attractive option for drug targeting (55,56).

While EGFR is a very prevalent gain of function mutation in GB, PTEN (tyrosine phosphatase/tensin homolog protein), a negative regulator of the PI3K/Akt pathway, is considered to be one of the most common loss of function genetic alterations (57). PTEN deletion occurs most commonly through loss of heterozygosity (LOH) of chromosome 10q. In LOH an entire gene and its surrounding chromosomal region is lost, and if the gene in question is a tumour suppressor then the remaining copy is left vulnerable to future mutations and subsequent malignant transformation (58). In the case of PTEN, loss of this tumour suppressor prevents negative regulation of PI3K which can lead to uncontrolled activation and proliferation, particularly in the context of additional mutations which constitutively activate

the pathway (59,60), as described above. PTEN has been associated with poor prognosis (61), is found more frequently in primary GB (62), and may represent an important early genetic step leading to the glioblastoma phenotype.

TP53 has been found to be mutated in up to 30% of primary GB, although mutations are more commonly detected in low grade astrocytomas and secondary GB (57). However, it is estimated that at least one component of the TP53 pathway is mutated in over 80% of all GBs (52). TP53 mutations are common to many cancer types as the normal tumour suppressor function of TP53 must be overcome for cancer cells to survive and proliferate (63). The TP53 pathway, when functioning normally, regulates cell cycle progression, response to DNA damage, and apoptosis. When the p53 transcription factor is activated, it promotes cell cycle arrest or apoptosis through activation of target genes. P53 activation also leads to the activation of MDM2 (an E3 ubiquitin ligase) which serves as an autoregulatory feedback loop to inhibit and degrade p53. MDM2 is itself inhibited by the tumour suppressor protein $p14^{ARF}$ (64). Therefore, mutation of TP53, amplification of MDM2, or deletion of $p14^{ARF}$ can ultimately lead to the inactivation of the p53 pathway and the survival of cancer cells (65). While the prognostic significance of TP53 mutations is unclear, it has been shown that TP53 overexpression may be associated with improved progression free survival (PFS) for patients who received long courses of adjuvant temozolomide (66).

Another tumour suppressor protein involved in the regulation of cellular proliferation and survival, retinoblastoma, is found to be deleted in a small number of GBs (50). Retinoblastoma normally binds E2F to prevent it from activating cell cycle progression target genes (67). The phosphorylation of Rb by cyclin-D1-CDK 4/6 complexes causes it to release E2F to allow G1-S progression (68). CDK4/6 can be overexpressed in GB leading to uncontrolled progression. A more common alteration in this pathway is the upstream regulator of CDK4/6, CDKN2A (2B less commonly). CDKN2A (or $p16^{INK4a}$) is a tumour suppressor protein that is encoded at the same locus as $p14^{ARF}$ and normally works to inhibit CDK4 from phosphorylating Rb (69,70). As with the TP53 and RTK pathways, any of the mediators mentioned above could be mutated to cause uninhibited cell cycle progression and enhanced survival of cancer cells bearing the Rb pathway mutation (71,72).

As seen by the WHO classification, isocitrate dehydrogenase (IDH) is an important molecular marker for delineating the evolutionary history of a GB. IDH, an enzyme involved in the citric acid cycle, is often mutated in low grade gliomas and secondary GBs (73) and in a

small subset of primary GBs (74). IDH mutations are conserved through cycles of malignant progression, suggesting that they are an early event in glioma development (75). IDH1 is the most commonly mutated enzyme and exists in the cytoplasm, while IDH2 exists in the mitochondria (76,77). Wild type IDH oxidatively decarboxylates isocitrate to α-ketoglutarate and carbon dioxide, but its altered enzymatic action in IDH-mutant gliomas yields reduced levels of α-ketoglutarate and increased levels of 2-hydroxyglutarate (2-HG). The elevated levels of 2-HG inhibit enzymes involved in histone and DNA demethylation leading to changes in epigenetic alterations and gene expression that impact various tumour-related pathways such as invasion, survival, and hypoxia signalling (78-80). It has been suggested that the epigenetic alterations induced by IDH1 mutations may be sufficient for the glioma hypermethylation phenotype. IDH1 mutations are often associated with younger patients, longer survival, and lower grade gliomas (74) and can be detected most often by R132H antibody specific immunohistochemistry (the most common amino acid change) (81). Other clinical implications of IDH mutations include higher rates of TMZ response (82), association with larger extent of surgical resection (83), and a novel method of non-invasive biomarker imaging of 2-HG on magnetic resonance spectroscopy (84). The inclusion of IDH mutation status in the WHO classification scheme reflects its relative importance in both prognosis and development of glioblastoma.

In addition to IDH mutation status, MGMT methylation status is also now routinely tested in GB patients due to its potential to predict prognosis and response to alkylating chemotherapy. The MGMT gene encodes for O6-methylguanine DNA methyltransferase, an enzyme involved in DNA repair. MGMT normally counteracts the alkylation caused by temozolomide by removing alkyl groups from guanine to its own cysteine residue so that the cell can survive and continue to replicate (85,86). When the MGMT promoter is methylated, the gene is effectively silenced, MGMT cannot repair the alkylation caused by TMZ, and cell death is initiated. Therefore, MGMT promoter methylation is associated with increased patient survival and improved response to TMZ (87,88). Interestingly, MGMT promoter methylation has also been shown to be predictive of improved response to radiotherapy (89). Inversely, if a GB expresses high levels of MGMT, then it can provide an avenue for TMZ resistance. However, MGMT is only a single component in the DNA repair response to chemotherapy. If MGMT is unable to remove alkyl groups, then normally the DNA mismatch repair system will recognize O6-methylguanine mismatches and trigger apoptosis after unsuccessful repair and induction of cytotoxic double-strand breaks. Unfortunately, mutations can also occur in MMR

genes (MSH2, MSH6, MLH1, MLH3, PMS1, PMS2). Mutations in MSH6, in particular, have been associated with GB (90,91) as MSH6 deficient cells cannot properly trigger cell cycle arrest in response to DNA damage caused by TMZ. If MGMT promoter methylation is coupled with MSH6 mutation/loss, then a GB becomes resistant to both the alkylation by TMZ and the killing which should be induced by that alkylation. The loss of normal MMR function in this context leads to an increased tolerance to mutagenic activity and thus a hypermutation phenotype observed in recurrent tumours (92). Our group has recently shown the impact of treatment pressures on DNA repair genes and hypermutation, as a patient who underwent three surgical resections with intervening treatments including alkylating chemotherapy demonstrated hypermutation after the final resection suggesting that acquired mutations in DNA repair genes may have allowed such extensive numbers of mutations to occur unhindered.

TERT (telomerase reverse transcriptase) and ATRX (alpha-thalassemia X-linked mental retardation protein) mutations are an important aspect of GB's ability to maintain replicative immortality despite ongoing divisions through telomere maintenance. As mentioned previously, for stem cells and cancer cells, elevated levels of telomerase leads to continual elongation of the telomeres and thus continual division (93). Point mutations (G>A transitions) in the TERT promoter leads to increased TERT expression and telomerase activity and increased cancer cell DNA viability (94,95). Alternatively, ATRX interacts with DAXX to form a complex that deposits H3.3 histone variants at telomeres to maintain their length (96). ATRX mutation/loss has been associated with IDH1 mutations and alternative lengthening of telomeres phenotype (ALT) through dysregulation of macroH2A1 telomere deposition, decreased binding of polymerase tankyrase 1 to macroH2A1, and lack of telomere sister cohesion resolution (97). ALT leads to longer telomeres compared to samples with TERT promoter mutations (98,99). TERT and ATRX mutations seem to be mutually exclusive in gliomas, possibly reflecting the similar survival advantage conferred by both mutation types (94).

While the above variants represent some of the most common mutations in GB, there is considerably more variation in GB. Therefore, in an attempt to stratify GBs based on recurring patterns within this heterogeneous group of tumours, various classification schemes have been proposed (100-103). One of the most commonly utilised classification schemes was proposed by Verhaak et al. and placed GB into Proneural, Neural, Classical, and Mesenchymal subtypes based on TCGA gene expression data (102). GBs in the Proneural subtype commonly exhibit mutations in IDH1, PDGFRA, and TP53. Patients in this subgroup tend to be younger

and tend to experience longer overall survival (OS), as would be expected for IDH-mutant GBs. The neural subtype is not characterized by particular mutations but by the expression of neuronal markers. Classical subtype GBs harbour frequent EGFR amplification, chromosome 7 amplification, and chromosome 10 loss. Classical GBs lack TP53 mutations and tend to have the best response to aggressive treatment. Lastly, the Mesenchymal subtype typically includes NF1 and PTEN deletions/mutations. The survival advantage after treatment is also significant for the mesenchymal subtype although patients in this subgroup have the worst prognosis overall.

Eckel-Passow proposed a simpler scheme by classifying GBs based on the presence of 3 molecular markers: IDH mutations, TERT promoter mutations, and 1p/19q codeletions (low grade gliomas) (104). GBs with TERT only mutations were the most common and patients were the oldest mean age at diagnosis, while IDH-only mutated GBs were associated with the youngest age at diagnosis. The molecular subgroups were not associated with overall survival in GB although TERT-only GBs had the shortest survival. With more recent TCGA findings, a new glioblastoma classification scheme has been proposed that includes not only biomarker expression but also DNA methylation profiles, gene expression patterns, and telomere length/maintenance description (98). While the classical and mesenchymal subtypes were mostly retained in this scheme ("classic-like" and "mesenchymal-like"), the proneural and neural subtypes were replaced with further subgroups. In particular, IDH-mutant gliomas (without 1p/19q co-deletion) were subdivided into G-CIMP-low and G-CIMP-high subgroups based on their relative levels of DNA methylation. G-CIMP (glioma-CpG island methylator phenotype) was demonstrated by gliomas with high levels of methylation at many loci (105). G-CIMP tumours are found in younger patients with better prognosis and are typically associated with IDH mutations (106). As discussed previously, IDH mutations and the competitive inhibition of α-ketoglutarate enzymes, such as ten-eleven translocation methylcytosine dioxygenase (TET) DNA demethylases, may represent the molecular mechanism for such hypermethylation (107). While patients with G-CIMP tumours of any type generally have a better prognosis than IDH-wildtype tumours, G-CIMP-high tumours had better prognosis when compared to G-CIMP-low tumours. The neural subtype was basically replaced with a small subset of IDH-wildtype GB which corresponded to the LGm6 methylation cluster assignment (LGm6-GBM). While these and other classification schemes are thought to provide information for patient stratification, prognosis, and treatment response (108,109), the importance of subtyping is ultimately unclear due to the observed intratumoral

heterogeneity (ITH) of GB which can lead to the presence of multiple subtypes within the same tumour (Figure 1.3).

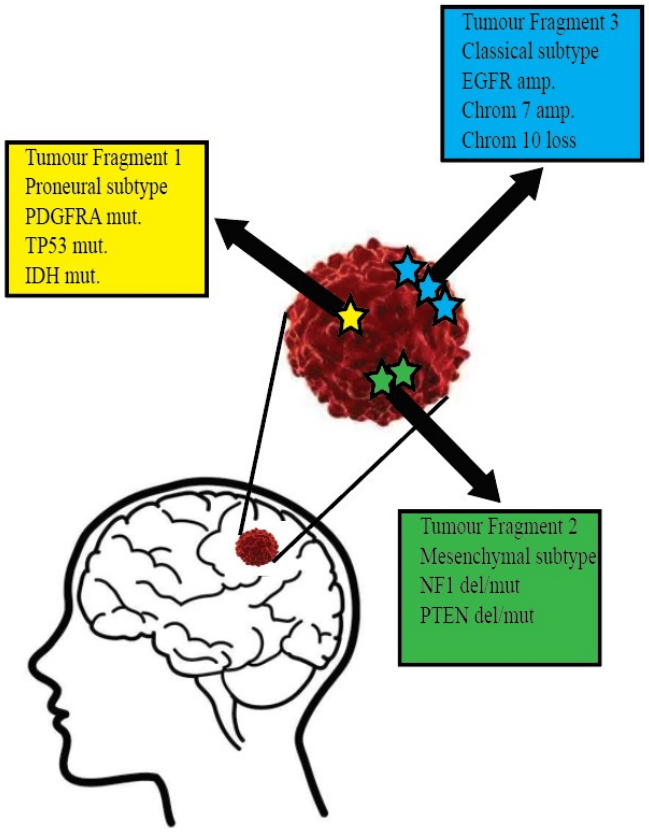

Figure 1.3 Glioblastoma intratumoral heterogeneity. An illustrated simple example of GB ITH in which spatially distinct tumour fragments may harbour different subtypes. Common mutations for each subtype are listed as an example of potential observable diversity, but ITH may also be observed in DNA methylation patterns, gene expression, and more. Separate clones may possess many similar mutations to other clones (linear evolution) or only a few similarities in probable early event mutations that are shared from ancestral precursors (divergent evolution).

1.2.2 Intratumoral Heterogeneity

While knowledge of common mutations, core pathways, and molecular subtypes is necessary and important, many of the above studies characterized genomic mutation patterns of GB based on single surgical biopsies and thus may not have captured the full genomic architecture of each tumour. In fact, it has been shown that a single tumour can harbour spatially distinct tumour fragments which correspond to different GB subtypes, making the utility of any classification scheme difficult. Sottoriva et al. utilised comparisons of copy

number alterations (CNA) and reconstructed tumour fragment phylogenies to examine the relative heterogeneity between spatially and temporally distinct tumour fragments within the same tumour (110). The prevalence of a given copy number event allows for inferring evolutionary trends. Common CNAs found in all fragments were considered to be early events in the evolutionary process whereas shared CNAs (found in more than one fragment) and unique CNAs (found in only one fragment) were considered middle and late events, respectively. For GB, CNAs in EGFR and CDKN2A were found to be early events whereas CNAs in PTEN and PDGFRA were considered to be late events. Tumour phylogenies were reconstructed through molecular clock analysis. Molecular clock analysis utilises a measure of mitotic distance between cells within a fragment, namely the number of cell divisions, to identify subclones. The genomic locus IRX2 has been shown to accumulate methylation errors linearly with age (111). By examining the relative amount of methylation on the IRX2 locus for a given cell population (a mitotic clone corresponds to a unique methylation tag), the composition and hierarchical relationships of mitotic clones within tumour fragments can be determined. As such, even within single tumour fragments, multiple mitotic clones with differing cell lineages were delineated. Another study which sequenced multiple tumour fragments found evidence of similar extensive ITH as only 51% of mutations were clonal and two of the treatment-naïve tumours even contained small fragments with hypermutator phenotype (112). Possible therapeutic targets were inconsistently identified within different fragments from a given tumour, demonstrating that a multi-sampling surgical and sequencing technique provides a more complete picture of a given GB's genomic makeup (112).

In addition to differences in genomic patterns, ITH has also been shown at the level of transcription. Patel et al showed by single-cell RNA-Seq of 430 cells from five GBs that diverse programs of transcription were variably expressed between cells from a single tumour. The cells within a given tumour corresponded to multiple GB subtypes further highlighting ITH and the potential limitations of utilising subtypes for treatment decisions. Another study based on RNA-Seq analysis found differences in molecular composition and GB subtypes between cells from the contrast-enhancing tumour core and cells from the non-enhancing tumour margin (mostly neural subtype). While the expression patterns of the marginal samples were contaminated with "normal" brain cells, the microenvironment could ultimately influence expression patterns of residual neoplastic cells within the parenchyma and contribute to observed differences in cell type-specific alteration patterns.

Differences in DNA methylation patterns (113,114) and drug sensitivity (115) have provided an even more comprehensive understanding of contributions to and implications of GB ITH. Such extensive ITH is thought to be a major factor behind the inevitable tumour progression, treatment resistance, and recurrence observed in GB (116-119), as multiple subclones with differential treatment sensitivity can exist within the same tumour. For example, single tumours were found to harbour amplifications in three different receptor tyrosine kinases (120), representing potential intrinsic resistance routes to treatments targeting a single specific RTK. EGFR, MET, and PDGFRA driver genes, which all contribute to protein production, were amplified in different cells coexisting within the same tumour. Similar results in which two or more RTKs were amplified within a single tumour were found in 34 TCGA cases (121). Furthermore, in vitro inhibition of the PI3K pathway for cell lines derived from gliomas expressing RTK coamplification required inhibition of both EGFR and PDGFR. The addition of therapeutic selection pressures to the context of ITH can lead to the contraction or expansion of various subclones and the potential for a recurrent tumour to be populated with resistant cell populations. The importance of this evolutionary process and its implications for effective treatment development necessitates further analysis of ITH and GB evolution in order to elucidate genomic patterns, early and late evolutionary events, and key, actionable branch points in a tumour's evolutionary history.

1.2.3 Treatment and Survival

Glioblastoma is a rapidly progressing and evolving disease. As such, patients who remain untreated experience an overall survival time of less than 6 months. After maximal safe surgical resection, the current standard of care for newly diagnosed glioblastoma, the Stupp Protocol, consists of fractionated radiotherapy (30 fractions of 2Gy) and concomitant and adjuvant temozolomide (TMZ) (122). Despite such radical treatment, the median survival is still only about 15 months. Glioblastoma has 5-year and 10-year post-diagnosis survival estimates of less than 6% and 3%, respectively, some of the lowest rates among all forms of cancer (41).

Surgical resection is important for both diagnostic purposes and to relieve tumour burden and mass effect on the brain. In addition to providing relief from symptoms and improving postoperative function (123), patients who underwent resection had increased

survival (124). Furthermore, those patients who received a more extensive resection enjoyed a greater survival advantage (125,126). In fact, partial resection or biopsy is associated with greater risk of postoperative complications such as hemorrhage, herniation, and oedema (127). While the preoperative performance status and location of tumour relative to eloquent brain areas must be considered to properly weigh the risk-benefit ratio, in general, the greater the resection, the better the outcome. This survival advantage is applicable to all glioblastoma patients, regardless of age (128,129). This may be due in part to the many surgical advances which have improved the safety of GB surgical resection. Intraoperative electrocortical stimulation, awake craniotomy, and neuronavigation provide surgeons with tools necessary to better avoid language and motor-associated areas. Intraoperative MRI and fluorescence-guided surgical resection have been developed to improve extent of resection. While both do improve resection, iMRI has not been clearly shown to improve survival for GB patients (130), while fluorescence-guided surgical resection has been associated with an increase in PFS (131,132). Fluorescence-guided surgical sampling involves the use of 5-ALA (5-Aminolevulinic acid; Gliolan) which is taken by the patient preoperatively to cause fluorescence of GB tissue when exposed to 405-nm wavelength blue light. Fluorescence is due to uptake of drug through the blood-brain-barrier (BBB) and into glioma cells where it is converted into protoporphyrin IX (fluorescent metabolite). The exact mechanism that leads to fluorescence has not been confirmed, but some hypotheses include low levels of ferrochelatase, high levels of metabolism, or disturbances in mitochondrial electron transport changes leading to accumulation of reactive oxygen species and ultimately reduction in heme synthesis (133-135). Regardless of the mechanism of action of 5-ALA, fluorescence-guided surgical sampling has also been important for studies on ITH as it aids in the collection of better-quality, spatially distinct tissue for downstream experimentation (110,136).

Another important benefit of surgical resection is the improved response to adjuvant therapy experienced by patients who undergo resection, particularly gross total resection. This benefit is evident for multiple modalities of therapy including radiotherapy after 5-ALA resection, temozolomide, standard chemoradiotherapy, and BCNU wafers (137). As seen with BCNU wafers, surgery also provides the opportunity to add therapies directly to the tumour cavity to treat GB locally and immediately after surgery, which will be discussed in more detail in Section 1.2.4. The cytoreductive results of maximal, safe surgical resection thus provide many benefits to the GB patient and should be included in first line GB treatment regimens whenever possible.

After recovery from surgery, typically 3-4 weeks, patients undergo conformal external-beam radiotherapy (discussed in Section 1.2.5) with concomitant daily temozolomide (75mg/m^2/d). After 6 weeks of combined treatment, patients will continue adjuvant temozolomide (150-200 mg/m^2/d) for 1 week per month for six monthly cycles. Except for occasional nausea/vomiting and myelosuppression, which is monitored by serial blood counts, TMZ is usually well tolerated. Many patients who experience myelosuppression are able to continue taking TMZ at a reduced dose. While many chemotherapies have been studied for survival benefit with GB (138), TMZ has emerged as the current standard chemotherapeutic agent due to demonstrated improvement in median survival when coupled with RT compared to RT alone (122). This benefit was confirmed in both the 2-year and 5-year survival follow-up (139), thus solidifying the use of TMZ for first line GB treatment with radiotherapy.

Many clinical trials have tested various alternative strategies for treating GB. In an effort to treat the disease by inhibiting a fundamental aspect of its biology, a monoclonal antibody (Bevacizumab) was developed to inhibit VEGF-A (140). Because GB is a highly vascular and quickly expanding tumour, angiogenesis inhibitors represent an attractive strategy to combat this biological feature and deprive the tumour of a potential mechanism of obtaining needed resources. The safety of bevacizumab was first established for recurrent GB. After successful phase II trials which demonstrated clinical activity, increased 6-month PFS compared to other recurrent treatment modalities, and decreased steroid doses required to control oedema, the FDA approved it for recurrent GB in 2009 (141-143). After its testing with recurrent GB, bevacizumab was then added to the Stupp protocol for newly diagnosed GB. Unfortunately, the results were even less clear than for recurrent GB, as the results from two randomised, double-blind, placebo-controlled phase III trials demonstrated only minor improvements in PFS and no change in median OS when comparing bevacizumab to placebo controls (144,145). Because bevacizumab can disrupt contrast-enhancement, pseudoresponses are common in which a tumour may appear to be stable radiologically even if the tumour is really growing. Such a phenomenon could explain why PFS was extended but not OS. Therefore, it seems that bevacizumab may not provide much clinical benefit for newly diagnosed GB. The lack of clinical utility coupled with an increased number of observed complications and severe adverse events in the bevacizumab group has limited its use.

Immunotherapies are becoming another popular method to inhibit a fundamental characteristic of GB; in this case immune evasion (146,147). The brain, due to the restrictions of the blood brain barrier, is not as easily accessible for immune cells as other parts of the body.

However, microglia within the brain are capable of immune responses (148) and bone marrow-derived macrophages can get recruited to brain tumours, particularly when the BBB becomes leaky or disrupted during tumour progression or treatment (149). Also, tumour-associated macrophages (TAMs) have been found in high grade gliomas and have been attributed to immunosuppressive phenotypes via STAT3 signaling (150). While there have been many efforts to more effectively harness intrinsic antitumour responses and to reduce the tumour's ability to evade the immune system, to date, immunotherapies against GB have not been extremely successful. A recent phase III trial (CheckMate-143) of nivolumab, a PD-1 checkpoint inhibitor, sought to inhibit the ability of GB to trigger immune suppression. PD-1 is expressed on activated T cells that secrete IFN-γ, but PD-1 receptor expression also leads to increased PD-L1 expression and resulting interaction on surrounding cells which triggers an inhibitory feedback loop to suppress T cell proliferation and enhance T regulatory cell development (151). The CheckMate-143 trial was stopped after interim analysis as nivolumab did not improve median OS over bevacizumab for recurrent GB patients (152). A phase II study of pembrolizumab, another PD-1 inhibitor, treated recurrent GB patients with pembrolizumab with or without bevacizumab and compared findings to historical controls of recurrent GBs treated with bevacizumab alone. The study found that pembrolizumab alone did not significantly contribute to an increase in median OS, further suggesting that checkpoint inhibitors may have limited activity as monotherapies (153). Many trials are ongoing which pair checkpoint inhibitors with various other forms of therapy in an effort to enhance clinical and immune responses.

There have also been several attempts at producing effective vaccines against GB. Rindopepimut, a peptide vaccine against EGFRvIII, showed promise in early clinical trials and in combination with bevacizumab. However, a phase III trial of the vaccine was halted at interim analysis due to a lack of OS benefit (154,155). Dendritic cell (DC) vaccines pulse a patient's own monocyte-differentiated dendritic cells with tumour antigens or resection lysates for delivery back into the patient to generate tumour-specific effector cells and immune response. A phase II trial for tumour lysate-pulsed DC vaccines demonstrated enhanced cytokine response in "vaccine responders" who had longer times to tumour progression and survival compared to nonresponders. Compared to patients who received chemotherapy only, both responders and nonresponders experienced longer survival when chemotherapy was added after vaccination, although higher fold responders experienced increased time to tumour progression after the addition of chemotherapy (156). While several phase I and II trials

demonstrate the safety and potential utility of DC vaccines, randomized control trials are necessary to establish clinical efficacy (157). In addition, subsets of responders and nonresponders need to be studied and compared in more detail to better understand the diverse mechanisms of immune evasion. Other strategies include viral vaccines, oncolytic viral therapy, and CAR-T cell therapy. Viral vaccines provide the opportunity for gene therapy centered around directly killing the cell or activating the immune system, and an early phase I trial established the safety and tolerability of adenovirus transduction of herpes simplex virus thymidine kinase with subsequent ganciclovir treatment (158,159). Oncolytic viral therapies lead to viral replication in tumour cells and subsequent lytic cell destruction. A phase I dose-finding and toxicity study of convection-enhanced, intratumoral delivery of poliovirus demonstrated a 21% overall survival rate at 24 and 36 months compared to 14 and 4%, respectively for historical controls (160). CAR-T cell therapy relies on the modification of T cells to target tumours based on selected antigens and then cause lytic killing of the identified tumour cells (161,162). However, CAR-T cell therapy is associated with high risk toxicities such as Cytokine-release syndrome and CAR-T-cell-related encephalopathy syndrome, and therefore requires intensive monitoring and patient workups. While many of these new treatment modalities are interesting, again, randomized control trials will ultimately be required to establish clinical efficacy. Several of these studies have produced a small subset of long-term survivors, similar to the standard of care Stupp protocol which provides a 2 and 5-year overall survival rate of around 10% and 5%, respectively. For younger or IDH mutant patients, the percentage of long-term survivors is higher. While a small subset of long-term survivors may not point towards significant clinical benefits, the underlying biology and characteristics of these long-term survivors need to be better understood so that future patients could potentially be stratified and treated based on their predicted response. This is especially important due to the potential significant toxicities associated with some of these modalities. As the difficulties with translating immunotherapies into clinical benefit makes clear, a better understanding of both primary and recurrent GB biology, the immune response, and the microenvironment is needed in order to improve combinatorial therapeutics for GB. These approaches must also take into account possible methods of GB resistance and evasion.

1.2.4 Local Delivery Strategies

One strategy for improving therapy is through bypassing the blood brain barrier. After resection, chemotherapeutics or other targeted modalities can be delivered directly to the tumour cavity for local treatment of residual disease. Local delivery also provides treatment in a therapeutic window of opportunity: the weeks during recovery from surgery in which patients currently receive no form of anti-neoplastic therapy. Many chemotherapeutic drugs have shown efficacy against GB cells in vitro or in vivo, but when translated to the clinic they do not display the same efficacy. It is hypothesised that one factor contributing to this lack of clinical efficacy may be the BBB preventing certain chemotherapies and other systemic drugs from entering the brain at high enough concentrations to produce an observable clinical effect. Thus, there are potentially many drugs and combinations of drugs which could be repurposed for GB if the BBB could be successfully and efficaciously circumvented (163).

Gliadel is a technology that bypasses the BBB by implanting carmustine-loaded, rigid polymer wafers into the cavity after GB resection. Like Bevacizumab, Gliadel is also one of the few therapies to have been FDA-approved for treatment of newly diagnosed and recurrent malignant gliomas in recent years. The wafers allow drug diffusion at higher than systemic concentrations over a period of several weeks to the tissue surrounding the cavity which contains residual cells. However, the utility of Gliadel has been controversial. While initial studies in recurrent GB demonstrated an advantage in median OS and 6-month survival for Gliadel versus placebo controls (164), trial results in newly diagnosed GB are less clear. A large phase III trial of 240 patients demonstrated an increased OS (13.9 months versus 11.6 months) for Gliadel with radiotherapy compared with placebo and radiotherapy (165). However, subgroup analysis revealed the GB subgroup did not experience a statistically significant survival advantage and that incidence of CSF leak and intracranial hypertension were elevated with Gliadel. A more recent trial which examined Gliadel implant after 5-ALA guided resection (14.2 months) showed no survival benefit over 5-ALA resection alone (14.3 months) and demonstrated an increased incidence of wound infection in the wafer group (166). Even though a single institutional study found no difference in perioperative morbidity after Gliadel wafer treatment (167), the potential for side effects shown in other studies coupled with the little to no increase in survival benefit, has limited the clinical adoption of this local delivery strategy (168). A potential cause of its limited clinical performance is the stiffness of the polymer which seems to make it difficult to achieve optimal tissue apposition and controlled

drug diffusion. The Melville Laboratory for Polymer synthesis has developed a hyaluronic acid-based hydrogel delivery system for the treatment of GB that avoids the pitfalls mentioned for Gliadel (169,170). These hydrogels represent a new avenue for local delivery of chemotherapeutics, radiosensitisers, and other drugs, and will be discussed in more detail in Appendix A.

1.2.5 The Role of Radiation for Glioblastoma

Because most GBs recur within 2 centimetres of the original tumour site (171-173), radiation of the tumour bed and the immediately surrounding tissue has been a major part of GB therapy for many years. Fractionated radiotherapy (3D conformal RT) up to 60Gy is the gold standard for treating newly diagnosed GB after resection as it has been shown to provide significant survival benefit alone (174,175) and an additive survival benefit when in combination with TMZ (139,176). RTOG guidelines for target volume delineation involve treating the FLAIR signal hyperintensity with a cone-down boost to the T1 MRI Contrast-enhancing region with a 2-cm expansion around the tumour region (177). In a phase III trial comparing standard TMZ with dose-dense TMZ for newly diagnosed GB, either RTOG or EORTC (more conservative target volume delineation that does not include oedema) guidelines were allowed for radiotherapy planning. Cox modeling demonstrated that the choice of radiation technique was not a significant predictor of overall survival in this trial (178,179), suggesting comparable outcomes between the guidelines. While randomized studies are needed to definitively compare efficacy between the two, use of the EORTC guidelines is associated with smaller irradiated normal brain volumes without an increase in recurrences at the margin (180). Importantly, intensity-modulated RT allows radiation oncologists to provide the prescribed RT dose while limiting radiation exposure to important neuroanatomical structures (brainstem, optic nerves, optic chiasm) (181-183). While hyperfractionation (184,185) and accelerated fractionation (186) protocols have undergone clinical testing, these regimens have shown no survival benefit or only similar benefit to standard fractionation, respectively, thus limiting their use in the context of GB. Interestingly, abbreviated (short course) RT protocols have shown clinical benefit by increasing survival and reducing risk for treatment of newly diagnosed GB in the elderly and patients with a poor performance status (187,188).

Other radiotherapy modalities have been examined for their potential to improve survival by providing boosts of radiation in addition to standard fractionation. Interstitial brachytherapy with iodine-125 failed to demonstrate a statistically significant increase in survival when compared with standard RT (189,190). Stereotactic radiosurgery (SRS) uses either a cobalt source (Gamma Knife) or a linear photon accelerator (LINAC) to achieve large doses of RT in the tumour volume while sparing the surrounding tissue. When SRS was coupled with fractionated radiotherapy for newly diagnosed GB, no survival benefit was attained. This lack of clinical improvement was consistent regardless of whether SRS occurred concurrently with fractionated RT (+/- chemotherapy) (191,192) or after fractionated RT (193). Thus far, SRS has been shown to have the most clinical utility for small, recurrent GB (194).

Despite standard of care treatment and many other experimental therapies, GB inevitably recurs which raises the issue of trying to identify the best recurrent treatment strategy. While there is not a consensus for best recurrent therapy regimen, and indeed such regimens may need to be individualized based on tumour volume, tumour location, patient performance status, and other factors, several institutions are testing reirradiation protocols to control tumour growth (clinicaltrails.gov). Early reports signal that fractionated reirradiation protocols may be a safe and effective tool for increasing PFS and OS for recurrent GB, but randomised controlled trials are needed to establish a clear clinical benefit (195-197). In addition to the utility of SRS for small, recurrent lesions, pulse-reduced dose rate RT may also be a beneficial way to provide reirradiation therapy while potentially reducing the risks of radiation retreatment (198).

An attractive method for improving a tumour's response to radiation both in the primary and recurrent setting, is the use of radiosensitisers (199). Historically, hypoxic cell sensitisers and halogenated pyrimidines were utilised to selectively isolate and sensitize hypoxic and rapidly proliferating tumours cells to RT, but these methods proved ineffective. More recently, targeted approaches which seek to exploit intracellular signaling pathways, particularly DNA repair mechanisms, have been developed. A few methods of improving radiosensitivity of GSCs (thought to be more radioresistant than other tumour cells) include, inhibition of HDAC (200), inhibition of mTORC1/mTORC2 (201), inhibition of ATM kinase (202), PARP inhibition (203,204), and inhibition of a combination of cell cycle checkpoint and DNA repair targets (205,206). A targeted, multimodal approach is also being explored through the use of cisplatin-infused gold nanoparticles in conjunction with RT (207). While there are many potential radiosensitisers available (208), selecting appropriate radiosensitisers based on a

more thorough understanding of radiation-induced GB evolution and underlying GB biology will no doubt lead to better sensitisation and response to radiotherapy.

1.3 Glioblastoma Evolution

The intratumoral heterogeneity of glioblastoma yields brain tumours with such a variety of genotypic and phenotypic cell populations that a given tumour may harbour subclones that are resistant to standard of care or experimental treatments even prior to undergoing such treatments. Yet the process of GB evolution becomes even more difficult and dynamic as we know that GB can also evolve not only in response to therapeutic challenge, but also in response to other selective pressures. The investigation of GB evolution after exposure to various selection pressures is important for understanding underlying GB biology and resistance mechanisms which have implications for developing more effective, better targeted therapeutics for recurrent disease.

1.3.1 Primary versus Recurrent Tumours

A common approach to examining cancer evolution is to compare genomic architectures between primary and recurrent tumours. By examining changes in genetic alterations, scientists can speculate on the relative effects of time, microenvironment, and treatment. Several studies have provided relatively large cohort analyses of whole-exome (WES) and whole-genome (WGS) sequencing of primary and recurrent patient-matched samples. Kim et al. found through TCGA genomic analysis and WES of matched tumours that TP53 mutations were strongly associated with an increase in subclonal mutations, including an increase in prevalence of G-CIMP methylation phenotype (209). Thus, the detected TP53 mutations could suggest a susceptibility to apoptosis suppression or increased DNA damage tolerance after treatment. Furthermore, WGS of 10 matched patient samples demonstrated two patterns of evolution: linear and divergent. Linear evolution, or clonal evolution, occurs when dominant clones present in primary tumours directly lead to regrowth of recurrent tumours

such that there are many shared mutations in addition to newly accumulated variants. Divergent evolution, or ancestral origin evolution, occurs when the recurrent tumour regrows from an "ancestral" clone that split early from the primary tumour's more dominant clones. When the dominant clones are removed by treatment, the ancestral clone which has accumulated many new mutations over time repopulates the tumour such that the primary and recurrent mutation patterns are quite different. Genomic analyses including WES, RNA-Seq, and array-comparative genomic hybridisation of 38 GB patients reveal that tumours that recurred distally were more likely to exhibit a branched (divergent) evolutionary pattern, with divergence in GB driver genes between paired tumours (210). This study also demonstrated that TMZ-induced hypermutation was rarely associated with IDH-wildtype primary tumours, suggesting that a GB's evolutionary history is affected by the complex interplay of baseline mutational architecture, early behaviour of heterogenous tumour cells, interaction with the microenvironment, and therapeutic selection pressures.

Similar results were found by Lee et al. through interrogation of multisector and longitudinal samples from 52 GB patients. Tumour fragments that were spatially proximal demonstrated more similarities in mutation and expression signatures, while distal foci and recurrences separated by longer periods of time were thought to have been seeded by distinct early clones reflecting a divergent pattern (115). The genomic similarity amongst spatially local fragments also corresponded to similar drug responses as cell lines derived from local samples exhibited similar responses to screened compounds while distant and longitudinal samples exhibited more diverse responses. These results from relatively large matched cohorts suggest that spatial and temporal proximity may have a correlation with genomic similarity, especially relative to distally and longitudinally separated recurrences. However, as previously discussed, fragments from the same tumour and even cells within the same fragment can display a large amount of ITH. Indeed, slightly conflicting results were found through the analysis of genetic alterations and COSMIC mutational signatures (211,212) of 10 presumably local recurrences (213). In this study, differences in genetic alterations were found between all paired samples, even in one case in which no intervention occurred between surgeries for the two recurrences, suggesting that both treatment and time (including interactions with the microenvironment) can lead to changes in genetic alteration patterns in locally recurrent tumours. It was also noted that even among the genetic similarities between paired tumours, the percent reads for given mutations varied widely, suggesting subclonal/clonal expansion and contraction.

Studies of paired primary and recurrent tumours demonstrate both the extensive ITH of GB and the evolutionary dynamics at work during disease progression. Therefore, longitudinal analysis of GB evolution must become a common feature of GB research, clinical evaluation, and treatment decisions. This priority is evidenced by the ongoing work of the Glioma Longitudinal Analysis Consortium (GLASS) which seeks to better understand the cellular and molecular changes involved in GB evolution in an effort to improve treatments and outcomes (214). While such longitudinal studies provide better insight into GB evolution and represent an improvement in GB genomic investigation from initial TCGA studies (based mostly on single biopsies of primary tumours), they still represent single snapshots in time of primary and recurrent tumours. Recent advances in liquid biopsies for GB provide the potential to incorporate more frequent disease interrogation for improved, up-to-date monitoring of patient response to targeted treatments (215-218). Therefore, liquid biopsies may provide an avenue for treatment improvements based on a better understanding of GB evolution and the selective pressures which drive that evolution for individual patients. Liquid biopsies provide an easier method for more frequent, longitudinal monitoring of tumour burden, treatment response, and clonal evolution. It provides the opportunity to examine whether treatments have led to resistance or even whether new susceptibilities may have arisen after a given treatment regimen. Liquid biopsies would prevent the risks associated with multiple surgical biopsies and could potentially capture more holistic genomic and transcriptomic profiles of the tumour than a focal biopsy. Furthermore, the ease and relative safety of longitudinal tumour response monitoring will allow for easier testing of targeted therapeutics in clinical trials. While more studies will need to be completed to optimize liquid biopsy protocols to make them more reproducible across studies, to pinpoint potentially useful biomarkers to correlate with response and prognosis, and to detect important evolutionary branch points to suggest initiation of matched target therapies, it seems clear that liquid biopsies could prove to be a very valuable tool for expanding personalized medicine options for GB patients.

1.3.2 Microenvironment as a Source of Selective Pressure

There are many potential sources of selective pressure that may contribute to GB evolution. The tumour microenvironment (TME) represents a complex source of non-tumour cells which interact with glioma cells and can influence glioma growth and evolution. Immune

cells, particularly microglia and macrophages (TAMs), are recruited to tumour sites and have been shown to influence GB growth and invasion (219). Reduction in the number of microglia has been shown to reduce in vivo glioma growth (220,221), which could be a function of the loss of supportive factors released from microglia such as EGF, STI1, IL-6, and TGF-β which stimulate proliferation, migration, and invasion (222-225). TAMs have also been implicated in glioma growth through their involvement in promoting angiogenesis via RAGE (receptor for advanced glycation end product) and VEGF signalling (226). An increased amount of TAM infiltration has been correlated with the mesenchymal transcriptional subtype and the transition from proneural to mesenchymal subtype has been correlated with activation of the NF-κB pathway (227). Such enrichment of immune cells in mesenchymal subtype GBs was corroborated through in silico cell sorting (CIBERSORT) experiments of TCGA data (228), further supporting the close interaction and mutual influence of GB expression and supportive TAMs in the microenvironment.

In addition to immune cells, GB is also influenced by resident astrocytes in the TME. In vitro experiments proved that astrocytes can enhance invasion and reduce radiosensitivity of GSCs (229,230). Activation of the JAK/STAT pathway of reactive astrocytes can lead to release of anti-inflammatory cytokines which promote unhindered GB growth through immunosuppression (231). Endothelial cells and other stromal cells may also play a role in the microenvironmental regulation of GB. Tumour cell niches have been described in the TME as locations in which cancer stem cells can directly contact, interact and communicate with non-neoplastic cells to promote tumour growth and survival. The perivascular niche, vascular-invasive niche, and hypoxic niche have been described and associated with angiogenesis, migration, and necrosis, respectively (232). The complex interactions of GB cells with the TME are important to assess, not only because of their direct impact on evolution, but also because the TME provides the in-situ context in which residual GB cells undergo treatment.

1.3.3 Therapy-induced Evolution

Therapeutic selection pressures are potentially some of the strongest drivers of evolution. A landmark study by Johnson et al. demonstrated chemotherapy-induced evolution as 6 out of 10 low-grade glioma that underwent alkylating chemotherapy with TMZ were found to be hypermutated when they recurred as high-grade glioma. The recurrent tumours displayed

acquisition of driver mutations in core GB pathways as a result of the hypermutator phenotype and its associated susceptibility to acquiring new mutations. Not only are low-grade glioma at risk of hypermutation after alkylating chemotherapy, but GB itself is susceptible to such evolution. It is estimated that around 50% of low-grade glioma that undergo malignant transformation and up to 20% of recurrent GBs express the hypermutator phenotype (233,234). Recurrent GBs have been shown to express the hypermutator phenotype in the context of MGMT promoter methylation and MSH2/6 mutation which increase susceptibility to DNA damage by TMZ and decrease a cell's ability to properly respond to such damage, respectively (Figure 1.4) (90,91). Such studies imply that chemotherapy drives evolution leading to the emergence of resistant clones. Consistent with studies of clinical specimens, temozolomide treatment of mice bearing brain tumour xenografts initiated from GB primary cultures also suggested the expansion of drug resistant clones (235).

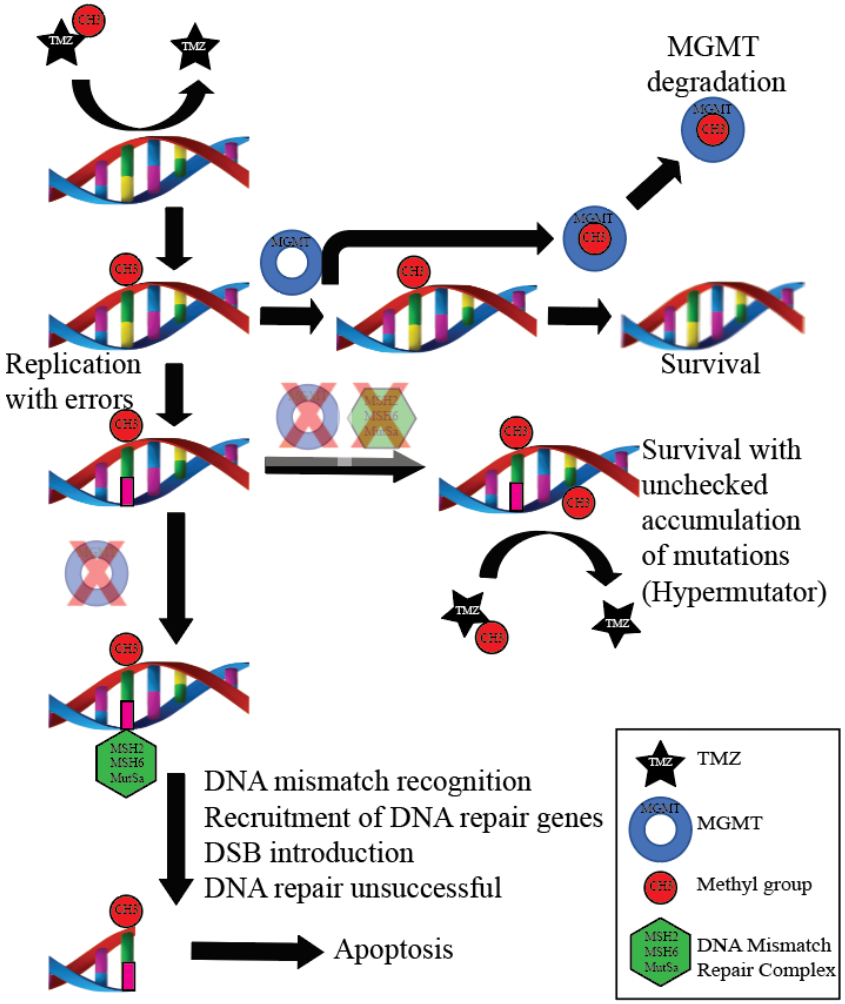

Figure 1.4 TMZ-induced evolution. Temozolomide alkylates tumour cell DNA. MGMT can remove alkyl groups from DNA and allow tumour cells to evade cell death. If MGMT promoter methylation is present, then MGMT does not function properly. In this case, the

DNA Mismatch repair complex MSH6-MSH2 can detect incorrect base pairing caused by replication after alkylation damage. Ultimately, DSBs are induced and cells undergo apoptosis after futile cycles of replication. However, if loss of function mutations in MMR genes are coupled with nonfunctional MGMT, then alkylation and C>T and G>A transitions will accumulate. This leads to survival of cancer cells with unchecked mutation accumulation resulting in the hypermutator phenotype.

While TMZ-induced hypermutator phenotype GBs can acquire a high number of new mutations following treatment, therapy can also lead to reduction of clonal diversity and selection of pre-existent clones. Targeted deep sequencing of 21 patients revealed that clonal diversity (variant burden) was reduced in non-hypermutated recurrent tumours, suggesting the selection of variants after treatment (236). Similar results were found by examining the branched evolutionary patterns of 114 patients after recurrence (237). Evolutionary rate models predicted that many recurrences emerged through the growth of clones that were present many years before diagnosis. These early clones had convergently gained "clonal replacement" mutations in key driver genes. Such results further support the removal of clonal populations prevalent in primary disease after treatment and subsequent selection and proliferation of early branching subclones to repopulate recurrent disease.

Treatment-induced evolution has implications not just for the therapeutic modalities which potentially induced the evolution but can also impact sensitivities to other targets. Longitudinal analysis of GB samples demonstrated a discordance between primary and recurrent tumours in 90% of the druggable targets tested after standard chemoradiotherapy (238), further supporting the concept that molecular analysis at initial diagnosis is not enough to capture the ITH of GB, particularly after treatment driven evolution. Indeed, while a study of the impact of standard of care treatment on 186 pairs of primary-recurrent GB found that approximately 80% of cancer gene mutations were stable at recurrence, many variants did demonstrate a change in status in subsets of patients (239). EGFR, a commonly targeted RTK, was one of the least stable mutations. In particular, 37% of patients with EGFRvIII in the primary tumour lost expression at recurrence, similar to a previous study (240), which implies that certain recurrent tumours need to be re-resected/re-biopsied in order to confirm mutation status of relevant variants with implications for precision medicine clinical trial inclusion. Several of the above studies have investigated the role of chemotherapy in GB evolution. However, despite the inclusion of radiotherapy in virtually all GB treatment regimens, little consideration has been given to the contribution of radiotherapy alone to GB evolution. In

order to assess the potential of radiation to drive evolution, a clinically and biologically relevant model is needed.

1.4 A Model for Studying Radiation-induced Evolution

Because glioblastoma is an evolutionary dynamic, genotypically diverse, and phenotypically heterogenous tumour, it presents a difficult challenge for researchers. Accurate models of this disease must be able to not only capture the underlying heterogeneity of the cancer, but also be able to recapitulate many of its histological, phenotypic, and clinical features. In the context of evolution, a cancer model is arguably most useful when it demonstrates a measured degree of treatment response (non-curative) followed by eventual progression and recurrence. Such a GB model would not only mimic the clinical course of the disease but would provide the opportunity to compare primary and recurrent tumours and the evolutionary processes that connect them. Glioblastoma stem-like cells (GSC) provide such a model.

1.4.1 Glioblastoma Stem-like Cells

Glioblastoma-stem like cells isolated from human GB surgical samples either through derivation and propagation in serum free, EGF/FGF-containing media (241) or through isolation of $CD133^+$ cells (242) were found to exhibit many of the same properties as adult somatic stem cells (243). Specifically, GSCs are undifferentiated cells with the ability to generate a heterogeneous population of fate-restricted cells, GSCs have the ability to self-renew, and perhaps most importantly, GSCs (sometimes called tumour-initiating cells) have the ability to initiate tumours (244). GSCs have also been implicated in treatment response, both chemoresistance and radioresistance (245,246), which may have implications for GB evolution and recurrence and also suggests their potential application for initial radiotherapy and drug response screening (247).

CD133 is thought to be one of several potential stem cell markers which can enrich for a clonogenic subpopulation of GSCs (244). Definitive markers of GB and GSCs are controversial because marker expression is known to fluctuate and some studies have demonstrated that cell populations lacking marker expression (CD133 or NG2) can sometimes still initiate proliferative tumours (248,249). Such results could indicate that self-renewal and tumour initiation capabilities may not be restricted to specific GSC populations. However, while CD133 sorting may not fully capture the genotypic and phenotypic heterogeneity of GSCs (136,250,251), it does provide a more uniform population of clonogenic cells with which to perform in vivo studies.

1.4.2 GSC-initiated in vivo Models of Glioblastoma

One of the shared, defining features of GSCs is the ability to produce tumours upon orthotopic implantation. Importantly, GSC-initiated orthotopic xenografts have been shown to replicate the genotype, phenotype and in vivo growth patterns of GB (252). While some GSCs are diffusely invasive and may serve as better models for glioma infiltration, others form discrete nodular and vascular masses and may serve as better models of tumour-associated angiogenesis (253). With respect to GB evolution, we have previously shown that after the initial implant of 100% CD133+ GSCs, xenografts at the time of morbidity are comprised of a variety of cell subpopulations including those expressing GFAP or βIII tubulin (254). This is consistent with tumour cells that have differentiated, at least partially, along astrocytic and neuronal pathways, respectively. In addition, there continued to be a small subpopulation (approximately 10%) of tumour cells expressing CD133, suggesting the enduring presence of GSCs.

GSCs isolated from paired surgical samples provide evidence for both linear and branched evolutionary patterns. GSCs were found to both accumulate mutations as a result of TMZ or to undergo positive selection in which a primary subclone (TP53 at low frequency prior to treatment) was positively selected and expanded to populate the recurrent tumour (255). Furthermore, GSCs isolated from a patient's tumour prior to and after EGFR-targeted therapy led to xenografts which recapitulated the disease genotype and phenotype (256). In particular, EGFR amplification seen in the initial tumour/xenografts was lost in the recurrent tumour/xenograft. In addition to demonstrating similar cell populations, the GSCs from the

initial tumour were found to be more proliferative in vivo and more sensitive to EGFR inhibition in vitro. A potential next step would be to treat the initial tumour-derived xenograft with EGFR inhibitor to determine if a recurrent tumour would regrow in vivo which mirrors the clinical outcomes and genotype/phenotype seen in the recurrent tumour-derived xenografts. In this regard, GSC-initiated orthotopic xenografts have already demonstrated efficacy as models of therapy-driven evolution. In a study by Chen et al., a Nestin-RTK-GFP transgene was utilised to label a subset of endogenous, quiescent GSCs. This labelled subset was found to regrow the tumour in a hierarchical fashion after treatment with TMZ initially caused arrest of proliferation (257). Chronic ganciclovir treatment, used to target GFP+ cells, led to tumour growth arrest, suggesting that the labelled glioma stem cell-like population was involved with treatment resistance, tumour cell proliferation and growth of recurrent tumours (257).

1.4.3 The Brain Tumour Microenvironment and Response to Radiation

Another reason that GSC-initiated xenografts closely replicate GB in situ is the interaction of GSCs with the brain tumour microenvironment. Many adult neural stem cells reside in neurogenic parts of the brain, including the subventricular zone of the lateral ventricles and the subgranular zone within the hippocampal dentate gyrus (258). Glioma stem-like cells have also been found to reside in such niches leading to the question of whether GSCs invade into or out of these areas during early tumourigenesis (259,260). In addition, integrin α6 has been identified as a possible GSC marker and its role as a receptor for the extracellular matrix protein laminin highlights the importance of microenvironmental interactions for GSC function and development (261). GSCs are not only influenced by the microenvironment but can also shape the microenvironment in return. This influence has been particularly evident regarding tumour vasculature. For example, GSCs have been shown to secrete high levels of VEGF which may induce angiogenesis (262). Further evidence suggests that GSCs may even transdifferentiate into vascular endothelial cells (263,264) as CD31+ endothelial cells were found to harbour GB-specific mutations (265). While such findings are controversial and warrant corroboration, they do present an interesting example of GSC-induced changes in the microenvironment.

To study the possible responses to radiotherapy in terms of evolution and therapeutic consequences, the GSC-derived xenograft model must also display ITH with respect to cellular

phenotype and radioresponse. Such ITH was demonstrated through analysis of γH2AX and 53BP1 foci induction and dispersal in GSC xenografts. Even though $CD133^+$ stems cells and $CD133^-$ differentiated cells have similar radiosensitivity in vitro, when irradiated as orthotopic xenografts $CD133^+$ cells were less radiosensitive than $CD133^-$ tumour cells (266). In vivo GSCs were less susceptible to foci induction, showed an increase in expression of genes related to reactive oxygen species, and experienced an increase in relative cell percentage after radiation (266). The microenvironment has also been shown to play a significant role in this radioresponse as tumour cells grown as orthotopic xenografts were able to more quickly disperse γH2AX foci following radiation therapy compared to cells grown in vitro (254). GSC-initiated xenografts exhibit the intratumour heterogeneity, microenvironmental interactions, and evolutionary dynamics necessary to simulate that of a GB in situ, thus providing a useful model for the study of radiation-induced GB evolution.

Chapter 2. Aims and Hypotheses

2.1 Aims

The extensive intratumoral heterogeneity of glioblastoma renders it susceptible to evolution when exposed to selective pressures. Such pressures as imposed by the tumour microenvironment and therapeutic regimens can lead to the expansion or contraction of various subclones depending on the relative fitness of each subclone as determined by its sensitivity to a given challenge. For example, a certain drug could remove all sensitive clones and thus provide the opportunity for resistant clones to expand quickly to grow a recurrent tumour due to competitive release. In this way, selective pressures drive evolution and contribute to tumour recurrence, progression, and treatment failure. While the role of chemotherapy in treatment-induced evolution has been studied, the impact of radiotherapy alone on glioblastoma evolution has not been determined.

As outlined in this thesis, I will endeavor to describe the effect of ITH on intrinsic radiosensitivity to determine whether spatially distinct regions of the same tumour may have different sensitivities. Then I will discuss whether radiation alone can drive the evolution of GSC-initiated orthotopic xenografts and whether it leads to the emergence of resistant subclones. In this context, the GSC-initiated xenograft model will also be proposed as a potential model system for studying recurrent GB and reirradiation protocols. Finally, I will report on biocompatibility and efficacy studies for a new hydrogel delivery system, which could provide immediate and local delivery of targeted combinatorial therapeutics, including radiosensitisers. Ultimately, by better characterizing the impact of radiation on glioblastoma evolution and by studying recurrent GB and retreatment strategies, we can harness insights related to recurrent glioblastoma biology and radiation biology for the production of more effective systemic and local therapies to improve outcomes for glioblastoma patients. With this thesis, I would like to answer the following questions: (1) Does ITH translate into differences in intrinsic radiosensitivities between patient-derived cell lines derived from distinct tumour fragments? (2) Does radiation alone drive glioblastoma evolution? (3) If radiation drives glioblastoma evolution, does it lead to the emergence of radioresistant clones? (4) Can the GSC-initiated xenograft model be used to study recurrent GB treatment strategies? (5) Are hyaluronic acid-based hydrogels biocompatible and effective at local drug delivery?

2.2 Hypotheses

(1) Does ITH translate into differences in intrinsic radiosensitivities between patient-derived cell lines derived from distinct tumour fragments?

Hypothesis: I hypothesised that patient-derived cell lines derived from spatially distinct tumour fragments would display intratumoral heterogeneity. Furthermore, I hypothesised that the heterogeneity between cell lines would extend to radioresponse such that different cell lines from the same tumour would display different intrinsic radiosensitivities.

After deriving cell lines from multiple spatially distinct tumour fragments from several patients, we examined differences in radioresponse through standard radiation biology techniques. Similarities or differences in radioresponse and extent of ITH were further interrogated through genomic analysis of these patient-derived cell lines and their corresponding tumour samples. If there are major differences in radioresponse and genetic alterations between cell lines derived from distinct regions of the same tumour, then it would suggest that multiple therapeutic targets are needed for holistic treatment of GB.

(2) Does radiation alone drive glioblastoma evolution?

Hypothesis: I hypothesised that, similar to other therapeutic modalities, radiation is capable of providing selective pressure sufficient to drive glioblastoma evolution.

GSC-initiated orthotopic xenograft models treated with fractionated radiotherapy were utilised to examine the survival, phenotypic, and genomic consequences of radiation. Due to the variability in tumour growth patterns and inconsistency in growth rates of the patient-derived cell lines utilised for Aim 1, those lines were deemed inappropriate for examining the effects of a therapeutic challenge. Therefore, GSC lines which have previously been shown to provide reproducible in vivo tumours with consistent radioresponse were selected for the study of radiation-induced evolution. Morphologic and histological analysis characterised potential

changes in recurrent GB biology. Viral integration site analysis (VISA) examined the impact of radiation on clonal diversity, while WES highlighted any changes in mutation patterns of GSC-initiated tumours before and after treatment with radiation. These measures were employed to provide evidence for radiation-driven GB evolution.

(3) If radiation drives glioblastoma evolution, does it lead to the emergence of radioresistant clones?

Hypothesis: As mentioned above, I predicted that radiation drives glioblastoma evolution. Furthermore, I hypothesised that such radiation-induced evolution would lead to the emergence of resistant clones which would contribute to the regrowth of a radioresistant recurrent tumour.

GSC-initiated orthotopic xenograft models were again applied to study the functional implications of possible radiation-induced evolution. Tumour cells were isolated from morbid control and irradiated tumours and were put back into culture. These xenograft-derived cell lines were subsequently tested for evidence of differential radioresponse through clonogenic survival assays and a reimplantation survival study. Such studies may provide valuable information on the potential functional implications of radiation-induced GB evolution.

(4) Can the GSC-initiated xenograft model be used to study recurrent GB treatment strategies?

Hypothesis: I predicted that through regular in vivo tumour growth monitoring, GSC-initiated xenografts could serve as models of recurrent tumour growth and could be successfully reirradiated to provide a clinically relevant model of recurrence and retreatment.

GSC-initiated xenografts underwent a first course of fractionated radiation. After treatment, the irradiated mice were followed by serial imaging to monitor for tumour regrowth. Once regrowth was noted, the same fractionated radiation protocol was reapplied. Survival analysis was performed to determine the in vivo radioresponse of recurrent tumours after

reirradiation. Such studies may not only demonstrate whether such models would be useful for studying recurrent treatment regimens, but may also serve as a more clinically relevant approach for determining functional implications of radiation-induced evolution.

Chapter 3. Materials and Methods

The following represent general methodologies employed throughout the work included in this thesis. Study-specific methods are described in Chapters 4-6 and Appendix A.

3.1 Human glioblastoma sample collection

Human glioblastoma tissue was collected from patients that underwent 5-ALA fluorescence-guided surgical resection at Addenbrooke's Hospital at the University of Cambridge. Fluorescent tumour tissue was collected for diagnosis, storage as fresh frozen tissue by the Addenbrooke's tissue bank, and derivation of patient-derived cell lines. Matched whole blood samples were also collected. Informed consent for tissue and corresponding clinical data to be used for research purposes was obtained from all patients prior to surgery. Tissue collection protocols were compliant with the UK Human Tissue Act 2004 and approved by the Local Regional Ethics Committee (LREC ref. 04/Q0108/60).

3.2 Cell culture of glioblastoma cells

3.2.1 Derivation and propagation of patient-derived cell lines

Primary tumour samples were placed in specimen tubes and immediately placed on ice for transport to the human tissue fume hood. Under the fume hood, tumour fragments were minced with scalpels separately, transferred to a 50mL Falcon tube, and incubated at 37.5°C and 5% CO_2 for 45-90 minutes with 2-5 mL of Accutase (Gibco), depending on the size of the tumour sample, to degrade extracellular material. After incubation, HBSS (without Calcium and Magnesium, Gibco) was added to the suspension for dilution. The single cell suspension was then filtered through a 40 μm cell strainer to remove debris, endothelial/vascular cells, and extracellular material. The resulting single cell suspension was spun down at 1200 g for 5 minutes. The supernatant was carefully discarded and 1-3.5 mL red blood cell lysis buffer was added to resuspend the pellet depending on the size and suspected level of blood content of the

pellet. After 10 minutes of incubation at room temperature, cells were spun down again at 1200 g for 5 minutes. The supernatant was carefully discarded and then 10 mL of HBSS was added to resuspend and wash the pellet. Washing occurred 1-3 more times depending on the size of the pellet. After a final wash and spin, the supernatant was discarded and the pellet was resuspended in serum free medium (SFM; Neurobasal A (Invitrogen, UK) with 20 mM L-glutamine, 1% PSF solution, 20 ng/ml hEGF (Sigma, UK), 20 ng/ml hFGF (R&D systems, UK), 2% B27 (Invitrogen, UK) and 1% N2 (Invitrogen, UK)). Cells were counted with a hemocytometer and then plated with SFM at a density of approximately 100,000 cells per mL in 25 or 75 cm^2 cell culture flasks and placed in a 37.5°C, 5% CO_2 incubator.

After 7-10 days, cells began to form floating neurospheres. Once there were enough neurospheres of sufficient size to be viable, neurospheres were removed from flasks, spun down at 1200 g for 5 minutes, washed with HBSS, resuspended in SFM, and added to cell culture flasks that had been pre-coated with extracellular matrix (ECM; Sigma). Neurospheres then plated down forming an adherent monolayer of glioma cells that were maintained and utilised for future experiments. To passage adherent monolayer cultures, media was removed from flask and 2-4 mL of Accutase was added for 10 minutes in 37.5°C incubator. Around 4 mL of SFM was added to floating cells and suspension transferred to 15 ml Falcon tube. If needed, Accutase step was repeated to remove remaining cells from flask. Cells were then spun at 1200 g for 5 minutes, resuspended in HBSS and spun again. The supernatant was discarded and SFM was added. Cells could then be counted, re-plated, frozen down, or utilised as needed.

3.2.2 Freezing and thawing patient-derived cell lines

Depending on the growth rate of individual, patient-derived cell lines, lines were passaged every one to two weeks. Typically, with each passage, cells were counted using a hemocytometer and 500,000-1 million cells in SFM were added to freezing media (SFM with 10% DMSO) to a total volume of 1 mL. Lines were then frozen down in isopropanol freezing containers at -80°C before being transferred to liquid nitrogen for permanent storage.

Individual patient-derived cell lines were thawed and re-established when necessary. Cells were removed from -80°C freezer or liquid nitrogen storage and placed on dry ice. 15 mL Falcon tubes with 10 mL of SFM were prepared. Then, cryovials were thawed by holding

in gloved hands. Once thawed, cells were quickly transferred to SFM and spun down. Supernatant was discarded and cells were washed with SFM or HBSS 1-3 more times, depending on the size of the initial pellet. Finally, 10 mL of SFM was added to pellet and solution was placed in a 75 cm^2 culture flask and placed in a 37.5^oC, 5% CO_2 incubator. A few days later, cells were transferred to ECM-coated flasks.

3.2.3 Glioblastoma stem-like cells and other glioblastoma lines

GSC lines NSC11, NSC20, and NSC23 were isolated from three human GB surgical specimens and were kindly provided by Dr. Frederick Lang (MD Anderson Cancer Center). They were maintained as neurospheres in stem cell medium composed of DMEM/F-12 (Invitrogen), B27 supplement (Invitrogen), and human recombinant bFGF and EGF (50ng/ml each, R&D Systems) at 37^oC, 5% CO_2, and 5% O_2, as previously reported (267,268). FACS was utilised to sort for CD133+ cells from each culture. To prepare cells, TrypLe Express (Sigma) was utilised to generate single cell suspensions from neurospheres. After 30 seconds of exposure, defined trypsin inhibitor (Sigma) was added and neurospheres were disaggregated. After washing, single cell suspensions were labelled with anti-CD133 antibody (PE-conjugated, Miltenyi) and FACS sorted under sterile conditions. CD133+ GSCs were expanded and utilised for all experiments. The U251 human GB cell line was obtained from the Division of Cancer Treatment and Diagnosis Tumour Repository (DCTD), National Cancer Institute (NCI), grown in Dulbecco's Modified Eagle Medium (DMEM) supplemented with 10% FBS (Invitrogen), and maintained as adherent cultures at 37^oC, 5% CO_2.

GSC lines and U251 cells were cultured less than 2 months after resuscitation. Cell lines tested negative for mycoplasma contamination by PCR analysis (Idexx BioAnalytics). All lines were transduced with lentivirus (LVpFUGQ-UbC-ffLuc2-eGFP2, provided by Viral Technology Laboratory, NCI Frederick) as single cells at a MOI of 1 to express both GFP and luciferase. GFP expression was monitored in vitro and, in some cases, cells were sorted for GFP positivity by FACS prior to in vivo implantation. For use in an in vitro experiment, GSC neurospheres were disaggregated into single cells, as described above, and seeded onto poly-L-ornithine (PO, Invitrogen)/laminin (Sigma-Aldrich) coated tissue culture dishes in stem cell media. Under these conditions, single-cell GSCs attach and grow as an adherent monolayer maintaining their CD133 expression and stem-like characteristics (269). Radiation was

delivered to in vitro cultures using a 320 kV Xray machine (Precision X-Ray Inc.) at a dose rate of 2.3Gy/min.

3.3 In vivo protocols

3.3.1 Orthotopic implantation of glioblastoma cell lines

CD133+ GSCs (1.0×10^5) or U251 (2.5×10^5) transduced to express luciferase and GFP were orthotopically implanted into the right striatum of 6-week-old athymic female nude mice (Ncr nu/nu; NCI Animal Production Program). A single cell suspension of the cells to be implanted were collected and then counted on a Coulter counter. Cells were then spun down and resuspended in sterile PBS such that the required number of cells could be implanted in 5µL per mouse. Mice were anaesthetized using isoflurane gas and transferred to a stereotactic surgical frame with continued isoflurane exposure and heat pads. Mice were secured with ear clamps. Meloxicam was provided subcutaneously prior to surgery initiation and Marcaine was provided topically after surgical incisions for post-operative pain relief. Scalps were scrubbed with iodine and 70% surgical grade ethanol three times prior to making a 1 cm sagittal incision to the right of midline with a sterile scalpel. The bregma was identified and a burr hole created with a 22-gauge needle 1 mm anterior and 2 mm lateral to the bregma. Once a hole was made in the skull, a Hamilton syringe pre-loaded with glioma cells was lowered to a depth of 3.5mm inferior to the skull surface and then raised 0.5mm. After a delay of two minutes, glioma cells were slowly injected over 4 minutes. Once all cells were injected, two minutes were waited prior to slowly removing Hamilton syringe. Mouse was removed from stereotactic frame and incision was closed with veterinary glue. Each mouse was monitored in a heated plastic chamber until fully recovered.

3.3.2 Bioluminescent imaging for monitoring tumour growth

On day 6 (U251) or day 21 (NSC11, NSC20, NSC23) after implantation, mice were randomised according to bioluminescent imaging (BLI) signal into two groups: control and radiation (RT). BLI was performed by injecting mice intraperitoneally with D-luciferin

(0.01ml/g body weight; 15mg/ml sterile PBS; GoldBiotechnology). After a period of approximately 15 minutes, mice were briefly anaesthetized with isoflurane and imaged with a Xenogen IVIS 200 imaging system (Caliper Life Sciences). BLI was performed weekly after irradiation until the first mouse of a given treatment group died. Subsequent BLI total fluorescence values were compared to the initial, pre-treatment total fluorescence value of a given mouse's tumour to provide BLI ratios. Tumour growth rate curves were generated in SigmaPlot by charting changes in BLI ratios for each treatment group as a function of time after irradiation.

3.3.3 Irradiation for treating in vivo tumours

After confirmation of tumour growth, mice randomised to receive irradiation were anaesthetized with an intraperitoneal injection of a ketamine/xylazine cocktail and placed in a well-ventilated Plexi glass jig with lead shielding of critical normal structures (e.g. torso, neck, ears). For GSC tumours, 5Gy was delivered for 3 consecutive days. For U251 tumours, 3Gy was delivered on 3 consecutive days. Radiation was delivered using an X-Rad 320 X-irradiator (Precision X-Rays, Inc.) at a dose rate of 2.9 Gy/minute. Immediately after receiving irradiation, mice were intraperitoneally injected with AntiSedan to reverse the effects of ketamine. Mice were placed on a warmer and monitored until fully recovered.

3.3.4 Subcutaneous injection of glioblastoma cells

To generate leg tumours 1.0 x 10^6 U251 cells per 100µl sterile PBS were subcutaneously (SC) injected into the right hind legs of 6-week-old athymic female nude mice while awake. Tumour size was monitored biweekly with digital calipers. Once the average tumour size of a cohort reached 150-200 mm^3, mice were randomised into control and radiation (3x3Gy) groups. Fractionated radiation was delivered locally with awake animals restrained in a custom designed lead jig which shielded all structures except for the tumour-bearing leg. Radiation (3Gy) was provided over three consecutive days utilising the same X-Rad 320 X-irradiator mentioned above. SC tumours were monitored biweekly with digital caliper measurements. Once an individual tumour reached a volume of 1500 mm^3 or 2 cm in any dimension, mice were humanely euthanised and SC tumours were collected for analysis.

3.3.5 Survival analysis

All mice were observed daily to monitor for onset of neurologic symptoms. Once mice reached morbidity, they were humanely euthanised utilising an approved schedule 1 method. Overall survival for each mouse was recorded and GraphPad Prism 7 (GraphPad Software) was used to generate Kaplan–Meier survival curves. The number of mice utilised for each study, based on previous work using established glioma cell lines, were estimated by a One-Way ANOVA analysis to allow 80% power to detect a 25% increase in growth delay/survival when the differences between the mean tumour volumes/survival times is 1.25 standard deviations different than controls. All in vivo experiments were performed as approved by the NIH Guide for Care and Use of Animals and conducted in accordance with the Institutional Animal Care and Use Committee. Additionally, all in vivo experiments performed in the UK were performed according to Home Office UK guidelines.

3.4 DNA and RNA extraction

3.4.1 Xenograft tumour collection

After humanely euthanising mice by cervical dislocation, cardiac perfusion was performed with chilled PBS. Briefly, the rib cage was removed, the right atrium was cut, a butterfly needle was inserted and clamped in the left ventricle, and the inferior vena cava was clamped shut. PBS was injected into the left ventricle into the blood stream to perfuse the brain to remove blood. If the brain was needed for histology, then 10% Formalin was perfused after the PBS. After cardiac perfusion, the scalp was cut and the skull opened to expose the brain. The entire brain was carefully removed and transferred to a PBS-filled petri dish for tumour removal or a container containing 10% Formalin for further fixation prior to histology preparation. GFP+ tumour tissue was visualised and dissected under a fluorescent stereoscope (Leica). Tumour tissue was transferred to a cryovial and snap frozen in liquid nitrogen prior to storing in a -80^{o}C freezer. When the fresh frozen tumour tissue was needed for DNA extraction, it was thawed on ice and then homogenised in the cryovial with a plastic pestle. A small amount of tissue was transferred to RLT buffer for initiation of the extraction process. Remaining tissue was returned to the -80^{o}C freezer for possible future experiments.

3.4.2 Homogenisation of patient tumour samples

Human glioblastoma fresh frozen tumour samples were requested and collected from the Addenbrooke's tissue bank. Small amounts of tissue (approximately 30mg) were transferred into Lysing Matrix D tubes containing ceramic spheres. 600µL of RLT buffer containing 10% β-mercaptoethanol was added and tubes run for two 15 second cycles on a FastPrep-24 homogeniser (MP Biomedicals). Once tissue was homogenised, samples were transferred into separate tubes and centrifuged for 3 minutes at top speed to remove tissue debris. Lysate was transferred to an AllPrep DNA spin column for further extraction.

3.4.3 DNA isolation

DNA isolation was performed with AllPrep DNA/RNA Mini kits (Qiagen) when both DNA and RNA were needed from a given sample. When only DNA was needed or when DNA was extracted from blood samples, DNeasy Blood and Tissue kits (Qiagen) with a similar protocol were utilised. To isolate DNA, tumour tissue or cell lysate was transferred to an AllPrep DNA spin column and centrifuged for 30 seconds at 8000g. The flow-through was utilised for RNA isolation as discussed below. The spin column itself was transferred to a new collection tube and 500µl Buffer AW1 was added prior to centrifuging for 15s at 8000g. Flow-through was discarded and 500µl Buffer AW2 was added and centrifuged for 2 minutes at full speed. The spin column was then placed in a new 1.5mL collection tube and 100µl EB Buffer was added directly to the membrane. The spin column was incubated at room temperature for 1 minute and then centrifuged for 1 min at 8000g for DNA elution. DNA was quantified with Nanodrop and stored in a freezer prior to use for downstream applications.

3.5 Histology and Immunohistochemistry

3.5.1 Histology preparation and H&E

Mice were euthanised and perfused with chilled PBS then formalin via cardiac puncture, as described. Brains were then removed and placed in 10% buffered formalin for at least 24 hours. After fixation, brains were transferred to cryowells and covered with 3% agarose gel. Once gel hardened, brains were removed from cryowell, attached to a plastic disc,

and transferred to a tissue chopper table (McIlwain). Brains were cut into 1 mm thick sagittal or coronal slices. Right hemisphere sagittal slices (medial slices containing right olfactory bulb and more lateral slices) and anterior coronal slices were then embedded in paraffin. Tissue slices were further cut into 6 µm thick slices and attached to positively charged histology slides. At least one slide per brain underwent hematoxylin and eosin staining. Unstained slides were also prepared for each brain for subsequent immunohistochemical staining.

3.5.2 DAB staining

FFPE right hemisphere sections of control and irradiated tumour-bearing brains were deparaffinized with Xylene and rehydrated in a descending concentration ethanol series. Heat-induced epitope retrieval was achieved using Citrate Buffer (pH=6) in a steamer for 1 hour. Slides were washed in TBS and once in 3% H2O2/TBS. Tissue was blocked at room temperature with Immpress 2.5% Horse Serum Blocking Buffer (Vector Labs). Human SOX2 primary antibody (Cell signaling, 1:250) was applied and incubated overnight at 4°C. Immpress HRP secondary (anti-rabbit, Vector Labs) was applied and incubated at room temperature for 30 minutes. Slides were washed in TBS and DI water. Four drops of ImmPACT DAB reagent were added to 4 ml of ImmPACT diluent (Vector Labs) and applied until visible colour change occurred (no more than 5 minutes). Slides were washed in tap water, counterstained with hematoxylin for 30 seconds, dehydrated with ascending alcohol series, dried, cleared in xylene, mounted with permount, dried overnight, and visualised with an AxioScan automated imager (Zeiss).

3.6 Whole exome sequencing

3.6.1 Library preparation and sequencing

Genomic DNA was subjected to WES, which was performed by the Center for Cancer Research Genomics Technology Laboratory. Extracted DNA underwent library prep according to the Agilent SureSelect XT (All Exon V5 +UTR) protocol and sequenced on an Illumina HiSeq4000 device using paired-end sequencing to an average sequencing depth of > 180x.

3.6.2 Variant calling

Mouse reads were removed as previously described (270). Alignment and tumour-only variant calling was performed with the Center for Cancer Research Collaborative Bioinformatics Resource (CCBR) pipeline (https://github.com/CCBR/Pipeliner). Read data was trimmed for the presence of adaptors and low quality using Trimmomatic v0.33 and the following parameter settings: Leading:10; Trailing:10; Sliding window:4:20; Minlen:20 (271). Reads were mapped to the hs37d5 reference genome using BWA-mem v0.7.17 with default parameter settings (272). Following alignment, BAM files were processed using SAMtools and PCR duplicates were marked using Picard v2.1.1 (273). Indel realignment and base recalibration were performed using the Genome Analysis Toolkit v.3.8 (GATK, Broad Institute, Cambridge, MA), following the GATK Best Practices (274,275). MultiQC v1.4 was used to aggregate QC metrics from FastQC, FastQ Screen, Picard, BamTools and Trimmomatic (276,277). Variant calling was performed using MuTect2 (278). Germline variants were excluded using a panel of normals (279). Only protein-altering variants were retained (280).

Chapter 4. Intratumoral Heterogeneity and Radiosensitivity

Glioblastoma is an extremely heterogeneous tumour type. Not only has heterogeneity been shown between individual tumours (50,98,102), but heterogeneity within individual tumours has been demonstrated, adding to the genomic and phenotypic complexity. As described previously, intratumoral heterogeneity has been established through multi-sampling surgical techniques, single cell RNA-seq analysis, and interrogation of DNA methylation patterns (112,113,281). Indeed, spatially distinct tumour fragments from a single tumour can harbour different genomic alteration and gene expression patterns, even corresponding to different GB subtypes (110). Because ITH is considered a requirement for cancer to undergo evolution, the functional implication of GB ITH is that selection due to external pressures may be a major cause of GB treatment resistance and recurrence (116,118,119).

Therapeutic selection pressures have the potential of causing the contraction or even elimination of treatment sensitive clones. After this contraction, treatment-resistant clones, or clones that were protected from the treatment due to a protective niche or temporary quiescent state, are then free to expand and repopulate a recurrent tumour. Such competitive release could lead to a more aggressive tumour with genotypic and phenotypic profiles different from the primary tumour. For example, coamplification of different types of receptor tyrosine kinases within different cells from the same tumour has been demonstrated in multiple studies (120,121). Such ITH could have potential implications for targeted treatments centered around RTK inhibition, such as EGFR inhibitors, as coamplification could provide a clear path to resistance. Thus, potentially effective treatments may only produce a response in a subset of glioma cells as targets may be inconsistently expressed within heterogeneous tumours (112). Some studies suggest that distal samples (and more longitudinally separated samples) may exhibit larger differences in treatment response compared to proximal samples (115). However, other studies demonstrate that locally recurrent tumours can display many genetic alterations and even variations in shared mutation prevalence, suggesting subclonal expansion and contraction (213). Because radiotherapy is a standard component of GB treatment, the ability of radiation to produce a consistent therapeutic response across spatially distinct regions of the tumour should be explored.

In this study, we sought to investigate the potential impact of ITH on intrinsic radiosensitivity by examining differences in in vitro radiosensitivity between cell lines derived from spatially distinct tumour fragments. Multiple cell lines from spatially distinct fragments from three different tumours were derived following 5-ALA fluorescence guided surgical sampling (136). Whole-exome sequencing of matched cell lines and tumour specimens demonstrated that the cell lines were good models of their tumour of origin, while still displaying heterogeneity between cell lines from the same tumour. DNA double-strand break foci analysis and limiting dilution assays demonstrate that while there were minor differences between some of the lines, there do not seem to be consistent differences in radiosensitivity between cell lines derived from spatially distinct tumour fragments. These results suggest that glioblastoma ITH does not lead to differential radiosensitivity of spatially (and genetically) distinct tumour regions. If this is true, then the heterogeneous tumour may have a relatively homogeneous response to irradiation.

4.1 Methods for studying radiosensitivity of patient-derived cell lines

Methods for deriving and maintaining patient-derived cell lines, extracting DNA, and performing whole exome sequencing can be found in Chapter 3. Methods described below were specifically utilised for the study of radiosensitivity of patient-derived cell lines.

4.1.1 γH2AX foci analysis

Poly-L-ornithine (PO) was added to each chamber of 2-chambered slides and slides were incubated overnight in 37°C incubator. PO was removed and washed twice with sterile PBS and then Laminin (Sigma-Aldrich) in PBS (1:500) was added to each chamber and incubated for at least 4 hours to overnight at 37°C. A single cell glioma cell suspension was created by adding Accutase (Gibco) to culture flasks or neurospheres. After incubation of up to 10 minutes, PBS was added, cells were disaggregated by pipetting, and cell suspension was filtered through a sterile 40µm cell strainer. Cells were spun down at 1000 rpm for 5 minutes,

resuspended in 5 mL sterile PBS, and counted with a Coulter counter. Cells were spun down for a final time and then plated at a density of around 50,000 cells per chamber in SFM. Cells were incubated on chamber slides at 37°C/5% CO_2/5% O_2 until cells reached 70% confluency. Slides were then irradiated at 2 Gy with a 320 kV Xray machine (Precision X-Ray Inc.) at a dose rate of 2.3Gy/min. After irradiation, slides were fixed at 1, 6, and 24 hours post-irradiation with 10% formalin for 10 minutes at room temperature. Cells were then washed three times with PBS and stored in PBS at 4°C for up to ten day prior to staining. For staining, cell membranes were permeabilised with 0.2% Triton/PBS for 10 minutes at room temperature and then rinsed with PBS-T. Blocking buffer (PBS-T, 5% Goat serum, 1% BSA) was added for 1 hour at room temperature with gentle rocking. Primary antibody to anti-phospho-histone H2AX Ser 129 (1:1000, Millipore) was then added in blocking buffer and incubated overnight at 4°C with gentle rocking. Next, cells were washed three times with PBS-T for 5 minutes per wash at room temperature. Secondary antibody (Alexa Fluor 488 or 555 goat anti-mouse IgG, 1:1000, Invitrogen) in blocking buffer was added and incubated for 2 hours at room temperature in the dark with gentle shaking. Cells were again washed three times with PBS-T and chambers were removed from slide. One drop of ProLong Gold/Diamond Antifade with DAPI was added to each chamber area and a glass coverslip was added. Weight was applied to remove bubbles and slides were allowed to dry overnight. Slides were stored at 4°C prior to imaging on a fluorescent microscope at 40x magnification. ImageJ was utilised to analyse TIF files and manually count the number of foci per nuclei. Twenty-five nuclei per condition and time point were counted.

4.1.2 Limiting dilution assay

For limiting dilution assays a single cell suspension was obtained as described above. Once cells were counted, serial dilutions were performed to obtain a suspension with 100-1000 cells per 100µl. Every well of a 96-well plate was first filled with 100µl SFM without bubbles. Then 100µl of the cell dilution made above was added to all wells in row A for a final volume of 200µl. With a multichannel pipette, solutions in row A were thoroughly mixed before removing 100µl from row A to transfer to row B. Next, row B wells were thoroughly mixed and 100µl of solutions were transferred to row C. This pattern was continued through row H. An example range would be: Row A (100 cells), B (50), C (25), D (12), E (6), F (3), G (1), H (0). A light microscope was used to visually verify that wells A-G contained single cell

solutions. Plates were then incubated at 37°C, 5% CO_2, 5% O_2. Twenty-four hours later, individual plates were irradiated with a range of radiation doses (1-3Gy) using a 320 kV Xray machine (Precision X-Ray Inc.) at a dose rate of 2.3Gy/min and then returned to the incubator. At 14 to 21 days post-irradiation, plates were removed from incubator and examined under a light microscope. The number of positive wells were determined and recorded. Wells were positive if they contained one or more spheres of approximately 30 cells. Number of spheres per well was also recorded. Finally, ELDA: Extreme Limiting Dilution Analysis online software was utilised to calculate the cancer cell initiating frequency and significance (http://bioinf.wehi.edu.au/software/elda/) (282).

4.1.3 Whole exome sequencing analysis: Correlation and superFreq

After sequencing, filtering, and variant calling, variant allele frequencies (VAF) were utilised to calculate Pearson's correlation coefficients for all combinations of samples. Next, the superFreq software was utilised to identify single nucleotide variants (SNV) and copy number alterations (CNA) and to predict and compare the number of clones in the samples (283)(https://github.com/ChristofferFlensburg/superFreq/). In brief, once SNVs and CNs are called in superFreq, genes with similar differential coverage and VAFs in a sample are clustered. SNV frequencies are converted to clonalities which are based in part on CN clonality estimates. SNV and CN clonalities are then tracked across samples from the same individual and mutations with similar clonalities are clustered into clones. Clones are then sorted based on the size of the predicted clone/subpopulation. Finally, SNVs are annotated with VEP and compared to COSMIC data (COSMIC will be further discussed in Chapter 5). All WES analysis done in collaboration with bioinformaticians within the Radiation Oncology Branch, National Cancer Institute, National Institutes of Health (Kristin Valdez and Dr. Uma Shankavaram).

4.2 Results

4.2.1 Glioblastoma surgical samples and patient-derived cell lines

After presentation and preoperative imaging suggestive of glioblastoma, patients underwent 5-ALA fluorescence-guided surgical resection at Addenbrooke's Hospital. Surgical specimens were both frozen for tissue bank storage and processed, as described in Chapter 3, to derive and establish GB cell lines. Tissue and patient-derived cell lines from three patients were chosen for inclusion in this study due to matching tissue availability and the successful derivation of multiple self-renewing cell lines from each tumour. While the inclusion of patient tumour samples able to generate multiple cell lines could potentially have selected for more proliferative, aggressive phenotypes, or at least tumours with phenotypes/genotypes more amenable to in vitro propagation, the need for multiple cell lines from the same tumour for in vitro radiosensitivity testing made this potential bias unavoidable. The clinical course of each patient and histopathological features of each neoplasm (Fig. 4.1D) are described below.

J3: A 54-year-old male presented with a two-month history of symptoms ranging from loss of confidence at work, short term memory loss, worsening of bipolar symptoms, and severe headaches to left-sided motor impairment and swallowing/speech difficulty. MRI showed a large right frontal heterogeneously enhancing glioma (7cm) with oedema and mass effect (Fig. 4.1A). Surgical resection was complicated as the tumour was very necrotic and vascularised. After tumour and clots were removed, haemostasis was difficult to achieve due to residual disease, resulting in the need to reoperate later in the day to remove an intracavitary haematoma. While histopathological analysis revealed a minor oligodendroglial component, 1p19q codeletion was not detected, thus providing a diagnosis of a WHO Grade 4 GB. The tumour was IDH1 mutation negative, MGMT promoter methylation negative, and had a MIB-1 of 40%. The patient was deemed too unwell to tolerate further treatments and palliative treatment was recommended. Unfortunately, he passed away 14 days later.

J7: A 73-year-old female who presented after a grand mal seizure had been experiencing a few weeks of headaches and 1 week of difficulty with memory prior to the seizure. Preoperative MRI showed a left frontal lobe tumour (4.2cm) with heterogeneous contrast enhancement involving cortex and white matter in the middle frontal gyrus with extension into the inferior frontal gyrus (Fig. 4.1B). Patient underwent 5-ALA fluorescence-

guided subtotal surgical resection with no postoperative complications. Histopathological analysis revealed a WHO Grade 4 GB. The tumour was IDH1 mutation negative, MGMT promoter methylation positive (46%), and had a MIB-1 of 15%. Patient received the Stupp protocol and completed radiotherapy and concomitant chemotherapy. Patient did not receive final adjuvant cycle of TMZ due to admission for siezures and sepsis. At last EMR review, patient had apparently stable disease, had survived for over a year since surgery, and was on conservative management and best supportive care.

J14: A 56-year-old male presented with a 12-day history of expressive dysphasia and word-finding difficulties and headaches. MRI showed a heterogeneously enhancing tumour (3.6cm) in the middle and posterior left temporal lobe with vasogenic oedema, left uncal herniation and minor midline shift consistent with GB (Fig. 4.1C). Patient underwent an awake craniotomy with 5-ALA fluorescence guided gross total surgical resection. Postoperative wound exploration, debridement, and resuturing was done due to CSF leakage from anterior part of wound. Histopathological analysis revealed a WHO Grade 4 GB. The tumour was IDH1 mutation negative, MGMT promoter methylation positive (26%), and had a MIB-1 of 15%. Patient received radiotherapy and adjuvant and concomitant TMZ at an outside hospital in Ipswich. At last EMR review, the Cambridge MDT had discussed the patient's follow-up MRI images taken during adjuvant TMZ treatment and found them to be inconsistent with recurrence. The recommendation was for the patient to continue standard adjuvant treatment protocol under the local oncology team.

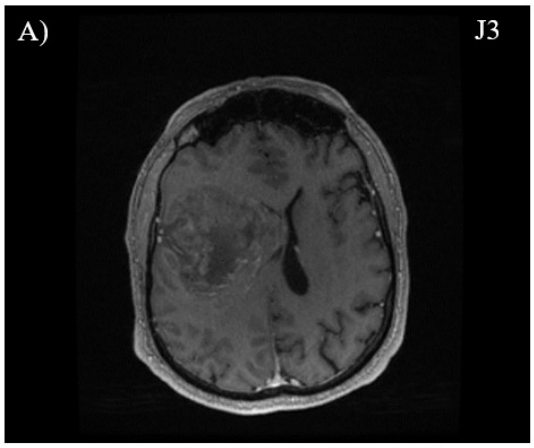

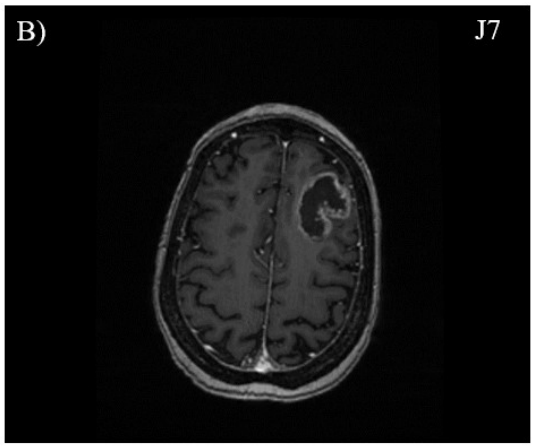

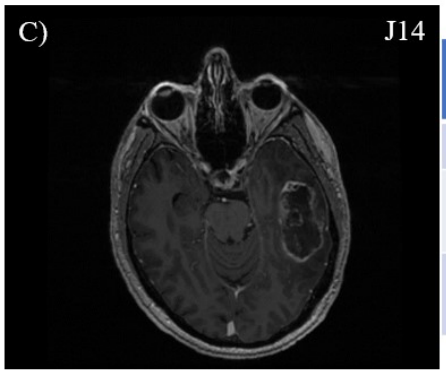

D)	IDH status	MGMT methylation	Mib-1 (%)	1p/19q Codel
J3	WT	Unmethylated	40	-
J7	WT	Methylated (46%)	15	-
J14	WT	Methylated (26%)	15	-

Figure 4.1 Glioblastoma samples. Preoperative T1-weighted magnetic resonance images of A) J3, B) J7, and C) J14 glioblastomas. D) Histopathology findings for each tumour.

4.2.2 Patient-derived cell lines as models of glioblastoma tumour fragments

Whole exome sequencing was performed on DNA extracted from spatially distinct glioblastoma surgical specimens, corresponding patient-derived cell lines, and matched whole blood controls to assess the ability of cell lines to serve as models of ITH between surgical samples. First, Pearson's correlation coefficients were calculated based on variant allele frequencies (VAF) for all samples. Comparison of correlation coefficients demonstrates that surgical specimens and cell lines from the same patients are much more highly correlated with each other than with samples from different patients (Fig. 4.2), suggesting that the derived cell lines are good models of their tumours of origin. Patient-specific analysis for J3 reveals that J3T1 and J3T4 cell lines are more similar to each other than to their respective tumour fragments (Fig. 4.3A). This similarity is evident by relatively few VAFs that are significantly different between the samples (indicated by red x's) compared to an abundance of shared non dbSNPs (likely somatic SNPs; blue dots on the diagonal). The relative similarity of the cell

lines could be the result of discrepancies in tumour tissue handling or biological changes imposed by the in vitro culturing environment (discussed further in Sections 7.2 and 7.3). The similarity between cell lines was also reflected in the copy number (CN) profiles of the samples (Fig. 4.3B). It should be noted that in the Super-Freq generated copy number profile, the J3T4 tumour sample seems to harbour a vastly different profile to the other samples, which was unexpected based on Pearson's correlation coefficients comparisons. Therefore, a different copy number caller (Sequenza) was utilised in an attempt to corroborate the difference. As shown in Figure 4.3C, the J3T1 and J3T4 tumour sample copy number profiles generated by Sequenza are very similar, suggesting that the differences seen in the initial profile may simply be a technical artefact.

The relationships between samples were further supported by superFreq analysis. Figure 4.4A displays an SNV heatmap generated by superFreq that compares the SNV frequencies for significantly changing somatic SNVs across all samples. SuperFreq also utilises SNV and CN data to group mutations into clones for comparing differences between matched samples. Figure 4.4B demonstrates that while several clones are preserved across all samples, there are observed differences between samples, particularly for the J3T1 tumour. The distribution of clones for J3 further supports that the cell lines are most similar to each other and are more similar to J3T4 tumour than J3T1 tumour. However, coefficients were still above 0.7 when comparing cell lines to their corresponding tumour fragments and all J3 samples were found to share mutations in specific GB driver genes (TP53 c.584T>C, PTEN c.181C>G, MECOM c.301G>A), again suggesting that the cell lines are good models of their tumour of origin. Even though the cell lines may not represent exact models of their corresponding tumour fragments, since J3T1 and J3T4 cell lines are not perfectly correlated (0.81) it is expected that some degree of heterogeneity is still present between the lines and would allow for further examination of ITH impact.

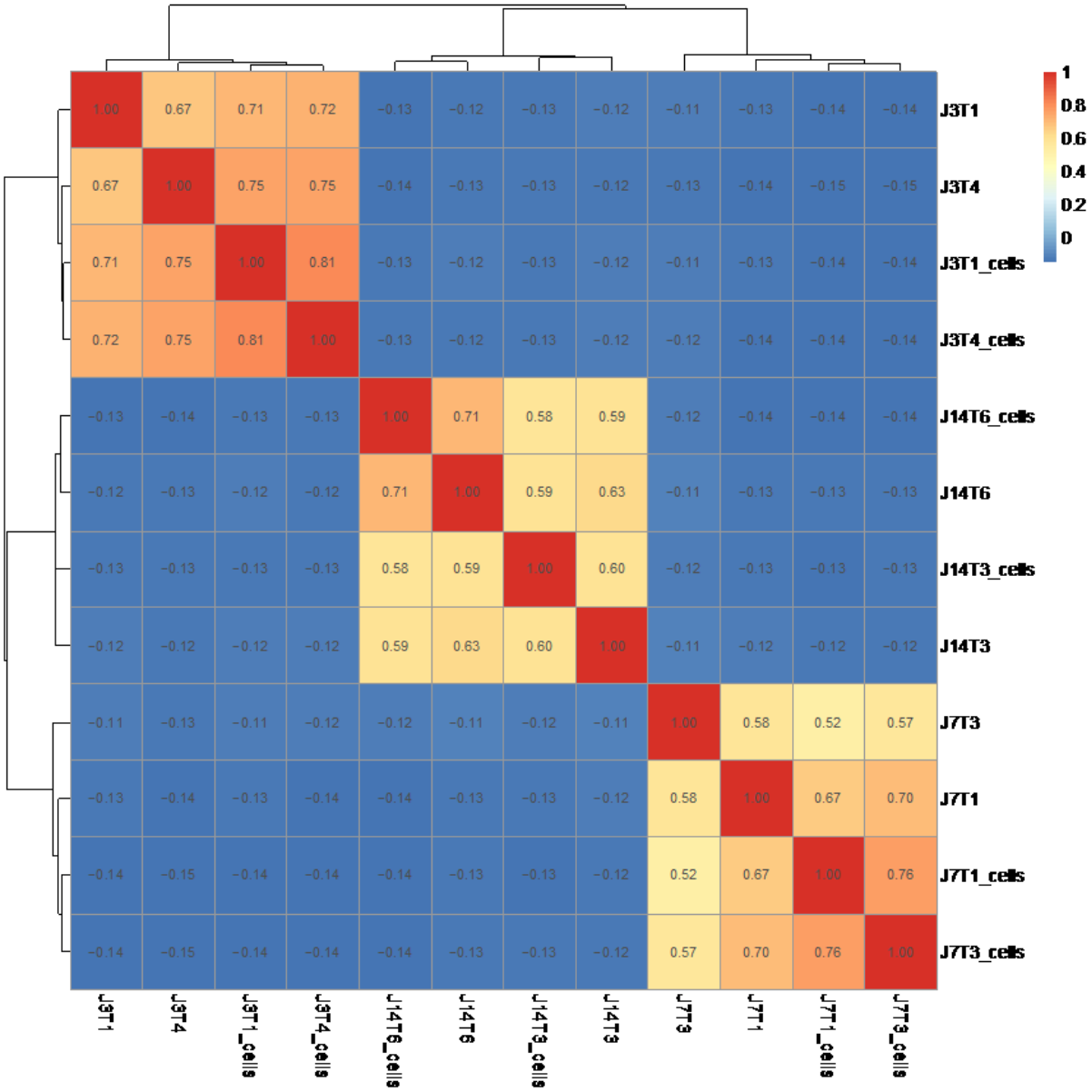

Figure 4.2 Pearson's correlation coefficients. Coefficient calculations are based on variant allele frequencies (VAF) of all J3, J7, and J14 samples sequenced. Germline variants were removed from this analysis.

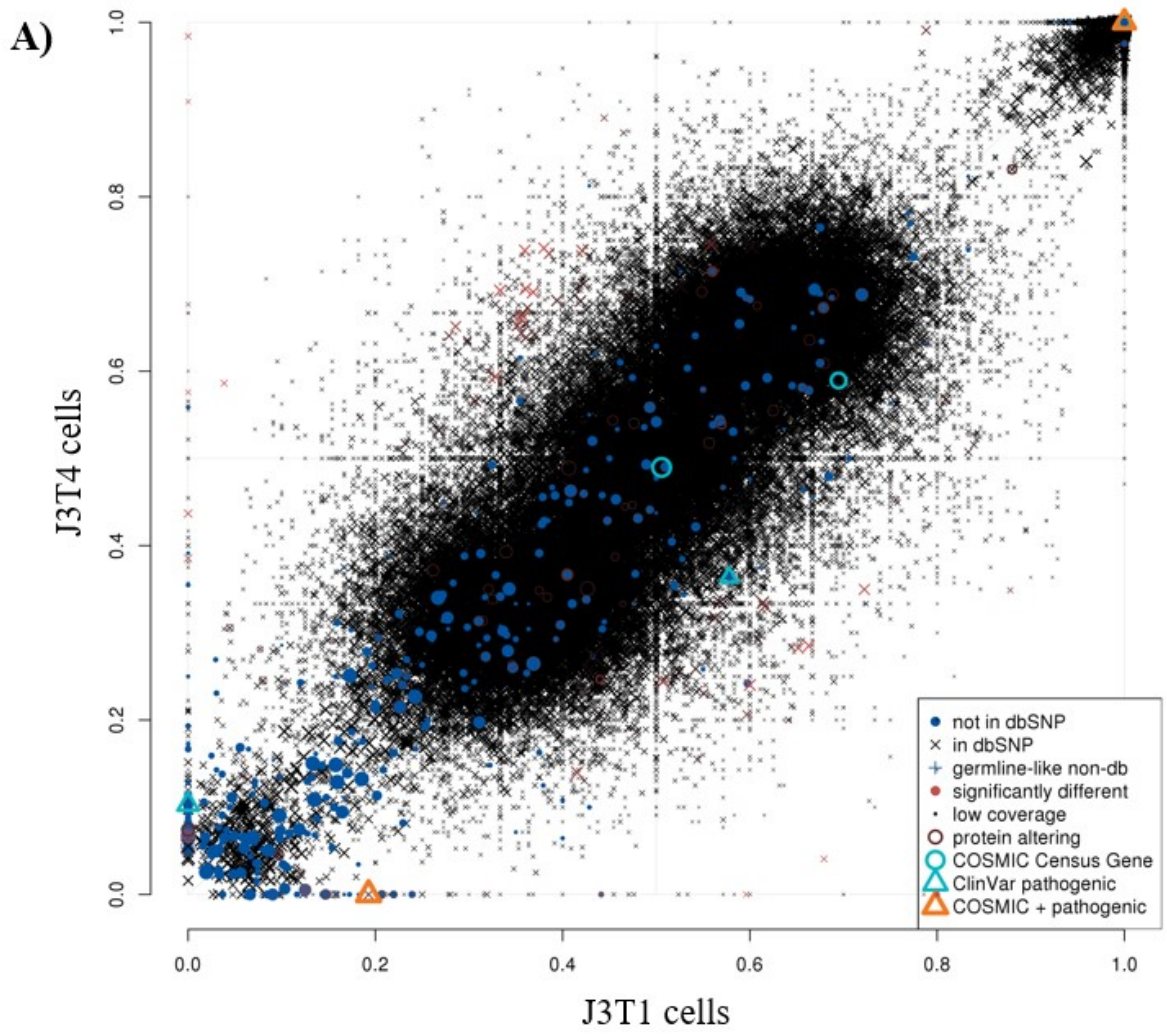

Figure 4.3 Comparison of J3 samples. A) VAF scatter plot comparing J3T1 patient-derived cell line and J3T4 patient-derived cell line. Red Xs indicate VAFs that are significantly different between two samples. Blue dots represent non dbSNPs (likely somatic SNPs). B) Copy number profiles for each J3 sample generated by SuperFreq (next page). C) Sequenza-generated copy number profiles for J3T1 and J3T4 to interrogate technical error observed in SuperFreq copy number calling for J3T4 tumour sample (next page).

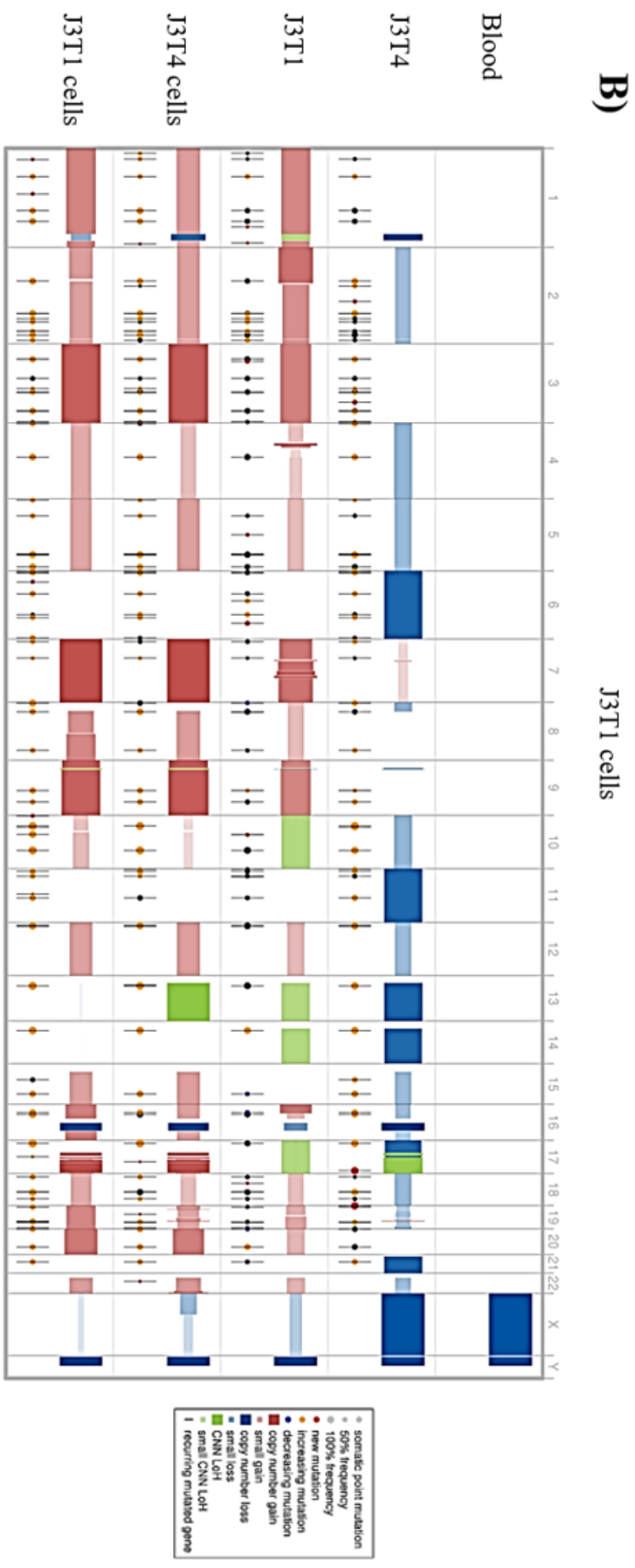
B)
J3T1 cells
Blood
J3T4
J3T1
J3T4 cells
J3T1 cells
1
2
3
4
5
6
7
8
9
10
11
12
13
14
15
16
17
18
19
20
21
22
X
Y
somatic point mutation
50% frequency
100% frequency
new mutation
increasing mutation
decreasing mutation
copy number gain
small gain
copy number loss
small loss
CNN LoH
small CNN LoH
recurring mutated gene

C)

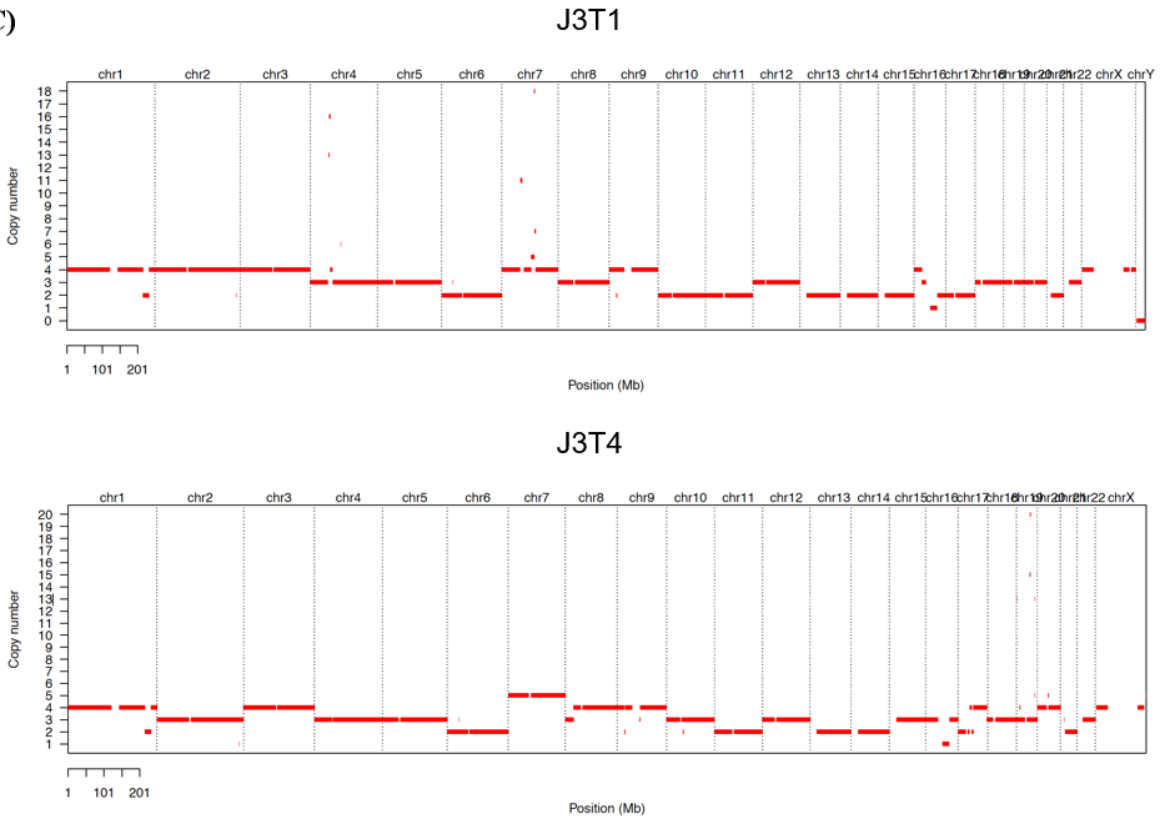
J3T1
chr1 chr2 chr3 chr4 chr5 chr6 chr7 chr8 chr9 chr10 chr11 chr12 chr13 chr14 chr15 chr16 chr17 chr18 chr19 chr20 chr21 chr22 chrX chrY
Copy number
0 1 2 3 4 5 6 7 8 9 10 11 12 13 14 15 16 17 18
1 101 201
Position (Mb)
J3T4
chr1 chr2 chr3 chr4 chr5 chr6 chr7 chr8 chr9 chr10 chr11 chr12 chr13 chr14 chr15 chr16 chr17 chr18 chr19 chr20 chr21 chr22 chrX
Copy number
1 2 3 4 5 6 7 8 9 10 11 12 13 14 15 16 17 18 19 20
1 101 201
Position (Mb)

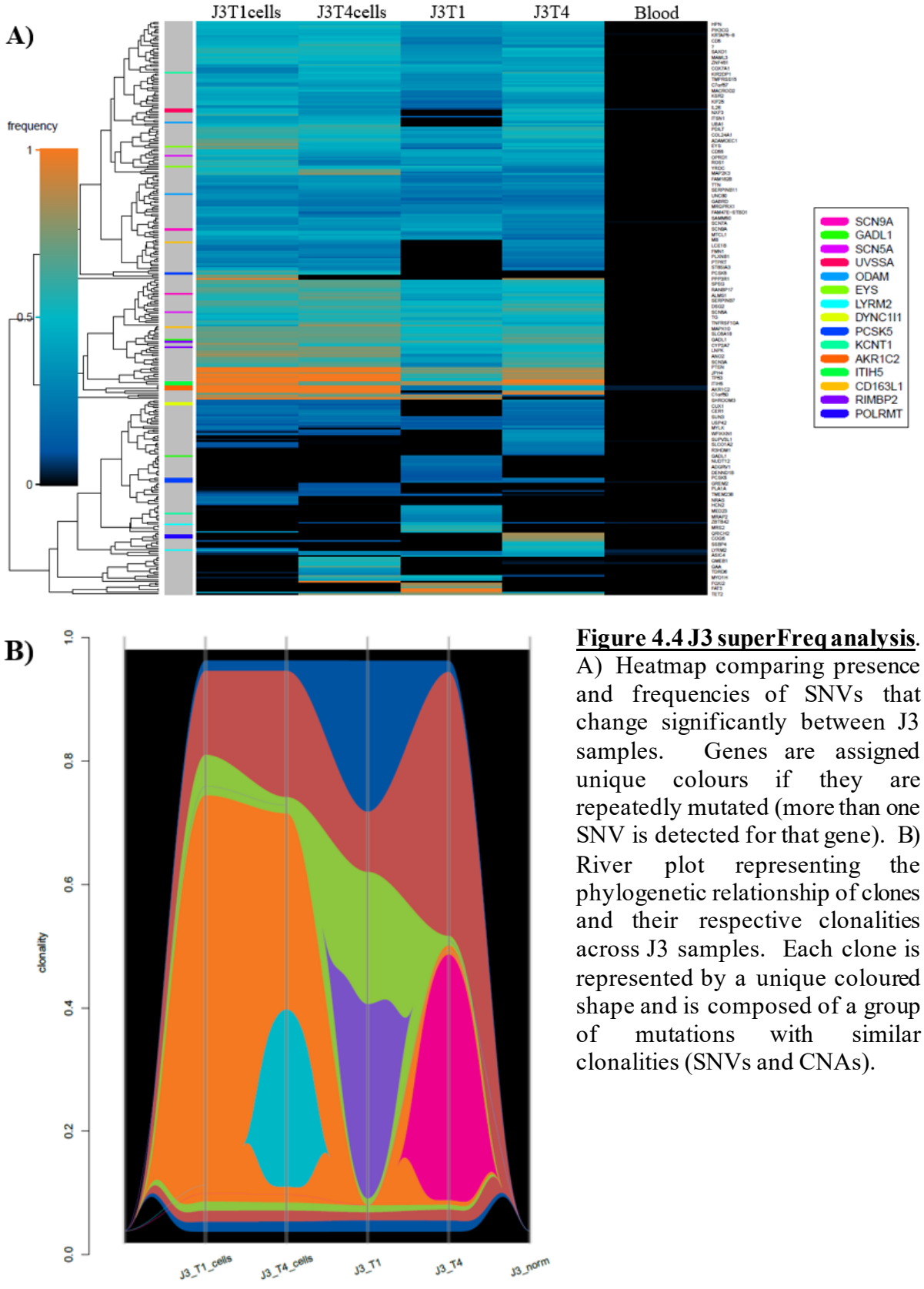

Figure 4.4 J3 superFreq analysis. A) Heatmap comparing presence and frequencies of SNVs that change significantly between J3 samples. Genes are assigned unique colours if they are repeatedly mutated (more than one SNV is detected for that gene). B) River plot representing the phylogenetic relationship of clones and their respective clonalities across J3 samples. Each clone is represented by a unique coloured shape and is composed of a group of mutations with similar clonalities (SNVs and CNAs).

Comparison of correlation coefficients for J7 samples suggest that, similar to J3, cell lines are more similar to each other than to their respective tumour fragments (Fig. 4.5A). As for J3, J7T1 and J7T3 cell lines were both more similar to one tumour fragment (J7T1) than the other. Copy number profiles were similar for all samples (Fig. 4.5B). The relationships between samples were further supported and represented by superFreq-generated SNV frequency heatmaps (Fig. 4.6A). While figure 4.6B indicates a more complicated distribution of clones for J7 than J3, it still displays a few highly conserved clones that are shared at high clonality between the two J7 cell lines and contribute to their similar makeup. When comparing cell lines to their corresponding tumour fragments, correlation coefficients were around 0.6. All J7 samples shared variants in a few GB driver genes (PIK3CB c.2884T>A, PERM1 c.4681C>T), while J7T1 tumour and J7T1 cell line shared a PTEN c.353A>T variant. The Pearson's correlation coefficient between cell lines was 0.76, again suggesting that the J7 cell lines represent a good model of the tumour of origin and that the cell lines maintain heterogeneity between lines.

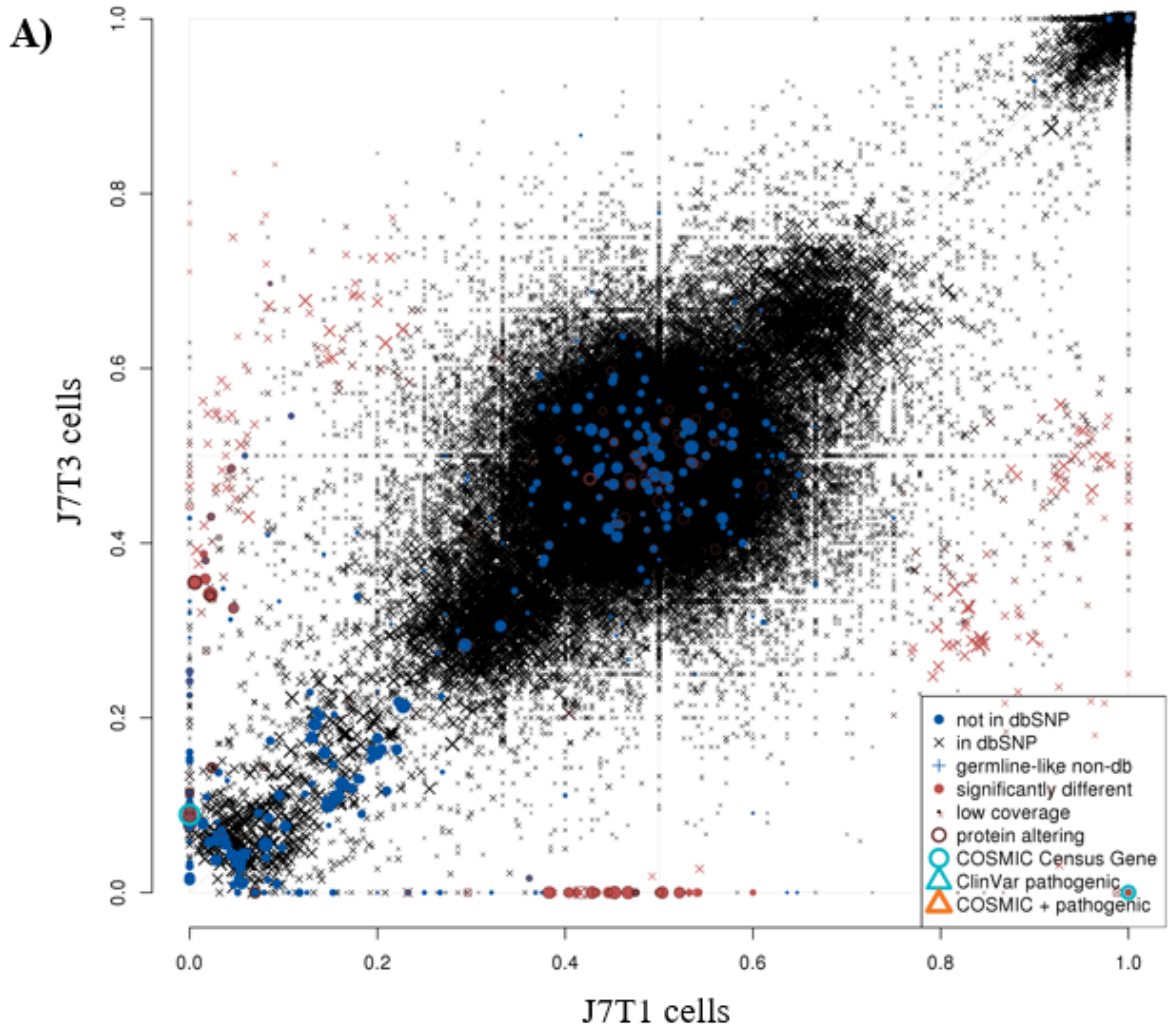

Figure 4.5 Comparison of J7 samples. A) VAF scatter plot comparing J7T1 patient-derived cell line and J7T3 patient-derived cell line. Red Xs indicate VAFs that are significantly different between two samples. Blue dots represent non dbSNPs (likely somatic SNPs). B) Copy number profiles for each J7 sample (next page).

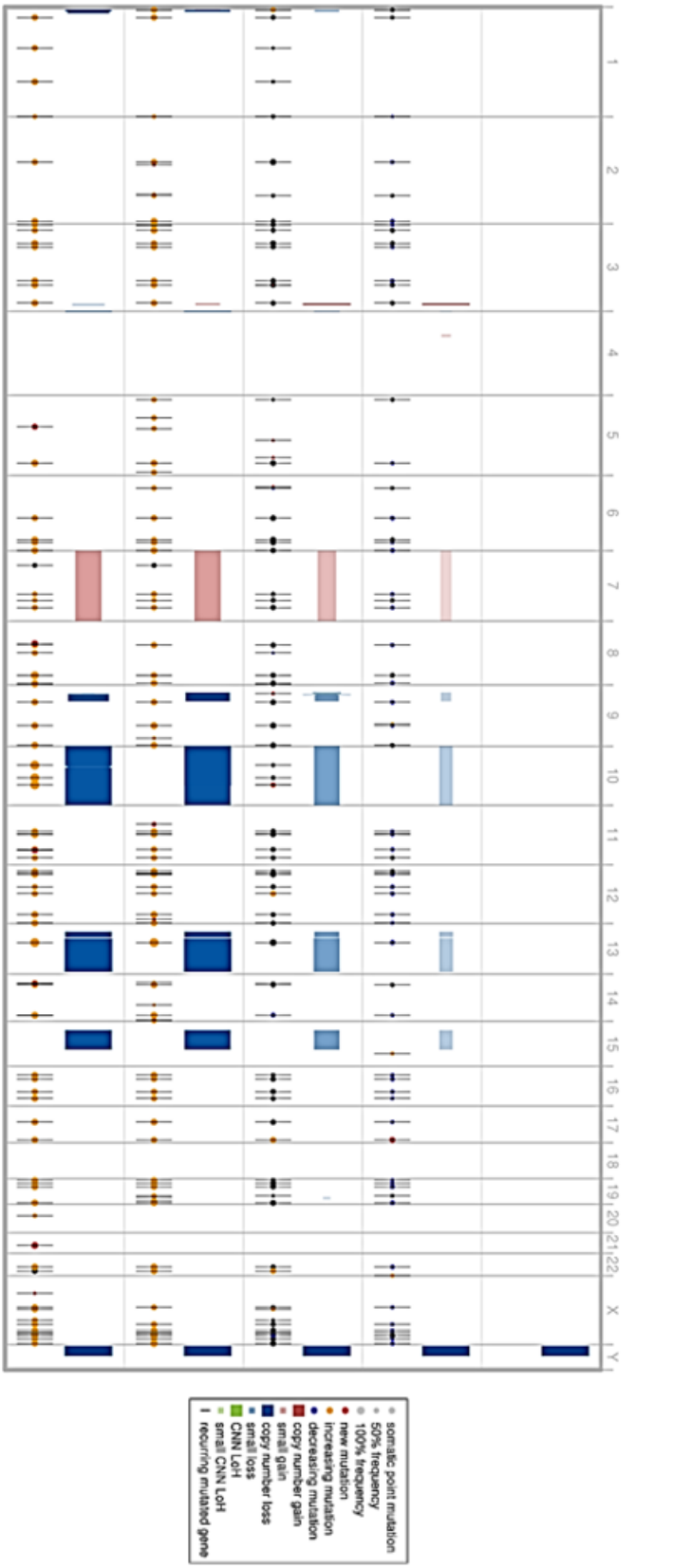
B)
Blood
J7T3
J7T1
J7T3 cells
J7T1 cells
1
2
3
4
5
6
7
8
9
10
11
12
13
14
15
16
17
18
19
20
21
22
X
Y
somatic point mutation
50% frequency
100% frequency
new mutation
increasing mutation
decreasing mutation
copy number gain
small gain
copy number loss
small loss
CNN LoH
small CNN LoH
recurring mutated gene

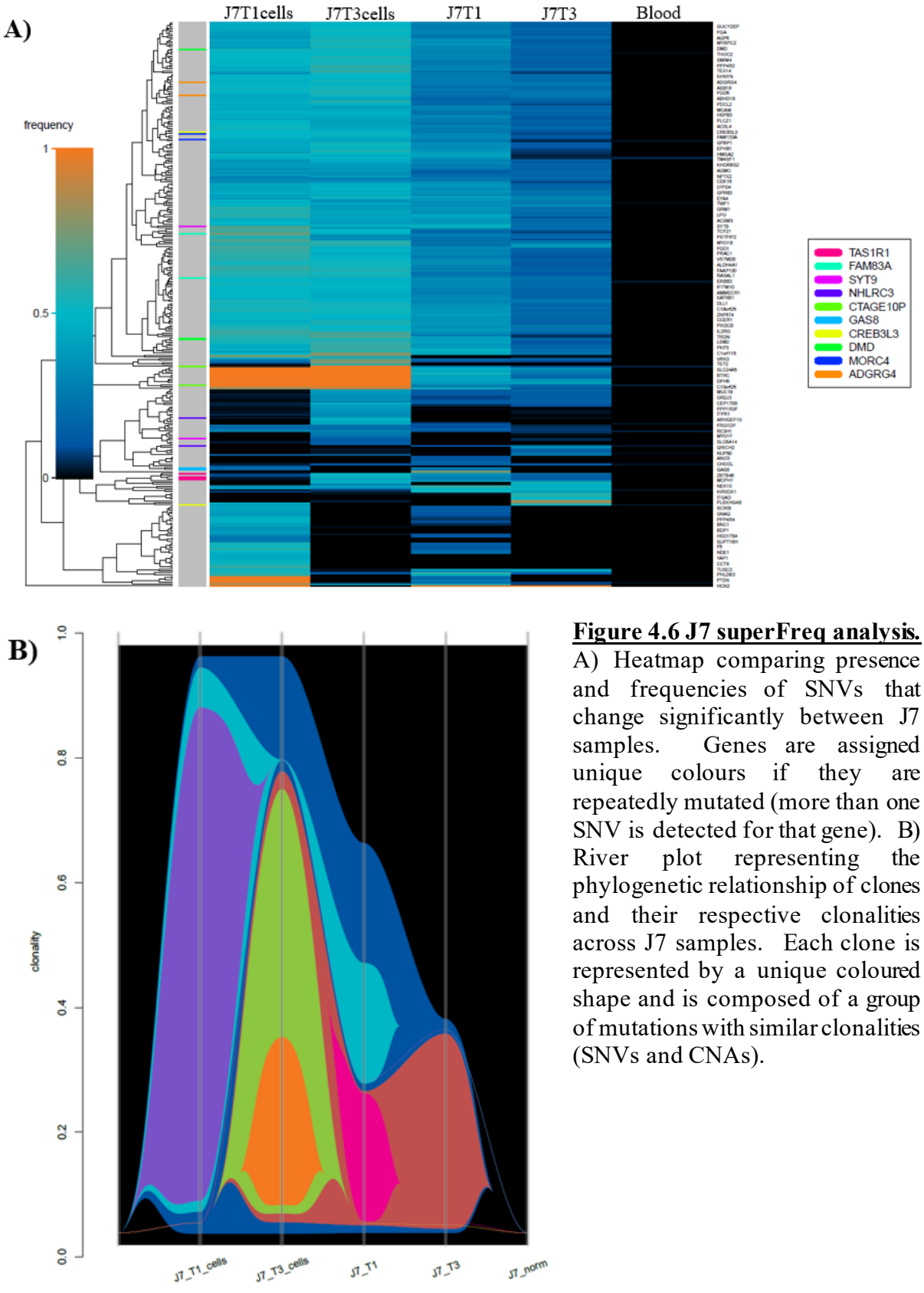

Figure 4.6 J7 superFreq analysis. A) Heatmap comparing presence and frequencies of SNVs that change significantly between J7 samples. Genes are assigned unique colours if they are repeatedly mutated (more than one SNV is detected for that gene). B) River plot representing the phylogenetic relationship of clones and their respective clonalities across J7 samples. Each clone is represented by a unique coloured shape and is composed of a group of mutations with similar clonalities (SNVs and CNAs).

In contrast to J3 and J7, J14 analysis demonstrates that J14T6 cell line is most similar to the corresponding J14T6 tumour fragment (Fig 4.7A). In addition, J14T3 cell line is most similar to its corresponding J14T3 tumour fragment, although it correlates almost equally well with all samples. CN profiles for J14 samples are displayed in figure 4.7B and demonstrate very similar profiles for J14T6 cell line, J14T6 tumour, and J14T3 tumour. The relationships between samples are further supported when comparing SNV frequency and clonal distribution (Figs. 4.8A and B, respectively). Figure 4.8B demonstrates three shared clones between J14T6 cells and tumour and two shared clones between J14T3 cells and tumour which support the similarities between these samples. Therefore, the patient-derived cell lines from the J14 tumour seem to be good models not only for the overall tumour of origin, but also for their respective tumour fragments. Taken together, these data suggest that while patient-derived cell lines may not be exact models for spatially-distinct tumour fragments in all cases, they do seem to be good models of their tumours of origin. Furthermore, the heterogeneity found to exist between cell lines, even when they resemble each other more closely than their respective tumour fragments, suggest that they can serve as potential models for studying the impact of ITH on radiosensitivity.

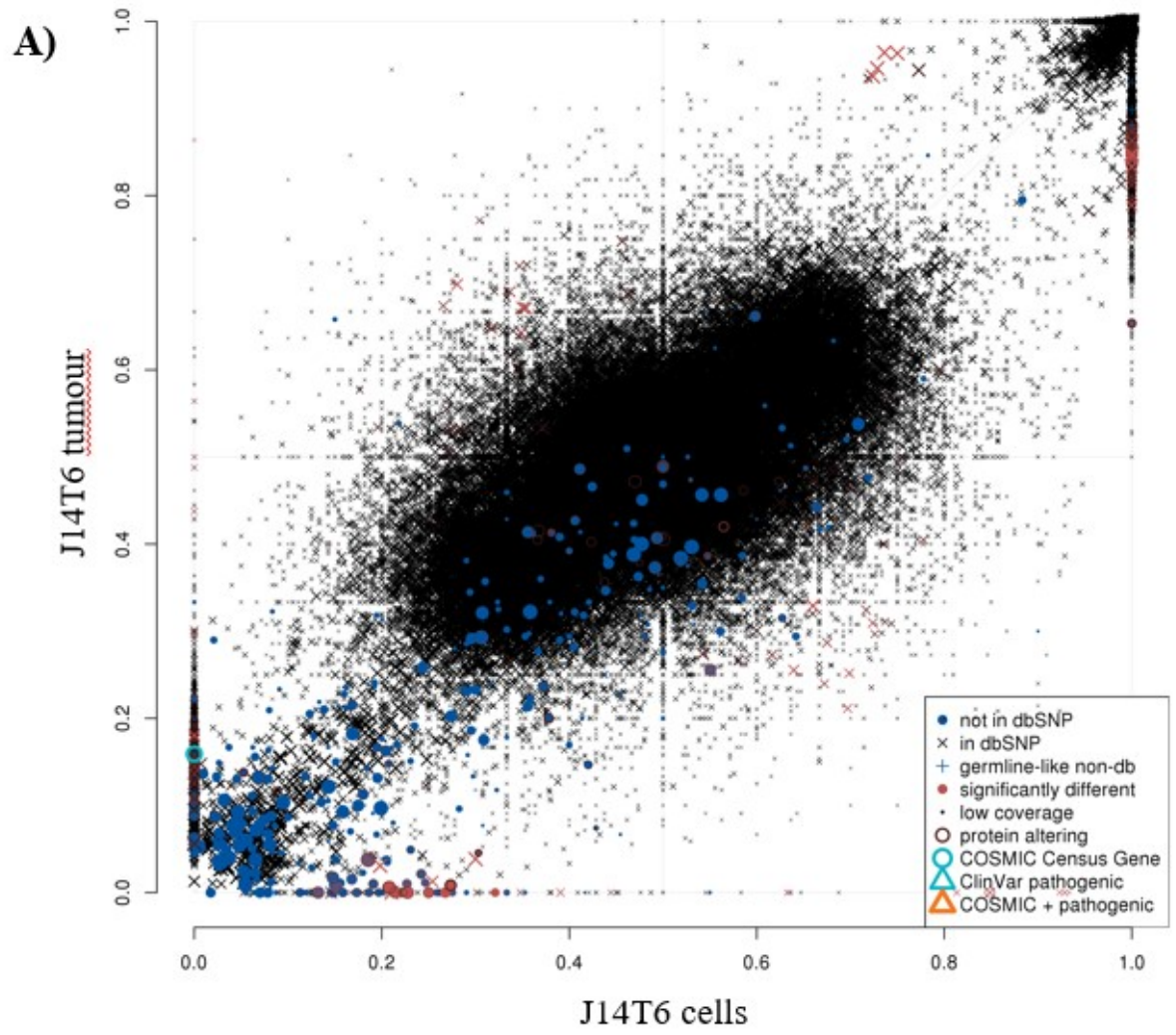

Figure 4.7 Comparison of J14 samples. A) VAF scatter plot comparing J14T6 tumour fragment and J14T6 patient-derived cell line. Red Xs indicate VAFs that are significantly different between two samples. Blue dots represent non dbSNPs (likely somatic SNPs). B) Copy number profiles for each J14 sample (next page).

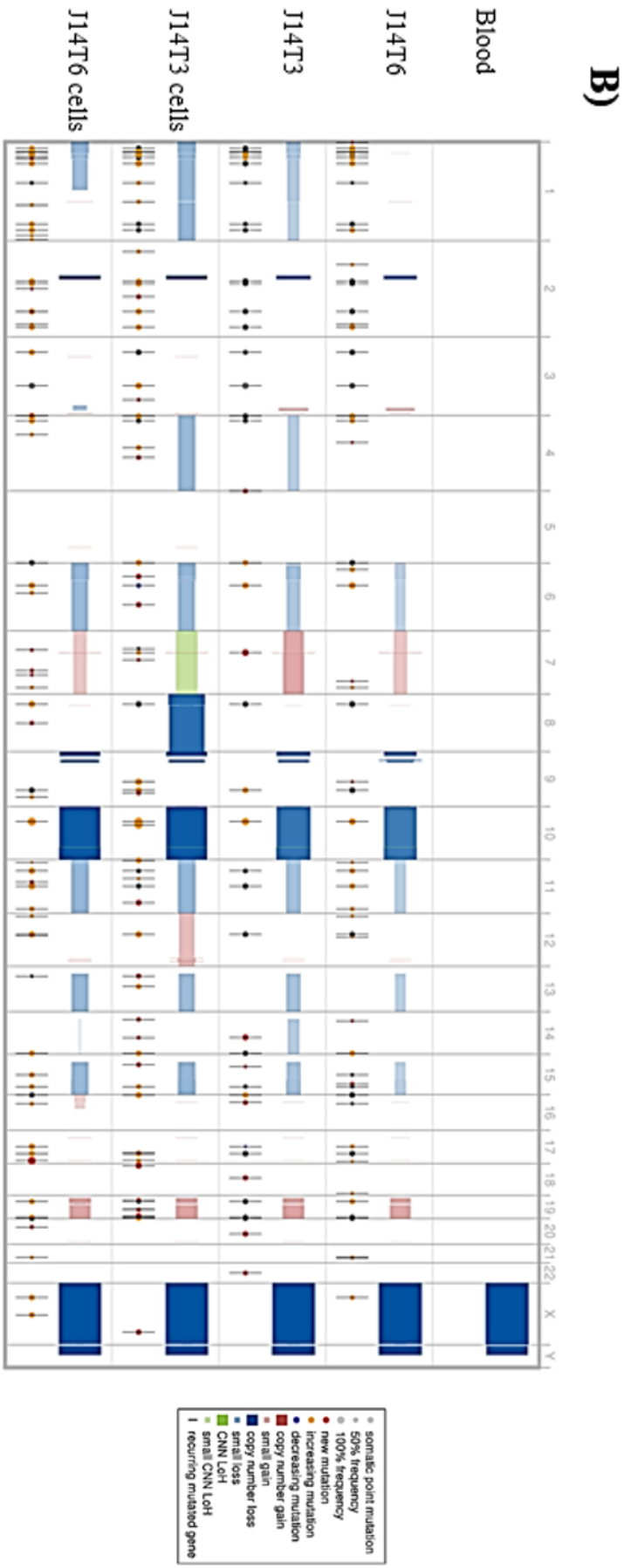
B)
Blood
J14T6
J14T3
J14T3 cells
J14T6 cells
1
2
3
4
5
6
7
8
9
10
11
12
13
14
15
16
17
18
19
20
21
22
X
Y
somatic point mutation
50% frequency
100% frequency
new mutation
increasing mutation
decreasing mutation
copy number gain
small gain
copy number loss
small loss
CNN LoH
small CNN LoH
recurring mutated gene

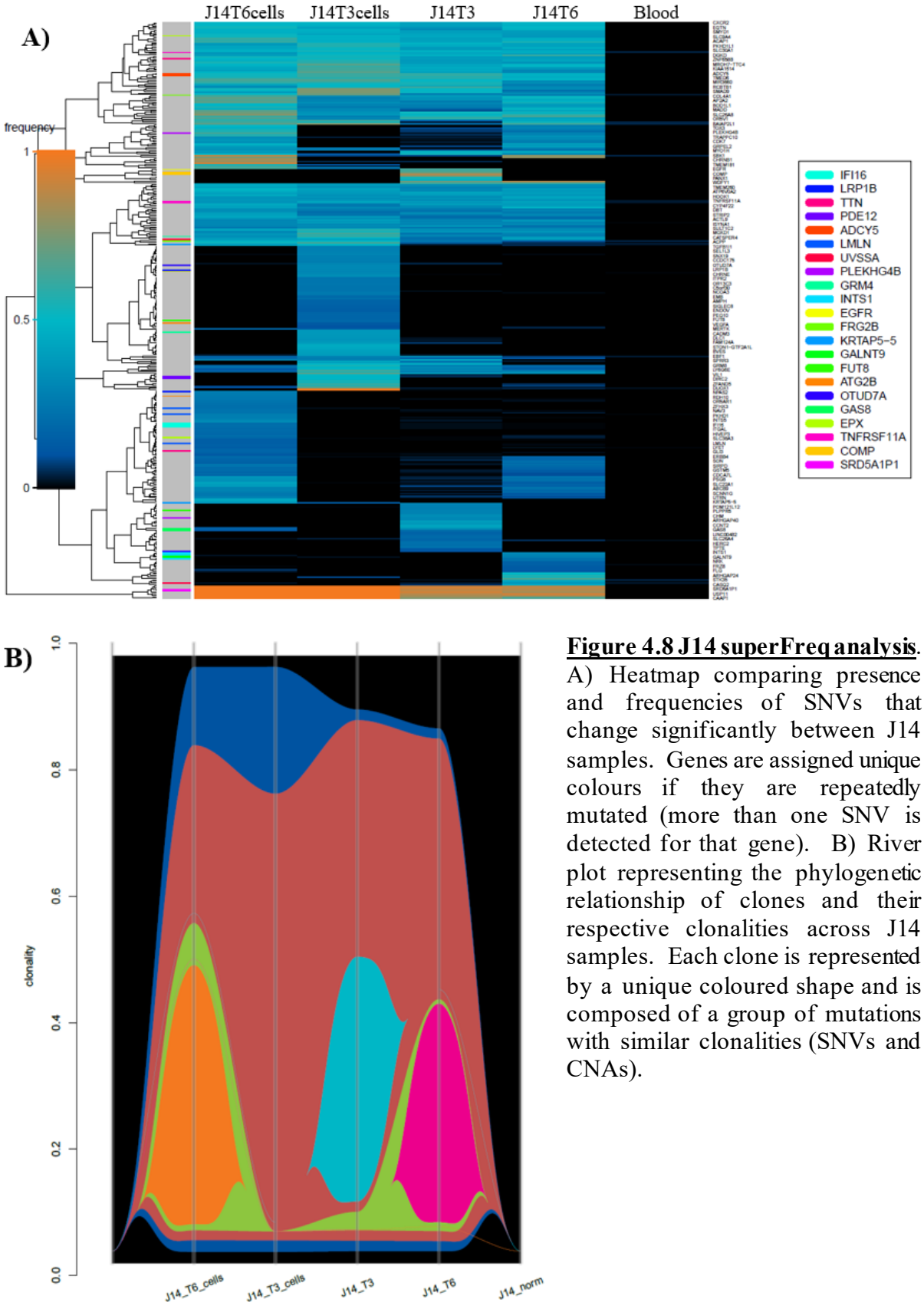

Figure 4.8 J14 superFreq analysis. A) Heatmap comparing presence and frequencies of SNVs that change significantly between J14 samples. Genes are assigned unique colours if they are repeatedly mutated (more than one SNV is detected for that gene). B) River plot representing the phylogenetic relationship of clones and their respective clonalities across J14 samples. Each clone is represented by a unique coloured shape and is composed of a group of mutations with similar clonalities (SNVs and CNAs).

4.2.3 γH2AX foci analysis

As an initial assessment of DNA repair competence, a component of intrinsic radiosensitivity, we analysed γH2AX foci. γH2AX foci correspond to radiation-induced DNA double strand breaks (DSBs) and their dispersal correlates with DSB repair (284,285). Because DSBs are the critical lesion in radiation-induced cell death, γH2AX foci can serve as a surrogate measure of radiosensitivity (286,287). Figure 4.9A demonstrates the average number of γH2AX foci counted for J3T1 and J3T4 cell lines at various time points after 2Gy of radiation (RT). Foci counts were compared to matched cells that received no treatment. J3T1 and J3T4 seem to be similar in DNA repair ability, particularly regarding their rates of dispersal (6 hr and 24 hr time points). There were no significant differences when comparing foci counts between the two J3 lines. Likewise, J14T3 and J14T6 display very similar repair competency based on similar foci counts between cell lines at each time point assessed (Fig. 4.9C). Again, no significant differences were found between the J14 lines. Only the two J7 lines exhibited differences in γH2AX foci counts (Fig. 4.9B). In particular, J7T1 harboured significantly more foci at the 1-hour post RT time point compared to J7T3 ($p=0.017$). In contrast, J7T3 harboured significantly more foci at the 24-hour post RT time point compared to J7T1 ($p=0.017$). The differences may suggest that J7T1 is initially more sensitive to increased DSB induction at 1 hr, but ultimately is better able to repair its DSBs (increased DSB dispersal at 24 hr). However, since there is discrepancy in the γH2AX foci trends between the two cell lines at early and late time points, the data may also suggest that overall, like J3 and J14, there are no clear differences between the J7 cell lines. While DNA repair for most cells is complete at 24 hours, as assessed by mean γH2AX foci, it may not be complete for cells with possible DNA repair pathway deficiencies or cells with lingering DSBs. If DSBs are not repaired properly, then the cell is likely to die and lose its clonogenicity. Therefore, a longer-term cellular assay which examines clonogenicity, such as a limiting dilution assay, is needed to better assess in vitro radiosensitivity.

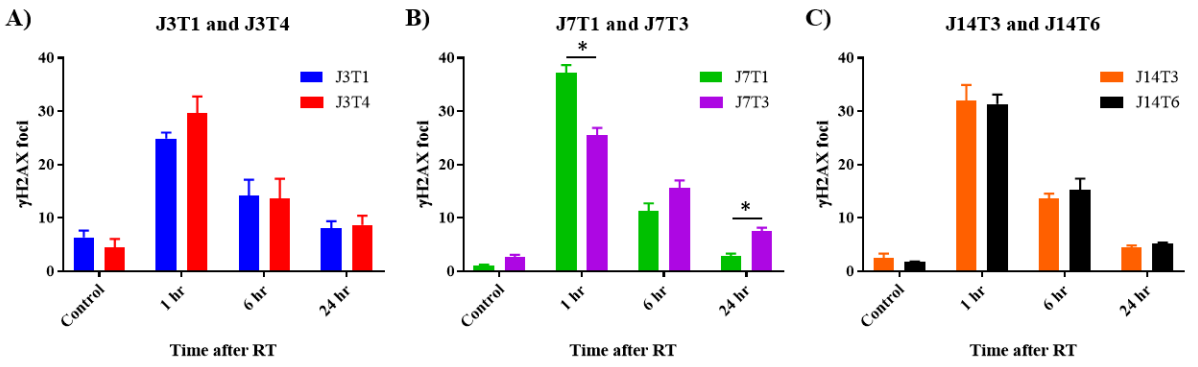

Figure 4.9 γH2AX foci analysis. Mean of γH2AX foci (with SE) for A) J3T1 and J3T4, B) J7T1 and J7T3, and C) J14T3 and J14T6. Foci were measured at various time points after 2Gy irradiation and also for untreated control samples. * $p < 0.05$

4.2.4 Limiting dilution assays

Limiting dilution assays (LDA) offer an alternative method for assessing in vitro radiosensitivity. Specifically, LDA determines the effects of radiation on clonogenicity, or the ability for cells to survive and continuously divide and grow into neurospheres. This longer term cellular assay reflects the two principal mechanisms of radiation-induced cell death: apoptosis and mitotic catastrophe (288). Clonogenic survival assays, the gold standard for in vitro radiosensitivity testing, also measure the consequences of radiation on clonogenic potential of cells. However, we found that several of our patient-derived cell lines were not amenable to clonogenic assays, thus necessitating the use of LDA. After adding serial dilutions of each cell line to 96-well plates, individual plates were irradiated (0-3Gy) and allowed to divide. After 2-3 weeks, the wells were scored as positive or negative, based on the presence of a neurosphere, and survival curves were constructed with ELDA: Extreme Limiting Dilution Assay online software (282). Figure 4.10A, B, and C display the stem cell frequency estimate curves generated with ELDA for the second replicates of J3T1 and J3T4, J7T1 and J7T3, and J14T3 and J14T6, respectively, as a function of cell number and radiation dose. Black, red, green, and blue lines correspond to 0, 1, 2, and 3Gy, respectively. The more parallel an individual line is with the y-axis, the higher the stem cell frequency for that condition and the lower the number of seeded cells needed to produce a positive, neurosphere-containing well. For each cell line, as more radiation was added, the stem cell frequency declined and wells with fewer seeded cells became less likely to be positive. J3T1 and J3T4 seem to have similar levels of stem cell frequency and thus clonogenicity after irradiation, as do J7T1 and J7T3.

These similarities in radiosensitivity are more easily visualised when the stem cell frequency estimates are converted to survival fractions by dividing the inverse of the ELDA-generated stem cell frequency estimate by the inverse of the stem cell frequency estimate of the control group (Fig. 4.10D). In contrast to J3 and J7, the survival curves for J14T3 and J14T6 suggests that there may be a difference in clonogenicity between the two J14 lines (Fig. 4.10D). J14T3 seems to have better survival and a corresponding increase in clonogenicity at each dose, but especially at 1Gy and 2Gy as the differences in surviving fractions at these doses are statistically significant ($p<0.05$).

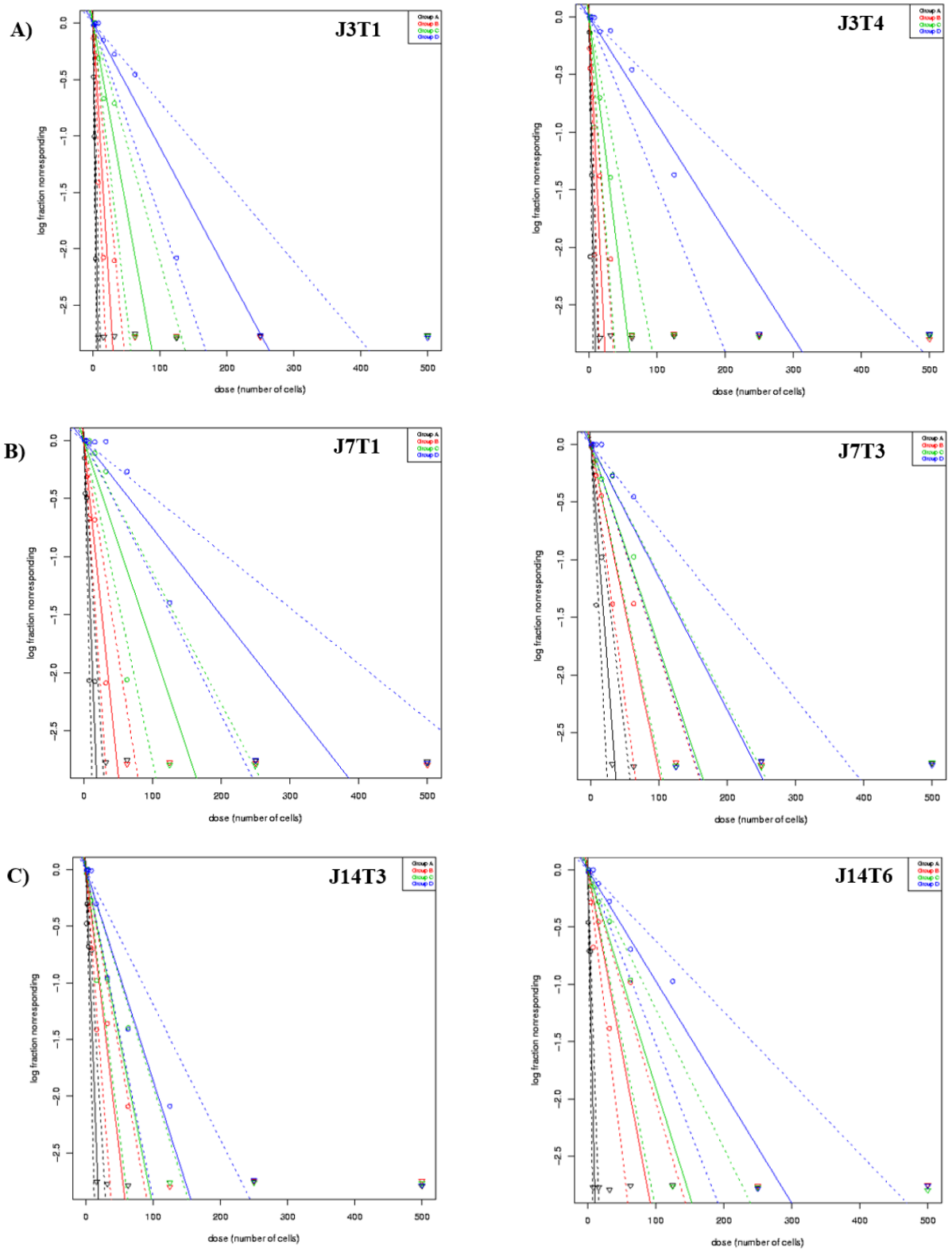
A)
J3T1
J3T4
B)
J7T1
J7T3
C)
J14T3
J14T6
log fraction nonresponding
dose (number of cells)
Group A
Group B
Group C
Group D

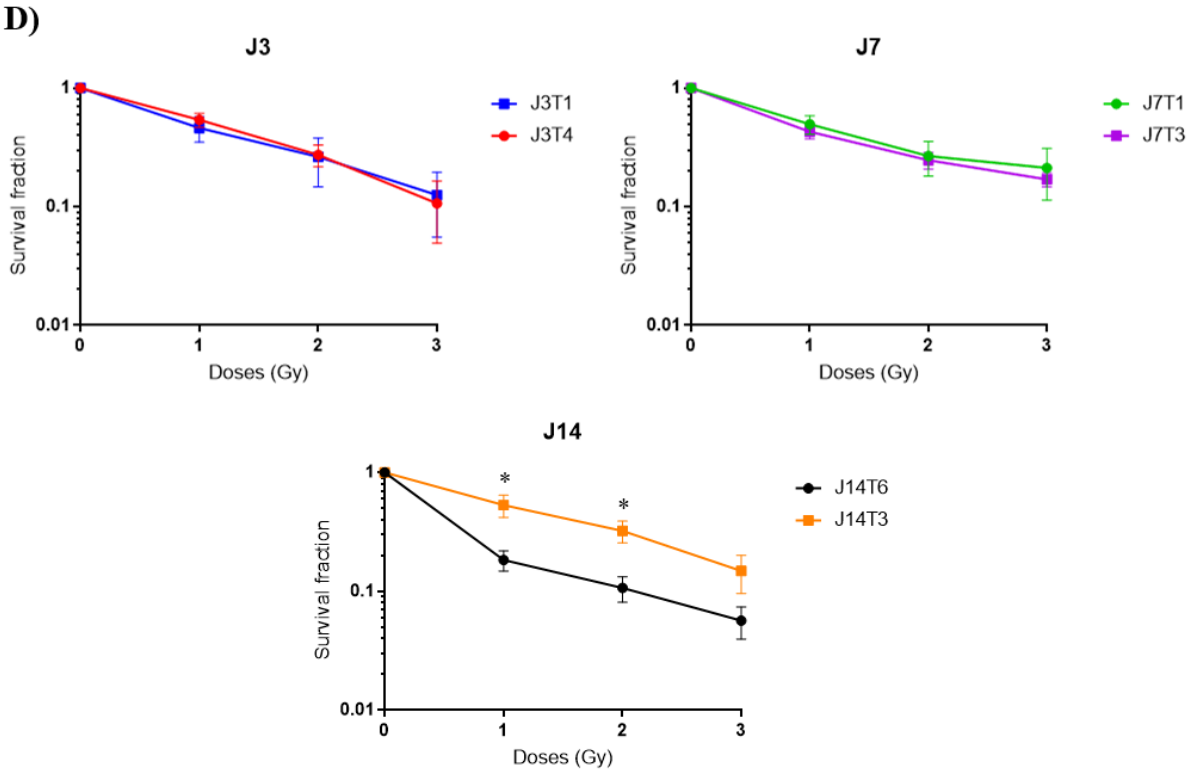

Figure 4.10 Limiting dilution assays. Stem cell frequency estimates (with confidence intervals) for A) J3T1 and J3T4, B) J7T1 and J7T3, and C) J14T3 and J14T6. Black, red, green, and blue lines correspond to 0, 1, 2, and 3Gy, respectively. D) Survival fraction as a function of radiation dose calculated from stem cell frequency estimates for J3, J7, and J14 cell lines. * $p<0.05$ by 2-way ANOVA.

J7 cell lines exhibited some differences by γH2AX foci analysis and J14 cell lines exhibited differences by LDA assay. Minor differences were also noted when comparing COSMIC mutational signatures and SNV profiles for these lines (Fig. 4.11). In addition to shared signatures, mutations in J7T1 cells mapped to signature 17 (unspecified aetiology), whereas mutations in J7T3 cells mapped to signature 6 (defective DNA mismatch repair) (Fig. 4.11A). Similarly, several genetic variants were detected in J7T1 samples (both cells and tumour) independent of J7T3 samples, and vice versa (Fig. 4.11B). While J14T3 and J14T6 cells had essentially the same COSMIC mutational signature profiles (Fig. 4.11C), they did possess variants that were unevenly distributed between sample types (Fig. 4.11D). The differences noted in COSMIC signatures and variant profiles provide further evidence for ITH between cell lines, which could contribute to the observed differences in radiosensitivity. When combining analysis of all tumours and lines, γH2AX DNA repair competence data was remarkably similar between lines (Fig. 4.12A). Beyond the previously noted differences in foci counts between J7T1 and J7T3, the only other statistically significant difference was between J3T1 and J7T1 at 1 hour after irradiation ($p<0.05$, 2-way ANOVA, multiple comparisons). In regards to LDA, all cell lines regardless of tumour of origin had a statistically significant difference in survival fraction after 1Gy compared to J14T6 (Fig. 4.12B; $p<0.05$, 2-way ANOVA, multiple comparisons). Additionally, J7T3 and J14T3 had a statistically significant difference in survival fraction after 2Gy. However, when taken together, differences in radioresponse between cell lines from the same tumour are not conserved across methods (Fig. 4.12A-B), suggesting that all cell lines from the same tumour tested may ultimately have relatively similar intrinsic radiosensitivities. Because of the overall complexity of radiosensitivity, there are many factors which could be contributing to the differences observed within and between individual assays such as LDA and γH2AX foci analysis, making it possible that these complex factors could cancel each other out. While these results may suggest that ITH does not translate to differences in radiosensitivity between different regions of the same tumour, future studies will need to interrogate other components of radiosensitivity, such as cell death and cell cycling, in order to develop a more holistic picture of the impact of ITH on radiosensitivity.

A)

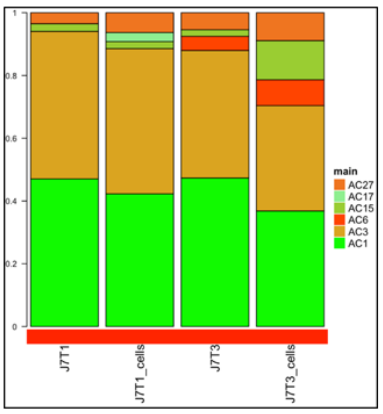

B)

Gene	SNV detected in J7T1	SNV detected in J7T3
CDH23	+	-
F5	+	-
FAM69A	+	-
LILRB2	-	+
PTEN	+	-
RASGEF1A	+	-
RNASE11	+	-
SCRIB	+	-
TRPA1	+	-
TTN	-	+

C)

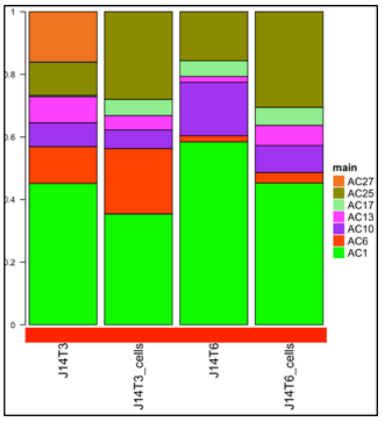

D)

Gene	SNV detected in J14T3	SNV detected in J14T6
EGFR	+	-
ARPP18	-	+
EPHBG	-	+
ERBB4	-	+
FAM124A	+	-
OR2D3	-	+
OR8G1	-	+
SCNN1G	-	+

Figure 4.11 COSMIC mutational signatures and SNV profiles. The relative contribution of mutations in A) J3 samples or C) J14 samples to pre-defined COSMIC signature profiles. Signatures were defined as positive when they had a cumulative normalized contribution over signature-specific cutoffs. B) Non-synonymous mutations differentially detected in J7T1 samples (cells and tumour) or J7T3 samples (cells and tumour). D) Non-synonymous mutations differentially detected in J14T3 samples or J14T6 samples.

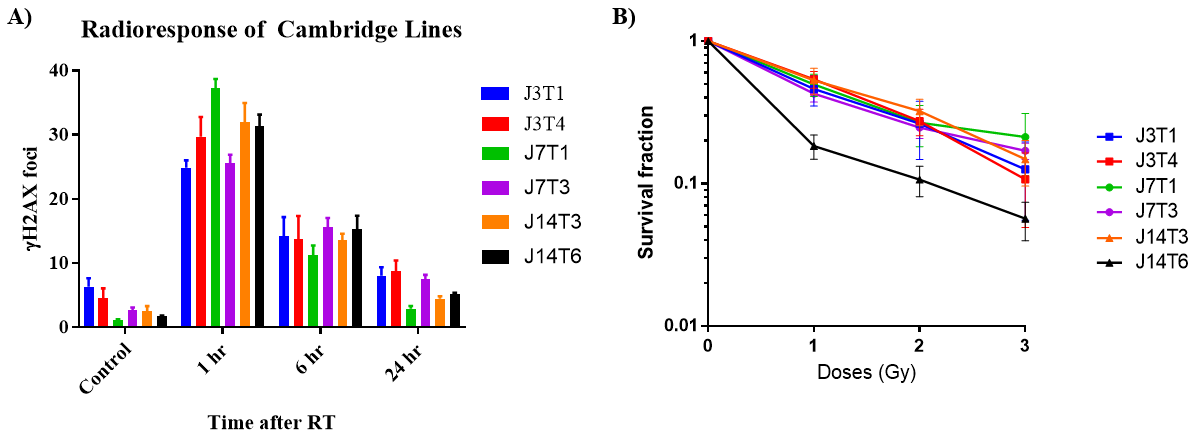

Figure 4.12 Intrinsic radiosensitivity. Combined radioresponse outcomes for all lines based on A) γH2AX foci analysis and B) limiting dilution assays.

4.3 Discussion

The goal of this study was to test the hypothesis that there are differences in intrinsic radiosensitivity between cells isolated from spatially distinct regions of human glioblastoma. Because ITH is thought to be a critical factor leading to GB resistance and recurrence, we utilised multiple cell lines derived from spatially distinct tumour samples as a model of GB ITH. Cell lines were derived from tumour fragments that were resected by 5-ALA fluorescence-guided surgery, a technique that has already been shown to capture ITH in both tissue samples (110) and patient-derived cell lines (136,247,250). In addition, patient-derived cell lines have been utilised for many types of cancer as effective models of the tumour of origin (289,290). While in vitro culturing can lead to phenotypic and genotypic changes of the cell lines over time (291-293), reflecting differences from the parent tumour, they have still proven an efficient model for studying cancer. Our WES results suggest that our patient-derived GB cell lines are good models of their parent tumours. In some cases (J14), the lines are also good models of the specific tumour fragment from which they were derived. Other cases demonstrated that the cell lines were more similar to each other in genetic alteration patterns than to their respective fragments. However, differences were observed between all samples from a given patient suggesting that ITH was preserved in the patient-derived cell lines. Therefore, our GB patient-derived cell lines represent viable models for studying the influence of ITH on radiosensitivity.

Patient-derived cell lines have been utilised extensively for studying cancer response to therapies, particularly chemotherapeutics and other drugs (289). Many large databases have been generated that combine cancer cell line genetic patterns and pharmacologic profiles to study response and resistance mechanisms (294,295). While many studies have centered around intertumour heterogeneity, there have also been studies that examine intratumour heterogeneity and its potential implications in cell lines (136,296). For glioblastoma, glioblastoma stem-like cells (GSCs) have been suggested as a potential source of ITH both in tumours and in cell lines (250,251). Such models of ITH are invaluable for efficiently studying potential heterogeneous responses to therapy. While the impact of ITH on differential drug sensitivity to some anti-GB agents have been performed (235,247,297-299), to our knowledge the influence of ITH on intrinsic radiosensitivity has not been previously addressed. Our results seem to indicate that only minor differences or even no differences in radiosensitivity may exist between cell lines derived from spatially distinct tumour samples. While differences were

observed in genetic alterations and clonal composition between samples, these differences, while reflecting ITH, may not contribute to significant differences in radiosensitivity.

If glioblastoma ITH does not have a significant impact on radiosensitivity, then it would suggest that spatially distinct tumour regions may have relatively uniform radioresponse. If this finding is applicable to the clinical setting, then the optimisation of radiotherapy, including treatment with radiosensitisers, would be expected to improve treatment outcomes for GB patients. It should be noted that this study was performed on treatment-naïve patient derived cell lines so the results may only be relevant in the primary disease setting. Therefore, the study of how radiation drives the evolution of GB may provide important insights on treatment resistance and recurrent GB biology. Ultimately, because ITH may not yield differential radiosensitivities, insights on treatment-induced evolution may lead to advances in treatment that improve radioresponse for the tumour as a whole.

Chapter 5. Radiation drives the evolution of orthotopic xenografts initiated from glioblastoma stem-like cells

Despite aggressive, multimodal treatment, glioblastoma inevitably recurs. Whereas the mechanisms mediating this consistent therapeutic resistance have not been defined, the clonal diversity and evolutionary dynamics inherent to GB is considered a major obstacle in the development of effective treatment (110,115,209,210,281). As previously mentioned, comparison of genomic data generated from glioma tissue obtained at initial surgery and at recurrence revealed an altered mutational profile, an effect that was attributed to temozolomide treatment (300). The implication of such studies is that the temozolomide driven evolution results in the emergence of resistant clones. Consistent with studies of clinical specimens, temozolomide treatment of mice bearing brain tumour xenografts initiated from GB primary cultures suggested the expansion of drug resistant clones (235). Given that GBs regrow after initial treatment, understanding the consequences of treatment-driven evolution may not only generate insight into the fundamental biology of recurrent GBs but also suggest novel therapeutic strategies.

While studies to date have focused on temozolomide (90,91,300), a role for radiotherapy as an independent driver of GB evolution has not been investigated. We have demonstrated that genetic diversity of cell lines derived from spatially distinct tumour fragments does not predict differences in in vitro radiosensitivity. However, in vitro radiosensitivity studies of treatment-naïve tumour-derived cell lines cannot address the ability of radiation to drive evolution. An in vivo model which provides microenvironmental context, mimics clinical radioresponse, and can be sampled after receiving either radiation or mock treatment is needed. Towards this end, orthotopic xenografts initiated from CD133+ GB stem-like cells (GSCs) would appear to provide a model system for testing the potential of radiation to influence GB evolution. As described, GSCs represent a clonogenic subpopulation considered to be critical in the development, maintenance and treatment response of GBs (241,242,245). Moreover, orthotopic xenografts grown from GSCs replicate the genotype, phenotype and in vivo growth pattern of GB (252). With respect to GB evolution, we have previously shown that CD133+ GSCs implanted into nude mice produce heterogeneous

tumours of differentiated cells while retaining a subpopulation of GSCs at morbidity (254). This GSC-initiated xenograft model has been utilised to demonstrate a role for the microenvironment in radioresponse (254) and the relative radioresistance of $CD133^+$ GSCs (266). Thus, the GSC xenograft model exhibits the intratumour heterogeneity and evolutionary dynamics that may simulate that of a GB in situ.

To investigate the potential of radiotherapy to influence GB evolution, the study described here defines the consequences of a fractionated radiation protocol on the growth pattern, clonal diversity and genomic architecture of GSC-initiated orthotopic xenografts. The data presented show that tumours that regrow after irradiation were less invasive and had different mutational signatures as compared to untreated tumours. In addition, based on viral integration site analysis (VISA), radiation exposure resulted in a reduction in intratumour heterogeneity (clonal diversity), an effect that was dependent on the brain microenvironment. These results indicate that radiation drives the evolution of the GSC-initiated orthotopic xenografts.

5.1 Methods for studying radiation-induced GB evolution

Methods for maintaining GSC (NSC11 and NSC20) and U251 human GB cell line cultures, initiating and irradiating brain tumour xenografts, and immunohistochemistry can be found in Chapter 3. Methods described below were specifically utilised for the study of radiation-induced GB evolution.

5.1.1 Viral Integration Site Analysis (VISA)

VISA was performed by Center for Cancer Research Genomics Technology Laboratory as described (301,302). Briefly, genomic DNA was sheared to an average size of 400bp and subjected to linker-mediated, nested PCR using a combination of long terminal repeat (lentivirus) and linker-specific primers. Illumina sequencing adaptors were added at the same time. The library was sequenced on Illumina MiSeq using 2x150bp PE reads. Integration site junctions were mapped to hg19 human reference genome. Insertion sites are expressed as a percentage of the total reads. To compare samples within an experiment, integration sites

detected in at least 2 of the samples were subjected to unsupervised hierarchical cluster analysis using R to visualise relative changes in clonal diversity.

5.1.2 Whole exome sequencing analysis: COSMIC and EXPANDS

Genomic DNA was subjected to WES and variant calling was performed with the CCBR pipeline as described in Chapter 3. COSMIC mutational signature analysis was performed with the YAPSA R package (v1.8.0) as described (212,303). The mutational catalogue was corrected to account for differences in triplet motifs between WGS and WES capture regions. Signature-specific cut-offs used can be found with the following R code: library(YAPSA), data(cut-offs), cutoffCosmicValid_rel_df[6,] (304). Tumour subpopulations were further defined using EXPANDS algorithm and R package (v2.1.2) with default parameters (305). EXPANDS determines cell-frequency probabilities by using copy number variation (CNV) and single nucleotide variant (SNV) allele frequencies to estimate the fraction of cells harbouring a SNV (SNVs and CNVs are filtered to remove variants on the X and Y chromosomes). SNVs are clustered and filtered based on cell-frequency probability distributions (305). For COSMIC and EXPANDS analyses variants were included when they were protein altering, present in at least 2 out of 3 replicates, and had vaf > 5%. All WES analysis done in collaboration with bioinformaticians within the Radiation Oncology Branch, National Cancer Institute, National Institutes of Health (Kristin Valdez and Dr. Uma Shankavaram).

5.2 Results

5.2.1 In vivo models of radioresponse

As a model system for investigating the impact of radiotherapy on GB evolution, orthotopic xenografts initiated from CD133+ GSC lines were used. While selection of cell populations prior to implant could potentially influence overall tumour heterogeneity or treatment response, it was necessary to start with a more homogeneous population with known in vivo growth dynamics and reproducible treatment responses. Since CD133+ GSCs have been shown to produce heterogeneous tumours and contribute to radioresistance, as previously discussed, this subpopulation of GSCs represent a good model for studying the impact of radiation on GB evolution. CD133+ GSCs were transduced with a lentivirus containing a bimodal expression vector fused with the bioluminescent protein ffLuc2 and fluorescent protein eGFP2 under UbC promoter control (LVpFUGQ-UbC-ffLuc2-eGFP2) (266). After in vitro expansion and confirmation of successful transduction by fluorescent microscopy and flow cytometry, cells were implanted into the right striatum of nude mice. At 21 days post-implant, upon reaching a size consistently detectable by BLI, tumour-bearing mice were randomised into treatment groups, control (mock) and 3x5Gy. As shown in figures 5.1A and B, this fractionated irradiation protocol resulted in significant survival increases for NSC11 or NSC20 tumour-bearing mice. This survival advantage was consistent with the delay in growth rate reflected by BLI as a function of time after irradiation (figures 5.1C-F). Given that 3x5Gy initiated at day 21 post-implant significantly delays tumour growth yet does not achieve curative effects, a situation not unlike that typically observed in clinic, this treatment protocol was used to test the hypothesis that radiation drives the evolution of GSC-initiated brain tumour xenografts.

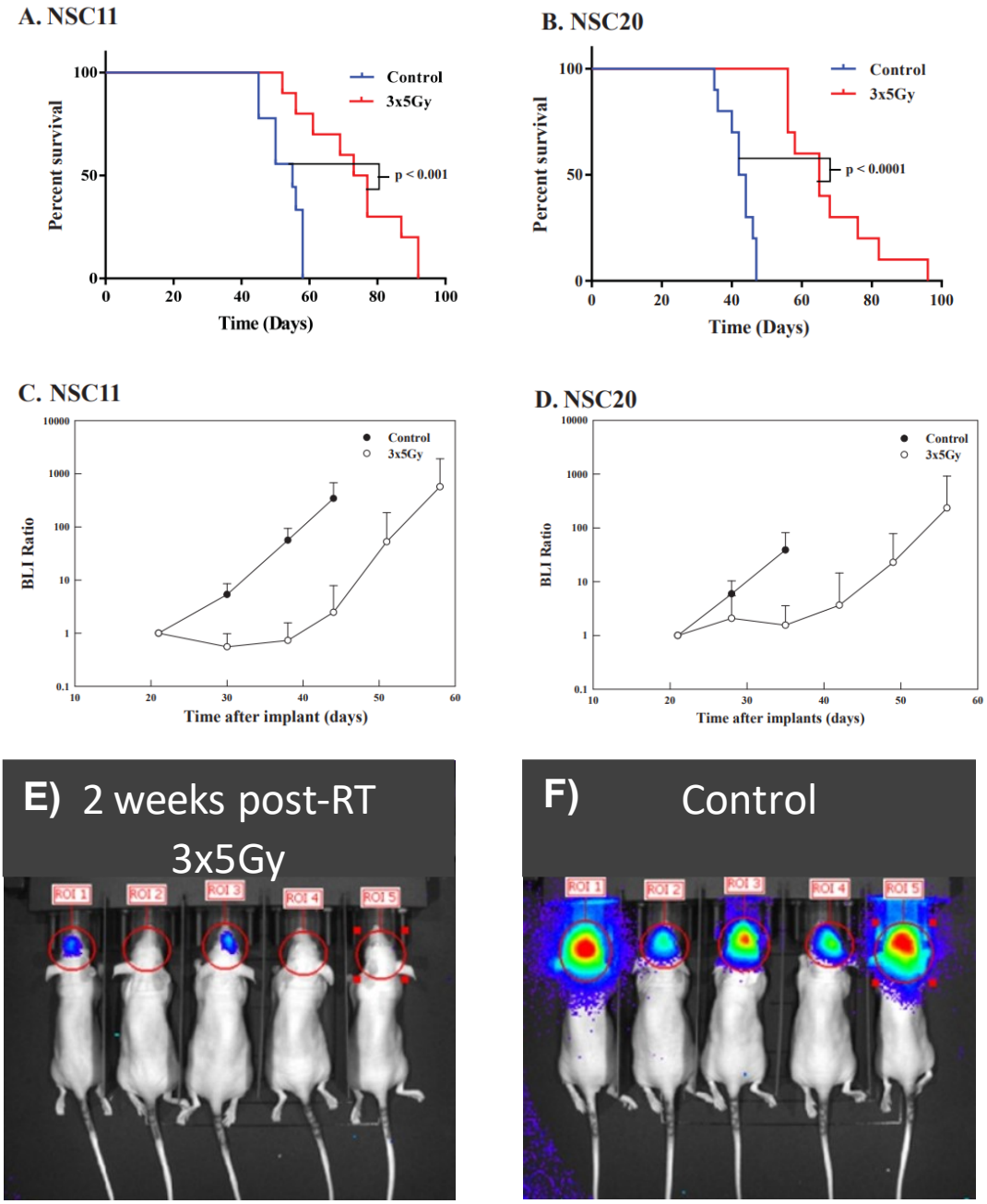

Figure 5.1 Radioresponse of GSC-initiated xenografts. On day 21 post-implant mice were randomised and treatment initiated the following day as described in text (3x5Gy). Kaplan–Meier survival curves were generated for A) NSC11 and B) NSC20 tumour-bearing mice (n=10 mice per group). Tumour growth defined by BLI ratio as a function of time after irradiation for C) NSC11 and D) NSC20. Representative images of NSC11 tumour-bearing mice two weeks after treatment for irradiated (E) and untreated (F) mice.

5.2.2 Radiation-induced changes in morphology and histology

As an initial assessment of the potential for radiation to influence GB evolution, the growth patterns of control and irradiated GSC xenografts were compared at morbidity. GSCs engineered to express GFP can be visualised in tumour-bearing brains using a stereomicroscope. Representative images (Fig. 5.2A) of control mice demonstrate GFP signal from NSC11 or NSC20 cells extends anteriorly and posteriorly throughout most of the right hemisphere, well beyond the right striatum implantation site, reflecting a highly invasive tumour. However, in irradiated mice, GFP fluorescence was more restricted and limited primarily to the anterior portion of the hemisphere. To determine whether these observations extended to the histological level, right hemisphere sagittal sections from control and irradiated NSC11 and NSC20 bearing brains were evaluated for human SOX2 staining, which is highly expressed in both lines. As shown in Figure 5.2C, GSCs in control mice were diffusely distributed with poorly defined margins and grey and white matter infiltration. In mice that received fractionated radiation, tumours were less invasive with more clearly demarcated borders and tumour core hypercellularity as compared to controls. While indicative of a reduced invasive propensity, in broader terms these results suggest that the fundamental biology of GSC-initiated tumours that regrow after irradiation diverges from that of untreated tumours. As a possible explanation, we hypothesised that morphological/histological modifications detected in recurrent xenografts reflected the radiation-induced selection of tumour cell subpopulations, i.e., radiation-driven evolution.

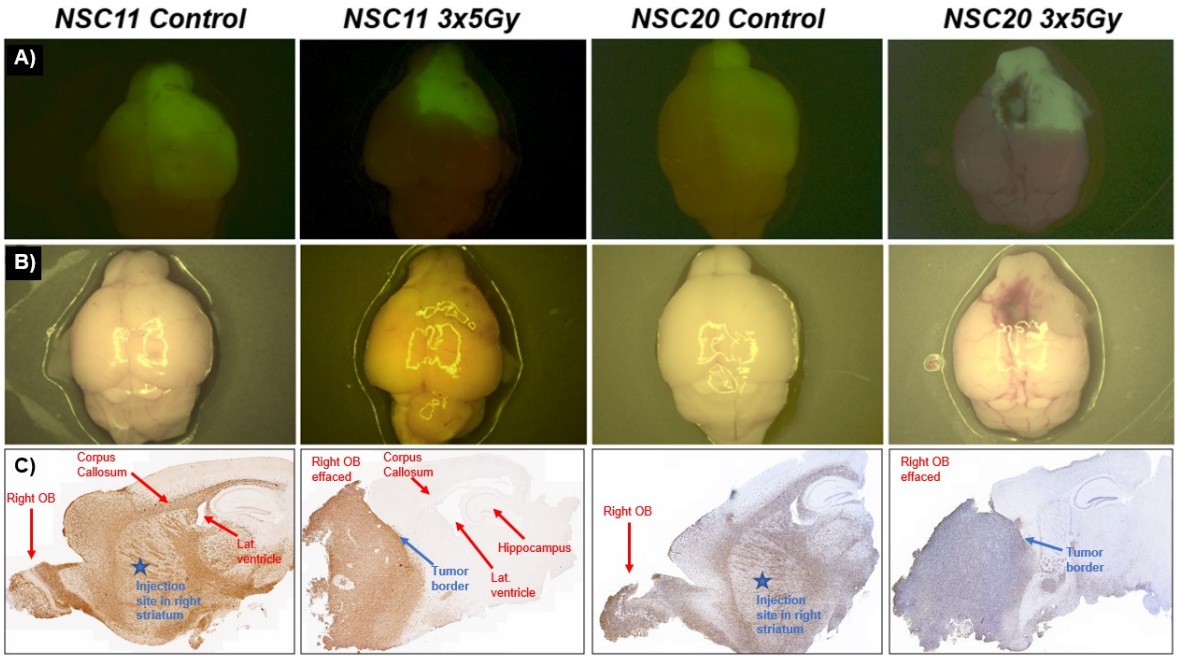

Figure 5.2 Morphology and histology of NSC11 and NSC20 tumours. A) Representative GFP fluorescence images of control and irradiated (3x5Gy) tumour-bearing brains at morbidity. B) Corresponding bright field images. Photos were taken on a stereoscope at 2.5x magnification. C) Right hemisphere sagittal sections at plane of injection site stained for SOX2 (magnification 20x).

5.2.3 Viral Integration Site Analysis

To directly address the question as to whether radiation modifies the clonal diversity (i.e., intratumoral heterogeneity) of GSC-initiated xenografts, viral integration site analysis (VISA) was used (301). Facilitating the application of VISA, these in vivo studies have centered on the use of GSCs transduced with the lentivirus LVpFUGQ-UbC-ffLuc2-eGFP2, which, as discussed above, allows for in vivo tumour growth monitoring and ex vivo visualisation. In addition to these attributes, the stable integration of the lentivirus into the genome at essentially random sites provides a unique tag for each cell in the transduced population, which is inherited by subsequent daughter cells. Because the integration site is largely within a transcriptional unit, sequencing of PCR amplified genomic DNA surrounding the lentiviral sequence allows for assigning each site to a single location/gene or nearest gene. Identifying the gene thus merely provides a method for easily cataloguing the integration site. The percent reads for a given gene/site corresponds to the size of the clone within the transduced population.

For this experiment CD133+ NSC11 cells were transduced with the described lentivirus; the culture was expanded and used for orthotopic implantation or collected for in vitro (IV) VISA. At 21 days post-implant, as for the survival studies, mice were randomised according to BLI into 2 groups: control (ic) and irradiated (icRT, 3x5Gy). At morbidity, mice were euthanised, GFP-expressing brain tissue grossly dissected, and DNA was extracted for VISA. The % reads detected at a given integration site (clonal frequency) were visualised for the individual xenografts and in vitro cultures in the heat map shown in figure 5.3A. As compared to NSC11 cells grown in vitro, there was a reduction in the number of clones detected (unique integration sites) in each of the 4 untreated xenografts (ic), suggesting a selection for clones that preferentially grow under in vivo orthotopic conditions. Moreover, as compared to the untreated tumours (ic) there was a further reduction in the total number of individual clones detected in the 4 xenografts that had been irradiated (icRT).

VISA and unsupervised hierarchical cluster analysis of clonal frequency were also performed on NSC20 samples (Fig. 5.3B). Although there was variability between xenografts in the control (ic) and irradiated (icRT) groups, as compared to NSC20 in vitro cultures, there was a reduction in clonal diversity in each of the orthotopic xenografts, with a further reduction evident in the irradiated tumours, similar to NSC11. The VISA results were also expressed in figures 5.3C-D as the average number of unique integration sites detected in each experimental

group. As shown, the largest number of integration sites was detected under in vitro conditions, which was reduced in orthotopic xenografts and further reduced after irradiation of xenografts. These results suggest that only a subset of the NSC11 and NSC20 cells proliferating in vitro will form a tumour after orthotopic implantation. Moreover, of those clones that grow orthotopically, after irradiation there is an additional reduction in clonal diversity, which is consistent with radiation-driven tumour evolution.

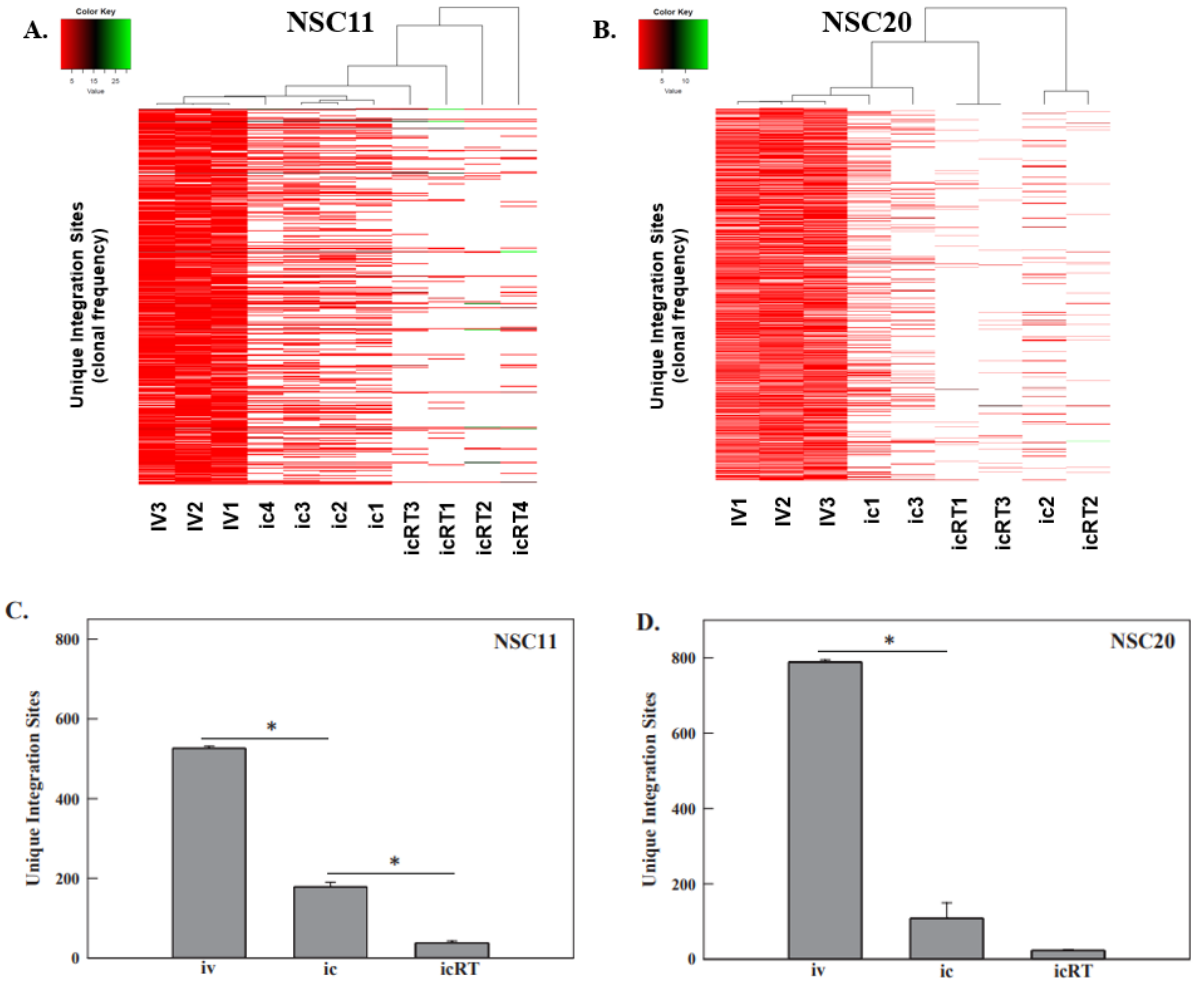

Figure 5.3 Viral Integration Site Analysis of NSC11 and NSC20. VISA comparing GSCs in vitro to those grown as intracerebral xenografts that had received mock treatment (ic) or 3x5Gy (icRT). Treatment protocol is as described in text. Unsupervised hierarchical cluster analysis of integration sites detected in A) NSC11 and B) NSC20. The absence of colour indicates the clone was not detected in a given sample (≤0.001% of total reads). The number of unique integration sites (mean ± standard error) detected by VISA in C) NSC11 and D) NSC20 samples. Because there was overlap of sites within each group, sites shared between samples of a given group were counted only once. * $p < 0.05$

To investigate the role of the microenvironment in the radiation-induced reduction in clonal diversity, VISA was performed on NSC11 cells irradiated in vitro. Twenty-four hours after plating, cultures received either mock (control), 4Gy (single dose), or 3x2Gy. Cells were harvested for VISA when they reached 70-80% confluency, which corresponded to 7, 19 and 21 days for control, 4Gy and 3x2Gy, respectively. Clonogenic survival analysis showed that the surviving fraction of NSC11 cells exposed to 4 Gy and 3 x 2 Gy was 0.008 ± 0.004 and 0.039 ± 0.031 (mean ± SEM, n = 3), respectively. As shown in Figure 5.4A, cultures did not cluster according to treatment group. Moreover, there was no significant difference in the average number of integration sites among the 3 groups (Fig. 5.4B). These results suggest that, in contrast to the orthotopic model, in vitro irradiation had no detectable effect on clonal diversity. These data suggest that the radiation-induced reduction in clonal diversity is dependent on the in vivo microenvironment.

To determine whether radiation-driven evolution was limited to xenografts initiated from GSCs and to further interrogate the role of the brain microenvironment, VISA was applied to the established glioma cell line U251. In this experiment, lentivirus transduced U251 cells were grown as intracerebral (ic) xenografts and as subcutaneous (SC) leg tumours. At 6 days after ic (when tumours were detectable by BLI) and 18 days after sc implantation (150-200 mm^3), U251 tumours received 3Gy for 3 consecutive days (3x3Gy), a regimen previously demonstrated to give a reproducible survival benefit for U251 xenografts. Irradiated and control ic tumours were collected at morbidity and sc tumours when the volume exceeded $1500mm^3$. Unsupervised hierarchical cluster analysis of the clonal frequency of the tumour samples as compared to U251 grown in vitro is shown in figure 5.4C with the average number of integration sites in each group shown in 5.4D. Whereas there was no consistent difference between control ic and sc tumours, the number of integration sites were reduced in each compared to U251 in vitro, although not to the degree as observed for the GSC ic tumours. In response to irradiation, the number of integration sites in sc tumours is reduced suggesting a decrease in clonal diversity. However, in ic U251 tumours irradiation induced a greater reduction in integration sites, suggesting that the radiation-mediated reduction in clonal diversity is not limited to xenografts initiated from GSCs. Moreover, these results suggest that the brain microenvironment plays a critical role in radiation-driven evolution of GB xenografts.

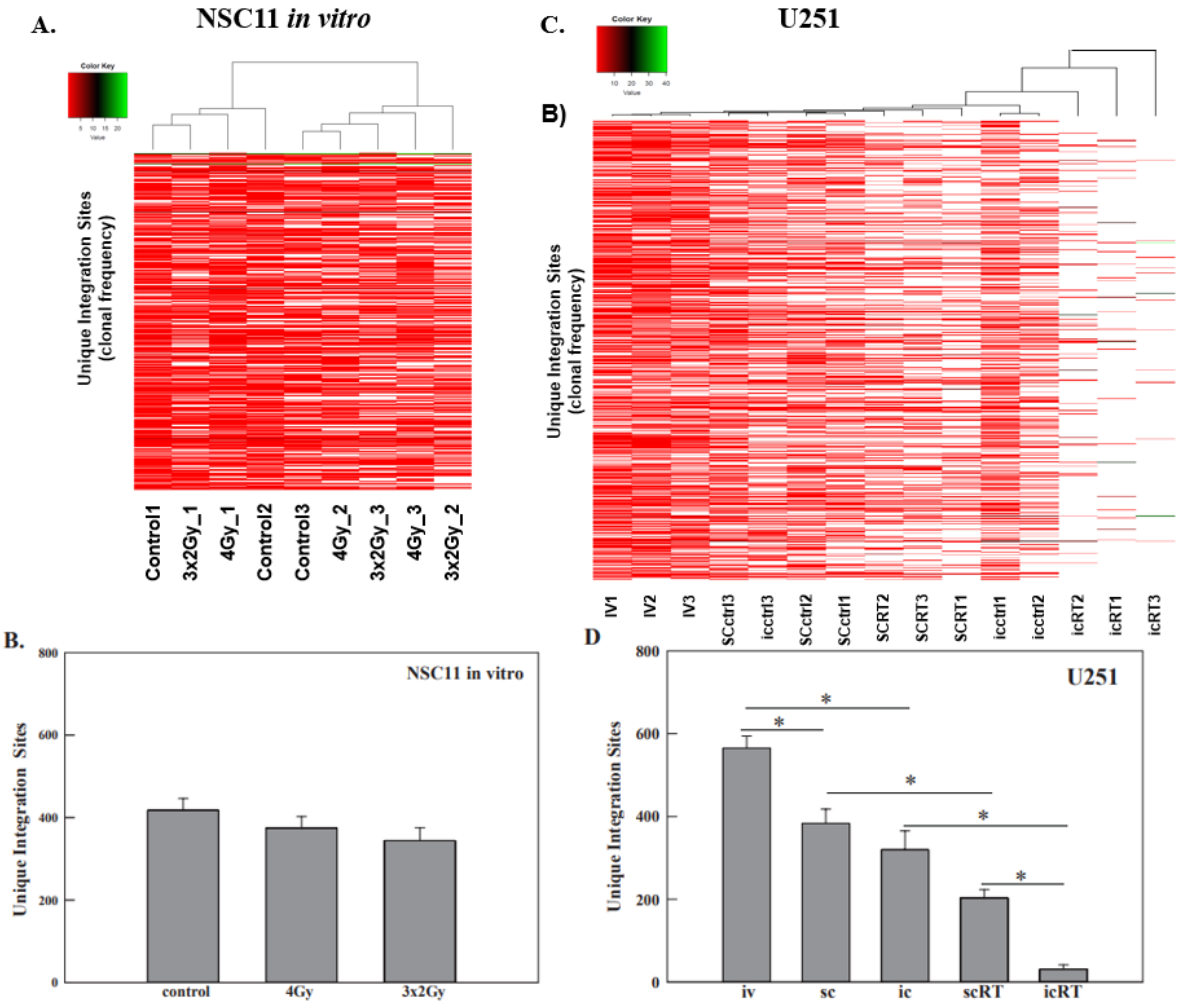

Figure 5.4 Viral Integration Site Analysis of NSC11 in vitro and U251. U251 cells were grown in vitro (IV) and as subcutaneous (SC) and intracerebral (ic) xenografts. A) Unsupervised hierarchical cluster analysis of integration sites detected in NSC11 cells that were untreated (control) or irradiated with a single dose of 4Gy or 3 daily doses of 2Gy (3x2Gy) B) Unsupervised hierarchical cluster analysis of U251 cells. U251 xenografts (sc and ic) received 3x3Gy as described in text. IV samples were initiated from the same pool of cells used for sc and ic implantation and collected when 70-80% confluent. C) Number of unique integration sites (n=3, mean ± standard error) detected in NSC11 in vitro. D) Number of unique integration sites (n=3, mean ± standard error) detected in U251 cells. * $p < 0.05$

5.2.4 Whole exome sequencing

Because investigations of tumour evolution typically apply WES to describe genetic ITH, this approach was used to evaluate the potential for radiation-driven evolution of GSC-initiated orthotopic xenografts. Genomic DNA extracted from morbid tumour samples were utilised for WES, similar to VISA experiments. Over 5500 SNVs + indels were detected in NSC11 tumours of which the majority were shared between control and irradiated tumours (Fig. 5.5A). Variants unique to control or irradiated tumours (private mutations) were consistently detected among the 3 samples in each group (Fig. 5.5B). The shared and private mutations in control and irradiated tumours were classified according to the mutational signatures generated from patient characteristics within large cancer cohorts using COSMIC mutational signature profiling (211,212,306). As shown in Figure 5.5C, the shared mutations distributed to mutational signatures 1 (Deamination of 5-methylcytosine), 5 (unspecified aetiology), 11 (TMZ treatment), 20 (Concurrent POLD1 mutation and mismatch repair deficiency) and 26 (Defective DNA mismatch repair). Mutations unique to control tumours associated with similar signature profiles. However, private mutations found in irradiated tumours did not include signatures 1, 5, and 20, but mapped to signatures 3 (Defective HR DNA repair: BRCA1/2 mutation), 6 (Defective DNA mismatch repair), and 15 (Defective DNA mismatch repair), which were not associated with the unirradiated tumours. These results suggest the emergence of different subpopulations in irradiated samples as compared to control NSC11 tumours.

These analyses were also performed on WES data generated from control and irradiated NSC20 tumours (Figure 5.6). In NSC20 tumours over 6000 SNVs + indels were detected with most of the variants shared between control and irradiated tumours with a similar number of private mutations detected only in control or irradiated NSC20 tumours (figures 5.6A-B). Using the shared mutations between control and irradiated NSC20 tumours the mutational signatures identified were similar to those in NSC11 tumours (signature #s 1,5,11,20,26) (Fig. 5.6C). In contrast, the signatures defined using the private mutations found in irradiated NSC20 tumours corresponded to increases in signatures 5 (unspecified aetiology) and 19 (unspecified aetiology) and decrease in signature 11 (TMZ treatment). Whereas these signatures were substantially different from those identified for irradiated NSC11 tumours, as for NSC11, these analyses suggest that irradiation modified the subpopulations comprising NSC20 tumours, consistent with radiation-driven evolution.

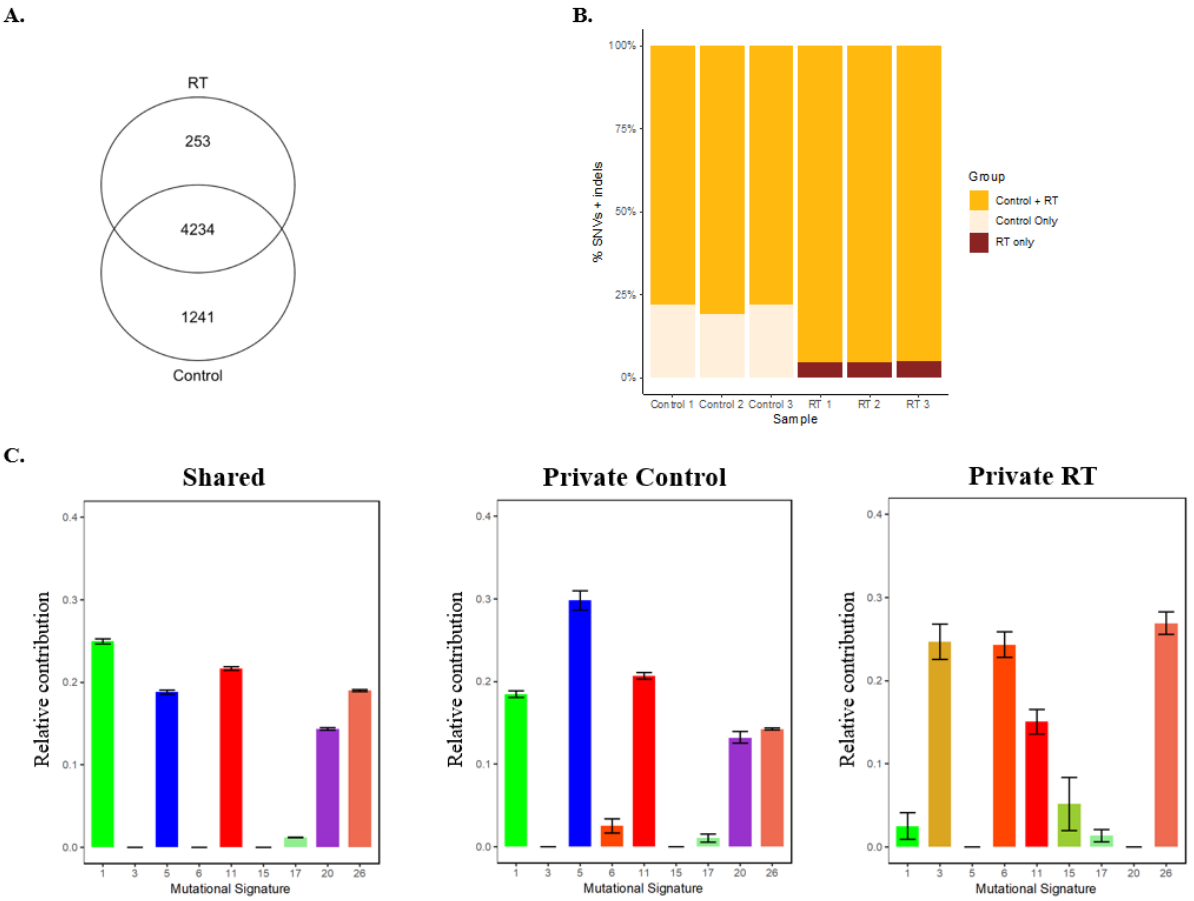

Figure 5.5 The influence of radiation on mutations detected in NSC11 xenografts. On day 21 post-implant, brain tumours (n=3) were exposed to 3x5Gy (RT) or mock irradiated (control) and collected for WES at morbidity. A) Venn diagram comparing the number of mutations between treatment groups. B) The relative percentage of shared or private variants for each tumour (control and treated). C) The relative contribution of shared and private mutations in control and irradiated tumours to pre-defined COSMIC signature profiles (211,212). Signatures were defined as positive when they had a cumulative normalised contribution over signature-specific cutoffs. In A and C, variants were included if they were protein-altering, were present in at least 2 out of 3 replicates, and had vaf > 5%.

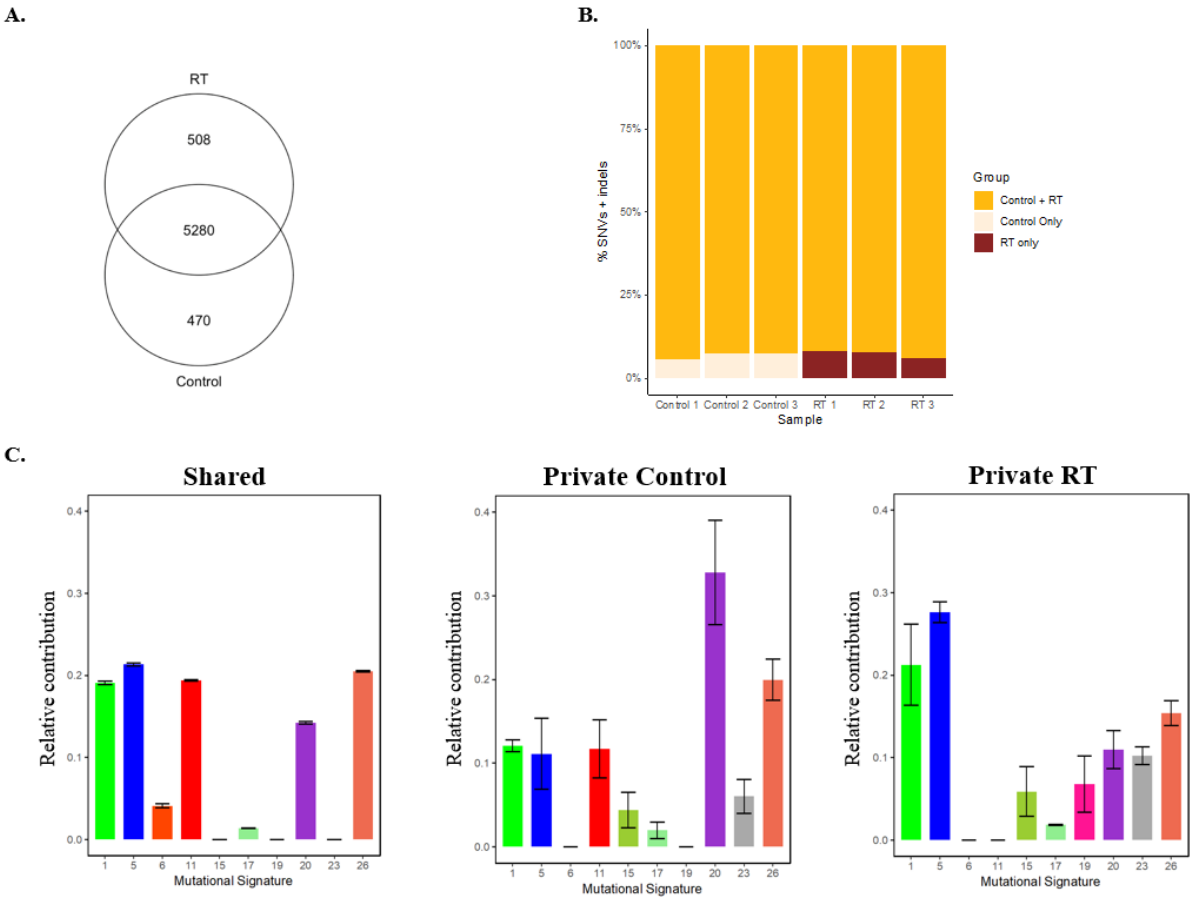

Figure 5.6 The influence of radiation on mutations detected in NSC20 xenografts. Treatment as in Figure 5.5. A) Venn diagram comparing the number of mutations between treatment groups. B) The relative percentage of shared or private variants for each tumour (control and treated). C) The relative contribution of shared and private mutations for control and irradiated tumours to pre-defined COSMIC signature profiles. Signatures were defined as positive when they had a cumulative normalised contribution over signature-specific cutoffs.

To investigate the effects of radiation on xenograft subpopulation heterogeneity in more detail, the bioinformatics tool EXPANDS was applied to the WES data set. EXPANDS utilises VAFs and copy number data to estimate cell-frequency probabilities (305). For this analysis, variants that were detected in at least 2 of the 3 replicates per group (control and RT) were included. Figure 5.7A depicts the 10 predicted subpopulations found in control and irradiated NSC11 tumours with the largest subpopulation (blue) at the bottom of the graph; each black dot corresponds to a variant predicted to be in a subpopulation. The lines indicate whether a specific variant in control tumours appeared in a subpopulation of the same ranking in the irradiated tumours or whether it had moved to another ranking. Whereas the majority of variants are conserved between the largest subpopulations of control and irradiated tumours (as depicted by straight lines), there was also a considerable amount of shifting from control tumours to a subpopulation of a different prevalence in irradiated tumours, which is especially apparent in comparisons of the smaller subpopulations (top of figure). Figure 5.7B shows 13 predicted subpopulations for NSC20 tumours. Again, the largest, most prevalent subpopulation (blue) is at the bottom of the graph. Similar to NSC11, while the majority of variants are conserved within the largest subpopulations, there is still substantial subpopulation shifting for variants between control and irradiated tumours.

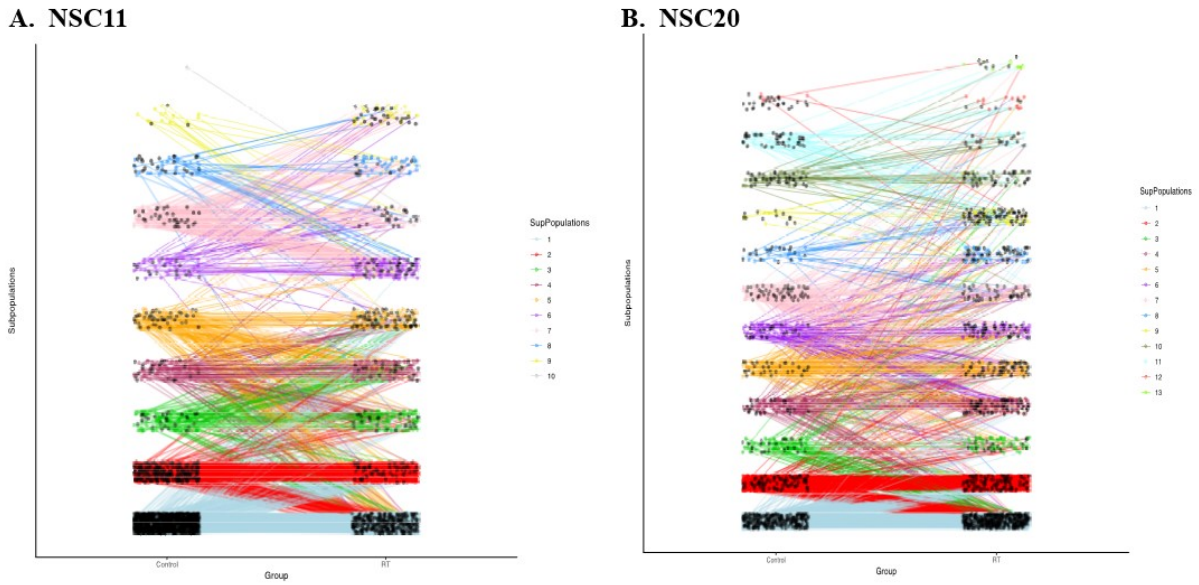

Figure 5.7 Influence of radiation on subpopulation dynamics. Orthotopic xenografts were treated and collected for WES as described in previous figures. Overall variant shifts within defined subpopulations of control and irradiated A) NSC11 and B) NSC20 tumours. The size of the subpopulations corresponds to its position on the y-axis, with the largest subpopulation at the bottom. The black circles correspond to individual variants.

These analyses were extended to driver gene mutations previously associated with GB (50,74,307,308). Initially, as shown in figures 5.8A-B, variants in driver genes were identified in each of 3 control and 3 irradiated GSC xenografts and classified as clonal (present in largest subpopulation), subclonal (present in smaller subpopulation), or both (multiple mutations for a given gene were individually found in both clonal and subclonal populations). In NSC11 tumours (Fig. 5.8A), multiple driver gene mutations were consistently lost in irradiated tumours, including AKAP9, FN1, SOX2, and SPTA1. There were also mutations that shifted in clonal status from control to irradiated tumours such as MAP4K3. Although there was more variability between individual tumours within control and irradiated groups, irradiation also resulted in changes in driver gene mutations detected in NSC20 tumours (Fig. 5.8B). Lost consistently after irradiation of NSC20 tumours were mutations in PIK3CA and CARM1. To further interrogate the observed GB driver gene mutation patterns, potential correlations between mutation changes after RT and survival and tumour growth were explored. Of the tumours that underwent WES, NSC11 RT1 and NSC20 RT1 were found to have the shortest survival for their tumour types, while NSC20 RT3 had the longest survival (Fig. 5.9A). NSC20 RT1 also had a noticeably faster growth rate compared to the other two irradiated NSC20 xenografts (Fig. 5.9B). Loss of TP53 mutation after RT was observed for both the NSC11 short survival tumour and the NSC20 long survival tumour and thus may not be correlated with survival (Fig. 5.9C). However, the loss of MEN1 and PIK3R1 mutations were observed for the NSC20 short survival tumour only which may suggest that these mutations could be beneficial for prolonged tumour survival. These data suggest that irradiation influenced the presence and clonality of GB driver mutations.

The shifts of these GB driver gene mutations between the previously defined subpopulations were then assessed (only subpopulations containing a GB driver gene variant were included). As in the overall WES data (Fig. 5.7A), the majority of NSC11 GB driver gene mutations were conserved within the largest subpopulations in control and irradiated samples (Fig. 5.8C). However, there were several mutations that became less prevalent after irradiation (for example, lines from control subpopulation 1 to RT subpopulations 2 and 4). There was also one mutation that become more prevalent after irradiation (line from control subpopulation 5 to RT subpopulation 1), suggesting that this particular subclone may have had a better survival rate after radiotherapy. Figure 5.8D displays similar subpopulation dynamics for NSC20 tumours, although more variant shifts between subpopulations were noted for NSC20 compared to NSC11, including at least 3 variants that increased in prevalence after

treatment. Changes in the distribution of mutations as a function of subpopulation size between control and irradiated tumours are consistent with subclone expansion and contraction, i.e. subpopulation evolution. Taken together, WES data support the radiation-driven evolution of orthotopic xenografts initiated from GSCs.

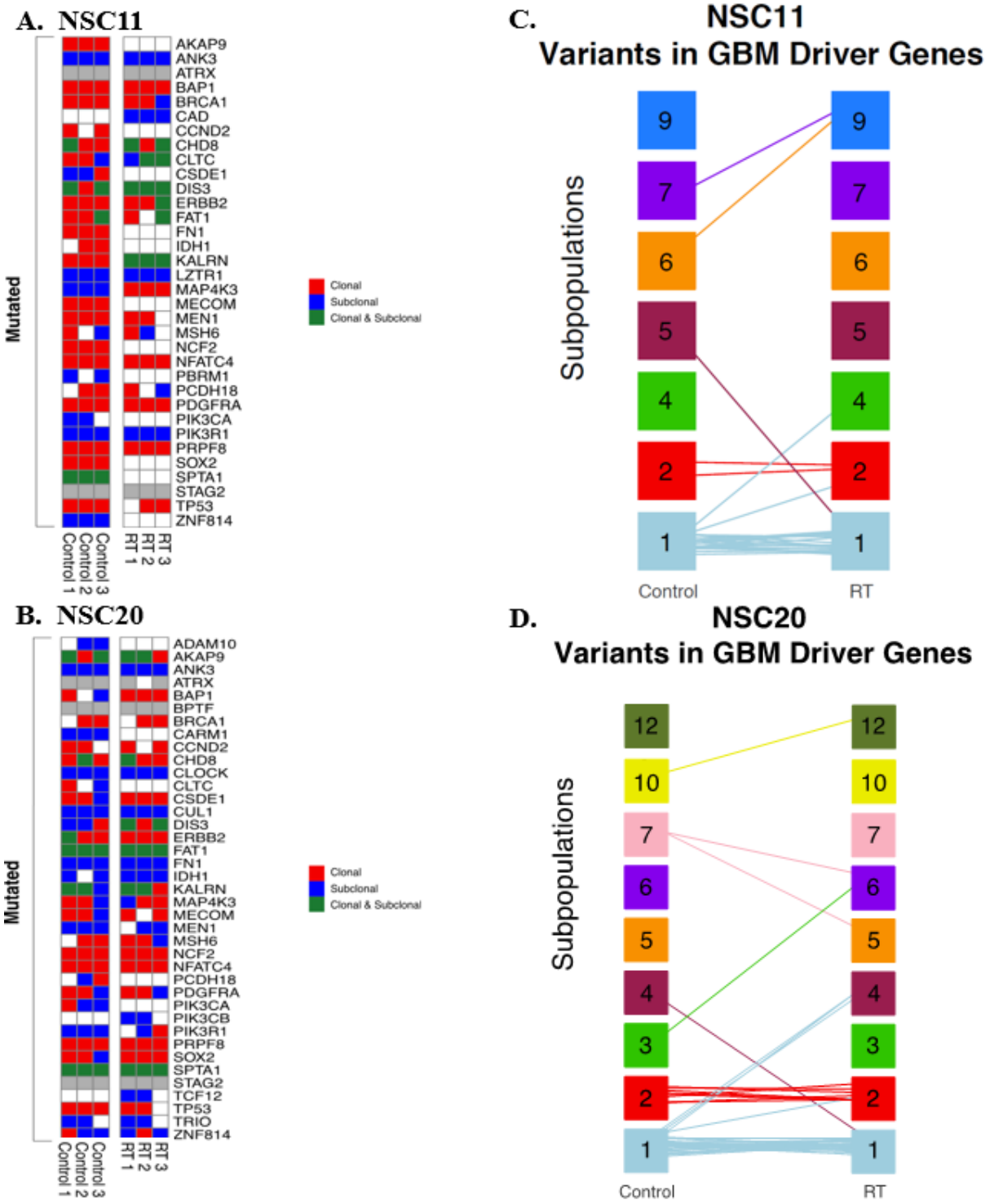

Figure 5.8 Influence of radiation on GB driver gene subpopulation dynamics. GB driver mutations in control and irradiated A) NSC11 and B) NSC20 tumours. Clonal variants were those in the sample's largest subpopulation; subclonal variants were those in any of a sample's smaller subpopulations. Gray boxes represent mutations other than autosomal SNVs (indels, X or Y chromosome SNVs), which are not included in EXPANDS. GB driver gene mutation shifts within the defined subpopulations of control and irradiated C) NSC11 and D) NSC20 tumours.

A.

Tumour Sample	Overall Survival (days)
NSC11 RT 1	61
NSC11 RT 2	73
NSC11 RT 3	75
NSC20 RT 1	79
NSC20 RT 2	90
NSC20 RT 3	108

B.

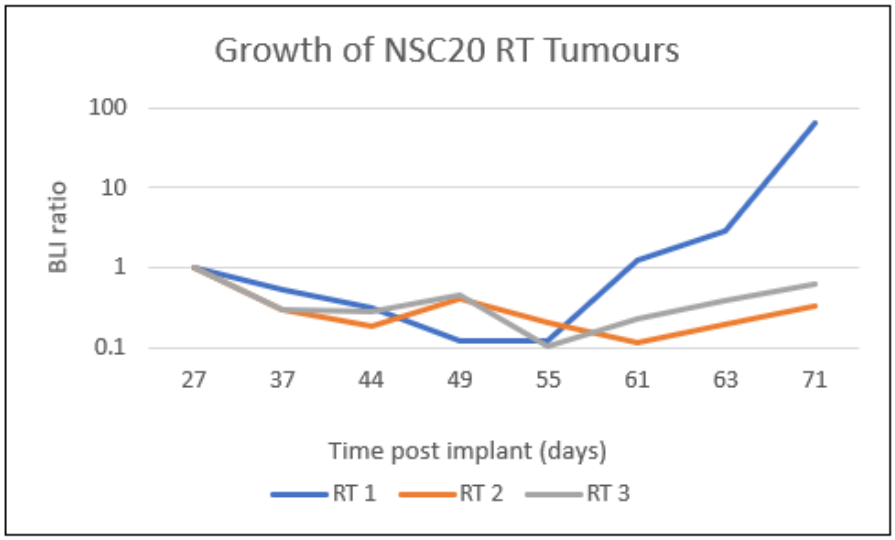

C.

Tumour Sample	Mutation Description
NSC11 RT 1	Loss of TP53 (after RT)
NSC20 RT 1	Loss of MEN1 (after RT)
	Loss of PIK3R1 (after RT)
	Never harboured BRCA1 mutation
NSC20 RT 3	Loss of TP53 (after RT)
	Did not gain PIK3CB
	Did not gain TCF12
	Never harboured TRIO mutation

Figure 5.9 Correlation of Mutation Changes with Survival and Tumour Growth. A) Overall survival of mice bearing the irradiated NSC11 and NSC20 tumours which underwent WES. B) Tumour growth defined by BLI ratio as a function of time after implant for sequenced NSC20 RT tumours. C) Description of the observed changes in GB driver gene mutations for NSC11 RT 1 (short survival), NSC20 RT 1 (short survival), and NSC20 RT3 (long survival).

5.3 Discussion

The goal of this study was to test the hypothesis that radiation drives the evolution of orthotopic xenografts initiated from GSCs. Given that ITH is a critical parameter mediating tumour evolution, VISA was used to assess the changes in clonal diversity existing in cell lines and tumour xenografts. In these analyses, in the absence of any radiation exposure, comparison of the GSC lines grown in vitro and grown as brain tumours showed a significant reduction in the clonal diversity with intracerebral growth. These results imply that, although isolated by CD133 expression, the GSC cultures are comprised of a heterogeneous population, which is consistent with previous reports (250,251,255,309) and that only selected subpopulations were capable of proliferation under orthotopic conditions. As compared to untreated tumours, there was a dramatic additional reduction in clonal diversity in GSC-initiated tumours that had been irradiated. These results are suggestive of radiation-induced selection of subpopulations within GSC xenografts with the ultimate consequence of a reduction in ITH. The radiation-induced reduction in clonal diversity was also detected in orthotopic xenografts initiated from the long-established GB cell line U251 indicating that the process is not unique to the GSC model and suggesting that radiation-driven evolution may be applicable to brain tumours in general.

Further analyses indicated that the reduction in ITH was dependent on the brain microenvironment. No change was detected in clonal diversity when VISA was performed on NSC11 cells irradiated in vitro. Moreover, comparison of U251 sc and ic xenografts showed that while there was a reduction in clonal diversity after irradiation of sc tumours, the effect was considerably more pronounced in ic U251 tumours, a reduction comparable to those detected in the GSC tumours. The implication of this reduction in ITH is that the brain microenvironment imposes radioresistance on only certain subpopulations of the GSC and U251 cells. Such a subpopulation selective effect could be attributed to normal tissue influence dependent on intrinsic characteristics of the cells implanted (e.g., genotype) or localisation into a radioprotective niche independent of tumour cell type. Whereas the mechanisms remain to be determined, the results presented emphasize the need to account for the brain microenvironment when investigating GB radioresponse.

As an alternative approach to evaluating radiation-driven evolution, studies were extended to WES, which has been the standard approach to evaluating tumour evolution. Comparison of untreated GSC tumours and tumours that had regrown after irradiation revealed a consistently different set of mutations as well as mutational signatures. There also appeared

to be a radiation induced shift in the genetic composition of the ranked sub-populations comprising the NSC11 and NSC20 xenografts. In evaluating the driver genes associated with GB (50,74,307,308), there was a reduction in the number of mutations in irradiated NSC11 tumours, which would be consistent with a reduction in ITH. In NSC20 tumours, although there was also a reduction in the number of GB associated gene mutations, the number of losses as well as the specific genes affected were different as compared to NSC11. The different mutation spectrums observed for NSC11 and NSC20 tumours with and without RT suggest that whereas radiation drives the evolutionary process, the specific events along with the functional consequences may be tumour dependent. For example, a PIK3CA mutation was consistently lost after RT in NSC20 tumour samples which may indicate that the gene/mutation contributes to radiosensitivity and furthermore may suggest that NSC20 tumours could be sensitive to PI3K inhibition. If future studies corroborate the sequencing findings through protein expression, then a PI3K inhibitor could be incorporated into in vivo studies. Thus, whereas WES results are indicative of radiation-driven evolution and may suggest potential therapeutic targets on a tumour-dependent basis, they do not provide any clear, generalizable insight into the mechanisms involved or the characteristics of the surviving tumour cells. Of note, the reduction in mutations detected in the irradiated xenografts is in contrast to the hypermutation reported for tumours treated with temozolomide (92,209,237,300). Whether temozolomide, a component of GB standard of care, influences radiation-driven evolution remains to be determined.

If radiation alters GB evolution, then the fundamental biology of the tumours that recur after an initially effective course of radiotherapy should be altered. An example appears to be the morphology/histology of the NSC11 and NSC20 xenografts that regrow after the fractionated radiation protocol as compared to untreated tumours. As shown, each tumour became less invasive with a more restricted growth pattern in response to irradiation. Although in conflict with reports showing that radiation increases the invasion propensity of glioma cells in vitro (310,311), these results agree with clinical observations indicating that > 80% of GB recur in the initial radiation treatment volume (180,182). The studies described here show that radiation alone drives the evolution of GSC orthotopic xenografts affecting their ITH, mutation profile and growth pattern. If a similar process is operative in a clinical setting, then therapeutic targets in a primary, untreated GB may differ from those in the recurrent tumour, as previously suggested (312). GSC xenograft tumours that regrow after an initial radiation exposure may thus provide a model system for testing therapies for recurrent GB. This would include re-irradiation alone as well as in combination with potential radiosensitisers.

Chapter 6. Glioblastoma stem-like cell-initiated orthotopic xenografts provide a useful model for studying reirradiation

After primary diagnosis and first-line treatment, which includes surgery, radiation, and chemotherapy, glioblastoma inevitably recurs, typically within a year of treatment initiation (74,122). The relatively rapid recurrence and progression of post-treatment GB demonstrates the ability of GB to evolve in response to harsh conditions (limited resources and therapeutic selective pressures) (24,31,35). Alkylating chemotherapy has been implicated in therapy-induced evolution by its ability to alter mutational profiles and lead to the emergence of temozolomide-resistant clones (235,300). Because we have shown that radiation has the ability to drive evolution of GSC-initiated xenografts, it is possible that radiotherapy may also lead to the emergence of resistant clones. The functional impact of radiation-induced reduction in clonal diversity and subpopulation selection must be interrogated due to its potential implications for recurrent GB treatment.

In particular, reirradiation protocols are a possible treatment option for recurrent glioblastoma. There are several potential risks for re-exposure of the CNS to radiation, including the development of symptomatic radionecrosis and damage to sensitive brain areas such as the brain stem and optic nerves. However, improved imaging to better define the tumour volume and advanced targeting techniques to more accurately provide radiation to the tumour while avoiding normal tissue are just a few of the methods used to mitigate the potential risks associated with re-exposure. Initial studies indicate the potential for clinical benefit after various forms of reirradiation (195-197,313-315). Shorter courses of radiation, which have been effectively employed in the elderly population (187,188), and pulse-reduced dose rate protocols may limit the additional radiation exposure for recurrent GB compared to standard fractionation techniques (198). Larger clinical trials of reirradiation are currently underway (https://clinicaltrials.gov/ct2/results?cond=Recurrent+Glioblastoma&term=radiation&cntry=&state=&city=&dist=), but the potential utility of reirradiation necessitates the investigation of GB models capable of studying retreatment protocols and their potential impact on and interaction with recurrent GB biology. For example, if radiation leads to the emergence of resistant clones which repopulate a recurrent tumour, then reirradiation would be expected to

have no clinical survival benefit and would not be recommended for patients. However, if radiation does not lead to the emergence of resistant clones, then patients may benefit from reirradiation and a more thorough understanding of radiation's impact on GB evolution may eventually suggest targets which may sensitise both primary and recurrent GB to radiotherapy.

To investigate the ability of radiation-induced evolution to positively select for radioresistant clones, potential functional implications of radiation on GSC-initiated orthotopic xenografts were examined through clonogenic survival analysis and in vivo reimplantation of xenograft-derived cell lines. Furthermore, the utility of GSC-initiated orthotopic xenografts for studying recurrent GB biology and retreatment protocols was investigated. Interestingly, tumour cells from control and irradiated tumours placed back into culture at morbidity did not demonstrate differences in radiosensitivity in vitro or in vivo. Furthermore, after the addition of a reirradiation protocol to GSC-initiated xenografts, recurrent tumours experienced a significant increase in overall survival, suggesting retained sensitivity to radiation. These results indicate that radiation-induced evolution of GSC xenografts does not lead to the emergence of radioresistant clones, which has positive treatment implications for GB patients. In particular, if this model is applicable to the clinical setting, then patients may experience further survival benefit with reirradiation protocols. Such reirradiation and recurrent GB treatment protocols and underlying recurrent GB biology and treatment response can be effectively studied with GSC-initiated xenograft models.

6.1 Methods for studying reirradiation and recurrent GB radioresponse

6.1.1 Clonogenic Survival Assay

Poly-L-lysine (PLL; Sigma) was added to each well of 6-well plates and allowed to stand 1 hour to overnight in 37°C incubator. PLL was removed, wells were washed twice with sterile PBS, and wells were allowed to dry in 37°C incubator for several hours to overnight. GSCs, typically maintained as neurospheres, were spun down at 800 rpm for 3 minutes at room temperature. Supernatant was aspirated and spheres were resuspended in 1 mL TryplE express.

After incubation for approximately 30 seconds at room temperature, 2 mL Defined Trypsin Inhibitor and 4 mL sterile PBS were added. After pipetting up and down to disaggregate the neurospheres, cell suspension was filtered through a sterile 40 µm cell strainer to ensure a single cell suspension. Cells were spun down at 1000 rpm for 5 minutes, supernatant was aspirated, and cells were resuspended in 5 mL sterile PBS. Cells were then counted with a Coulter counter. Cells were spun down a final time and resuspended in stem cell media at $1x10^5$ cells/ml in a 50 ml conical tube. Serial 1:10 dilutions were performed in stem cell media until desire dilution was reached. Appropriate number of cells were added to PLL-coated plates. Cells were incubated overnight at 37°C, 5% CO_2, and 5% O_2 to allow cells to attach prior to radiation treatment. After allowing time for cell attachment and recovery, plates were irradiated (0, 1, 2, or 3Gy) using a 320 kV Xray machine (Precision X-Ray Inc.). After irradiation, plates were returned to a 37°C, 5% CO_2, and 5% O_2 incubator and fresh stem cell media was added up to twice per week. At approximately 21 days post-irradiation, wells were stained with 0.5% crystal violet for up to 5 minutes. Plates were rinsed by immersion in a large bowl of water and crystal violet was properly disposed. After drying, plates were counted for number of colonies per well with a stereomicroscope. Colonies were defined as containing at least 25 cells (corresponding to 4-5 divisions). To generate a radiation survival curve, surviving fraction (SF) for each dose of radiation was calculated by determining the plating efficiency (PE) (number of colonies divided by the number of cells seeded x 100), which was then divided by the PE determined for the untreated control sample. Survival curves were constructed by plotting the surviving fraction versus radiation dose. The control (0Gy) SF is set at 1.0 on the y-axis with the remaining SF data points plotted on a log scale (decreasing from 1.0); the x-axis corresponds to the radiation dose and is plotted on a linear scale (a semi-log plot

6.1.2 Flow cytometry

A single cell suspension of GSCs was prepared as described above. Cells were centrifuged and pellet resuspended in 800µL PBS and 200µL 10% Formalin for 10 minutes at room temperature. Cells were centrifuged and resuspended in 500 µL of fixed cell staining buffer (PBS, 0.5% BSA, 0.1% Triton-X-100, 0.05% Tween20, 5% FBS). Cells were aliquoted into Eppendorf tubes for appropriate samples and controls (unstained, Hoechst control, secondary control, CD133-1 and CD133-2). To 100µL of cells, 20µL of pure CD133-1 and

CD133-2 (Miltenyi; PE-conjugated) were added. Cells were incubated with antibody for 1-2 hours at 4°C in the dark. Stained cells were centrifuged and resuspended in PBS with Hoechst 33258 (1:50,000). Samples were filtered through a 40µm nylon mesh into flow tube. Flow cytometry was performed on a BD LSRFortessa and analysis performed with FACSDiva software.

6.1.3 Immunocytochemistry

Poly-L-Ornithine (PO; Sigma) was added to chamber slides and allowed to stand overnight in a 37°C incubator. PO was removed, chambers were washed twice with sterile PBS, and PBS with Laminin (Sigma, 1:500) was added. Chambers were incubated at 37°C in Laminin for 4 hours to overnight. A single cell suspension of GSCs was prepared and cells were counted with a Coulter counter as described above. 50,000 cells per chamber were added with 2mL stem cell media. Cells were checked daily and were utilised for staining once cells reached approximately 70% confluency. Media was removed and slides were washed twice with PBS. Cells were fixed with 10% Formalin for 10 minutes at room temperature. Formalin was removed and cells washed with PBS once prior to incubating in blocking buffer (PBS, 5% FBS, 0.5% BSA, 0.1% Triton-x-100) for one hour at room temperature. Next, the primary antibody (CD133, Proteintech, 1:200) in antibody buffer (PBS, 5% FBS, 0.5% BSA, 0.1% Triton-X-100, 0.05% Tween20) was added and incubated overnight at 4°C with gentle shaking. Cells were washed three times with PBS and gentle shaking for 10 minutes prior to adding secondary antibody (Alexa Fluor 555, Invitrogen, 1:1000) in antibody buffer. Cells were incubated for 1 hour at room temperature in the dark. Cells were washed three times with PBS and gentle shaking for 10 minutes and chamber slides were removed. Anti-fade with DAPI was added and slides covered with coverslips. Slides were dried overnight and images taken with a fluorescent microscope (Zeiss).

6.1.4 Xenograft Reirradiation Protocol

Orthotopic implantation of CD133+ GSCs into the right striatum of female athymic nude mice, initial bioluminescent imaging, randomisation, and treatment with fractionated radiation (3x5Gy) were completed as described in Chapter 3. After the first course of treatment

(control or 3x5Gy), tumour growth was monitored weekly by BLI. Once the average BLI ratio of irradiated tumours demonstrated an observable increase (approaching 10 on the logarithmic scale), the irradiated mice were re-randomised into two groups: control (previously received 3x5Gy) and reirradiation (3x5Gy-3x5Gy). Mice in the reirradiation group received three consecutive days of 5Gy. After the second course of treatment, tumour growth was monitored by BLI out to morbidity. Kaplan-Meir survival curves were generated in GraphPad Prism 7.

6.2 Results

6.2.1 Clonogenic survival analysis of in vivo tumour cultures

As an initial test of whether radiation-induced evolution leads to the emergence of radioresistant clones, xenograft-derived cell lines were established from in vivo NSC11 control and irradiated tumours. For this experiment, once NSC11 tumour-bearing mice reached morbidity, mice were euthanised and GFP-expressing tumour tissue was dissected under a microscope. Tumour tissue was immediately placed in Trypsin-EDTA and mechanically dissociated with sterile scalpels. After inhibiting the trypsin, cells were washed with sterile PBS and spun down several times before adding stem cell media containing antibiotics. Cells were monitored, washed, and given fresh media for several days until neurospheres began to form and proliferate. After an antibiotic taper, xenograft-derived cell lines from both control and irradiated tumours were plated on PLL-coated plates for clonogenic survival assays to assess radioresponse. Figure 6.1A demonstrates no difference in survival fraction as a function of dose between cell lines derived from control xenografts (NSC11ic Control) or irradiated xenografts (NSC11ic 3x5Gy). While the colonies for NSC11 are typically small, there was no difference in colony size or morphology between the control and 3x5Gy cell lines (Fig. 6.1B) or between untreated cells (pictured) and irradiated cells. Furthermore, flow cytometry analysis for CD133 positivity demonstrated similar levels of CD133 expression for both NSC11ic control xenografts and NSC11ic 3x5Gy xenografts (Figs. 6.1 C and D, respectively). Flow cytometry results were supported by immunocytochemistry demonstrating fairly uniform CD133 expression (green fluorescence) of cultured cells (Figs. 6.1E-F). While the derivation protocol itself could perhaps be expected to generate a high percentage of CD133+ GSCs

regardless of xenograft characteristics, the GSCs composing each xenograft-derived cell line seem to display relatively similar radioresponses, regardless of treatment history (Fig. 6.1A).

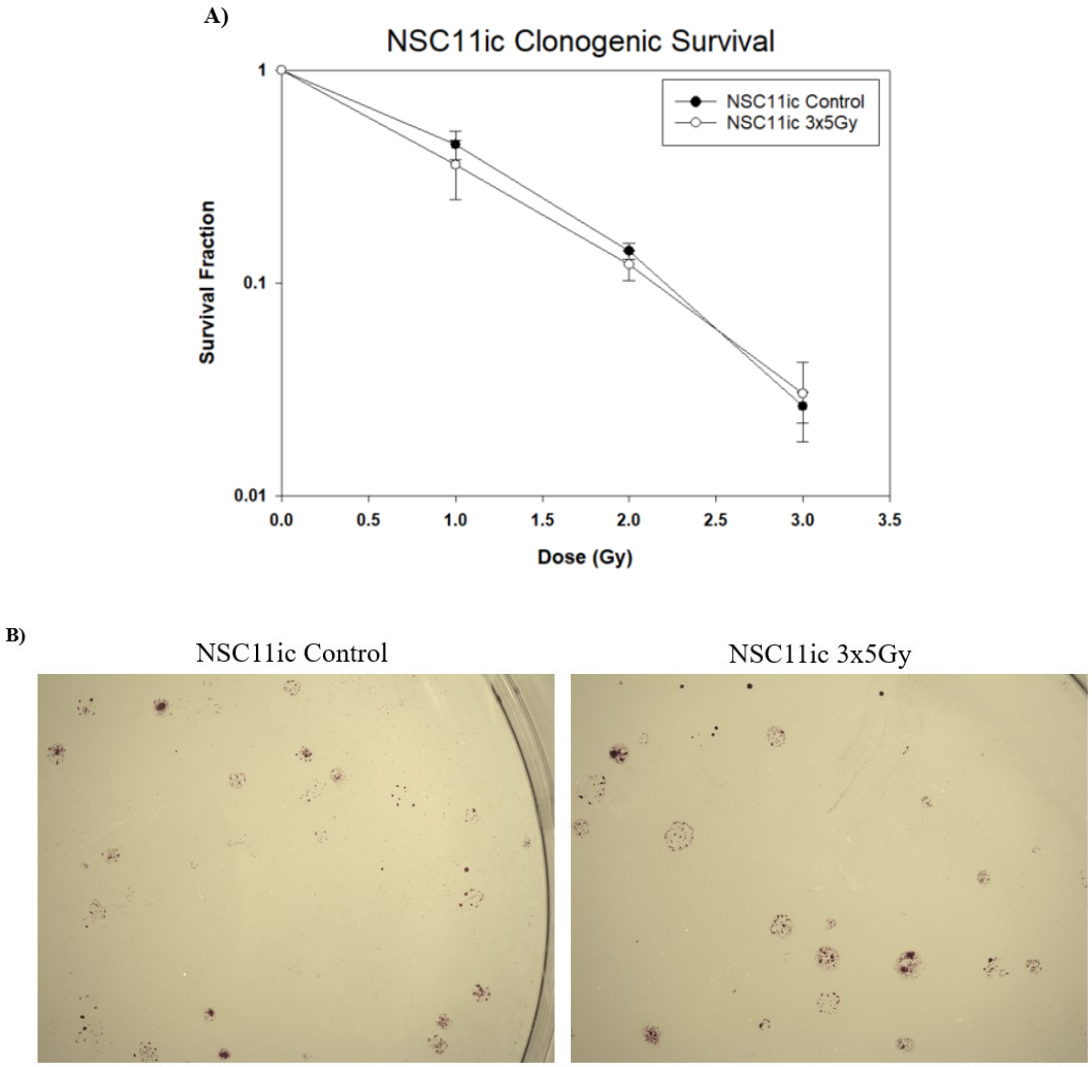

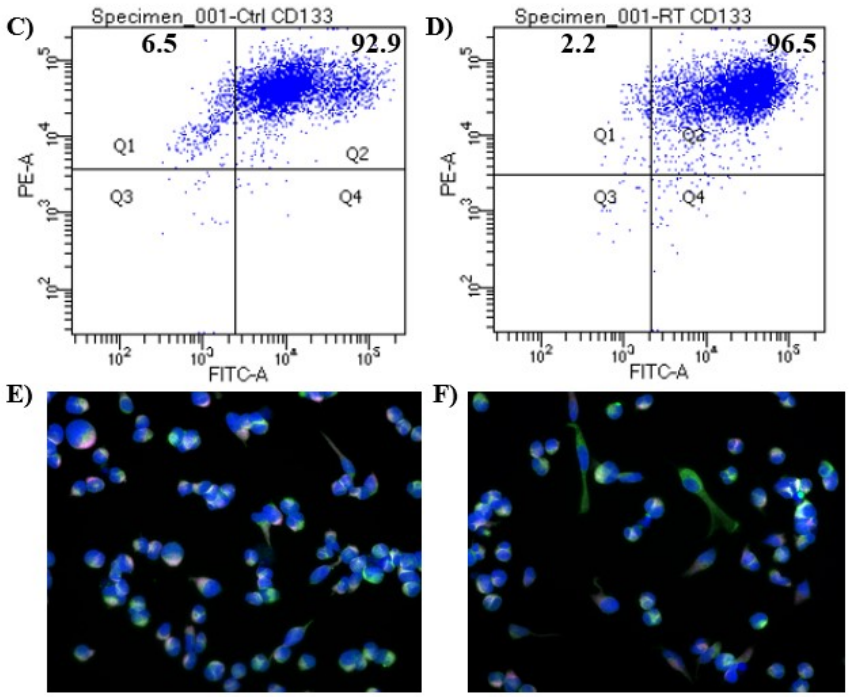

Figure 6.1 Clonogenic survival assay and GSC proportion analysis. A) Clonogenic survival curve comparing the survival fraction as a function of radiation dose between cell lines derived from control and irradiated (3x5Gy) xenografts. B) Representative images of NSC11ic Control and NSC11ic 3x5Gy clonogenic assay colonies (0 Gy). Flow cytometry dot plot demonstrating the percentage of GFP+ (FITC+) tumour cells which express CD133 (PE+) from C) control or D) irradiated xenograft-derived cell lines. Fluorescence images of attached E) control or F) irradiated xenograft-derived cells (blue=nuclear DAPI stain) which express CD133 (green) and Nestin (pink).

6.2.2 Reimplantation Study

To ensure that the lack of difference in radiosensitivity between xenograft-derived cell lines with different treatment histories was not attributable to in vitro culturing, a reimplantation study was performed. NSC11 cell lines were derived from xenograft tumour tissue as described for clonogenic assay experiments. Once clonogenic neurosphere cultures were generated and antibiotics tapered, xenograft-derived cell lines from control (icCtrl) or irradiated (ic3x5) tumours were reimplanted into the right striatum of nude mice. The tumour take rate for xenograft-derived cell lines was around 95%, similar to standard GSC implantation studies. As in prior in vivo experiments, at day 21 post-implant, after visualisation of tumours with BLI, mice from both cohorts were randomised into control and fractionated radiotherapy (3x5Gy) groups. After treatment, mice were followed out to morbidity with BLI

and overall survival was recorded. As shown in figure 6.2A, a statistically significant difference in survival based on xenograft-derived cell line treatment history was not observed. While the median survival for the control tumour-derived cell line implants was higher than irradiated tumour-derived cell line implants (83 days vs. 72 days, respectively), Kaplan-Meir survival curve comparison demonstrates a clear lack of significant survival advantage (p=0.9889). Similarities in survival between xenograft-derived cell lines were consistent with similarities in tumour growth delay for each reimplant type as assessed by BLI as a function of time after irradiation (Fig. 6.2B). These data suggest that radiation-induced evolution does not select for radioresistant subclones.

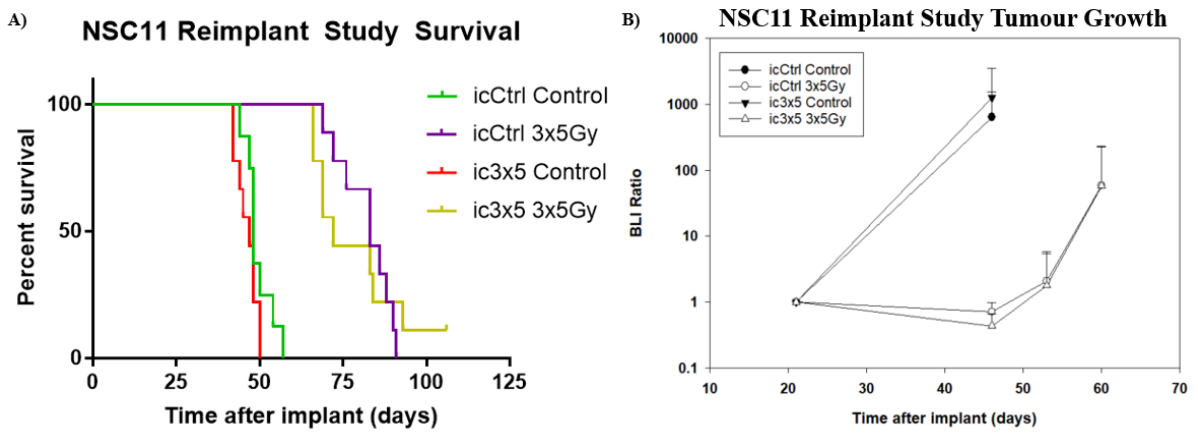

Figure 6.2 Radioresponse of reimplanted NSC11 xenograft-derived cell lines. Reimplanted xenografts were randomised and treated (3x5Gy) on day 21 post-implant as described in text. A) Kaplan-Meier survival curves were generated for control tumour-derived reimplants (icCtrl) and irradiated tumour-derived reimplants (ic3x5) that received no treatment (Control) or fractionated radiation (3x5Gy) (n=8-9 mice per group). B) Tumour growth defined by BLI ratio as a function of time after irradiation. Day 21 represents initial, pre-treatment BLI baseline imaging prior to randomisation and irradiation.

6.2.3 Reirradiation of GSC-initiated orthotopic xenografts

Because our reimplantation study contained an intervening period of in vitro cell line derivation, it is possible that the in vitro environment led to a loss of potential differences in radiosensitivity that may have been gained by GSCs after treatment in the brain microenvironment. Therefore, as a final, more clinically relevant assessment of radiation's potential to induce the emergence of radioresistant subclones, we added a reirradiation protocol

to our GSC-initiated xenograft model. Orthotopic implantation of CD133+GFP+GSCs, initial BLI, and first course of treatment (control or 3x5Gy) were completed as described previously. After completion of the initial course of treatment, tumour growth of control and irradiated tumours were followed weekly with BLI. Once the irradiated tumours began to regrow, as determined by a consistent increase in BLI ratio as a function of time after irradiation, the mice were re-randomised into two groups: control and fractionated radiotherapy (3x5Gy). After the second course of treatment, mice were followed out to morbidity with BLI and overall survival recorded. Figure 6.3A shows that NSC11 tumour-bearing mice that underwent reirradiation experienced a significant increase in survival compared to mice that only received one course of fractionated irradiation. Similar survival advantages from the reirradiation protocol were also observed in NSC20 and NSC23 tumour-bearing mice (figures 6.3B-C). Consistent with increased survival, tumour growth delay was detected by BLI after both the initial and second courses of fractionated irradiation (figures 6.4A-C), suggesting that recurrent tumours that regrow after initial treatment remain sensitive to irradiation. Finally, the fundamental change in recurrent GB biology, as evidenced by reduced invasive propensity, which was observed after one course of radiation (Fig. 5.2), was similarly observed in reirradiated NSC11 and NSC20 tumour-bearing brains at morbidity (figures 6.5A-B). Taken together, these results suggest that radiation-induced evolution does not lead to the emergence of radioresistant clones and that GSC-initiated xenografts represent useful models for studying recurrent GB biology and retreatment protocols.

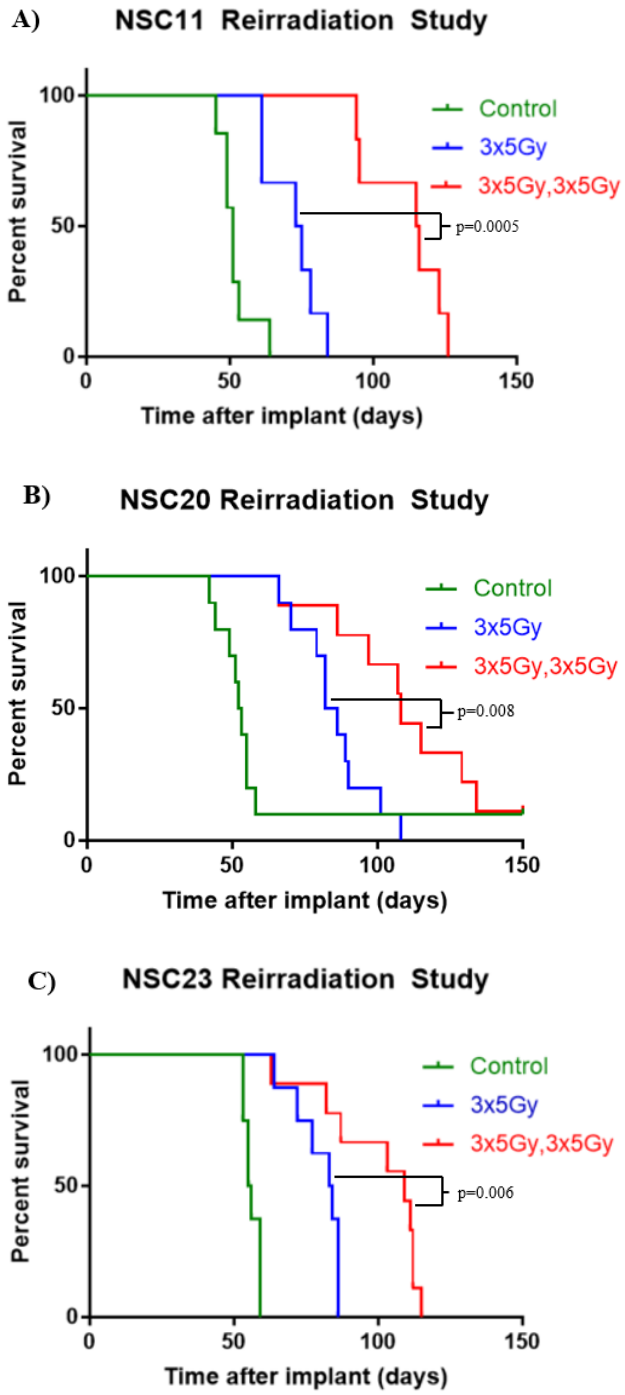

Figure 6.3 Survival of GSC-initiated xenografts after reirradiation. After initial randomisation and treatment (3x5Gy), mice were followed by BLI weekly to monitor tumour growth. Once the average BLI ratio of irradiated tumours demonstrated an observable increase (approaching 10 on the logarithmic scale), the irradiated mice were rerandomised and reirradiated (3x5Gy, 3x5Gy). Kaplan-Meier survival curves were generated for A) NSC11, B) NSC20, and C) NSC23 tumour-bearing mice (n=6-10 mice per group). Log-rank (Mantel-Cox) test utilised for statistical analysis of survival benefit with GraphPad Prism 7 software.

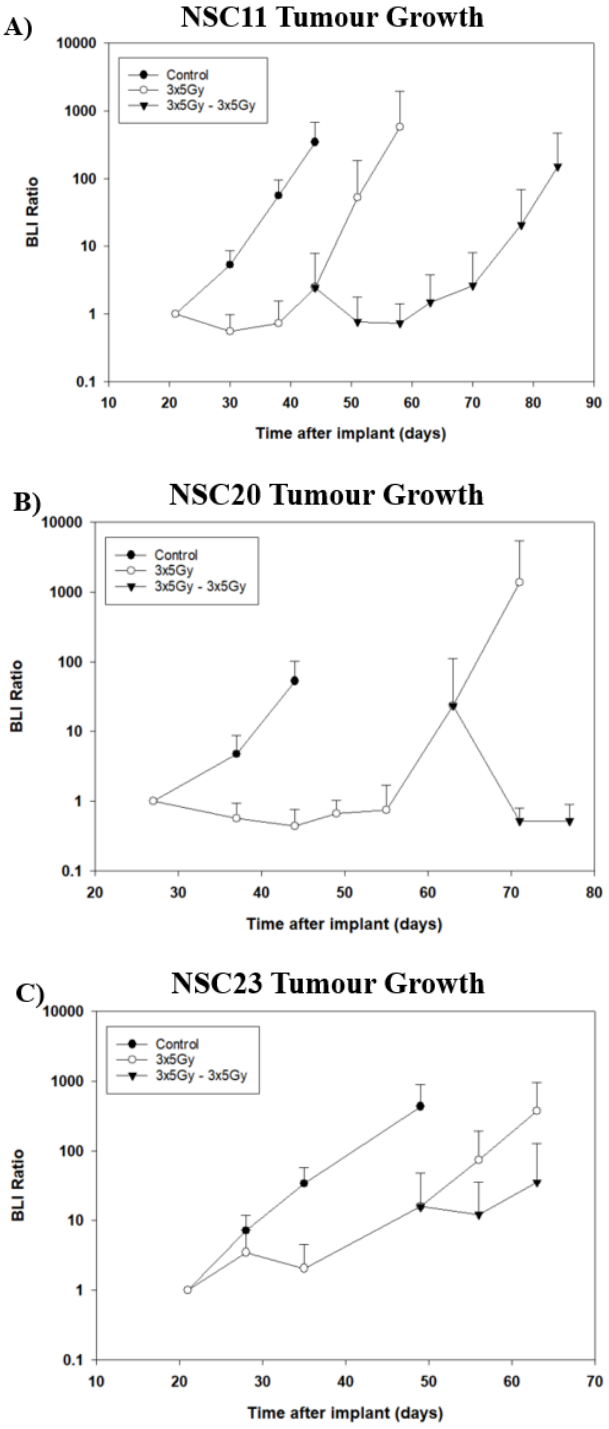

Figure 6.4 Radioresponse of GSC-initiated xenografts after reirradiation. Tumour growth defined by BLI ratio as a function of time after irradiation for A) NSC11, B) NSC20, and C) NSC23 tumours.

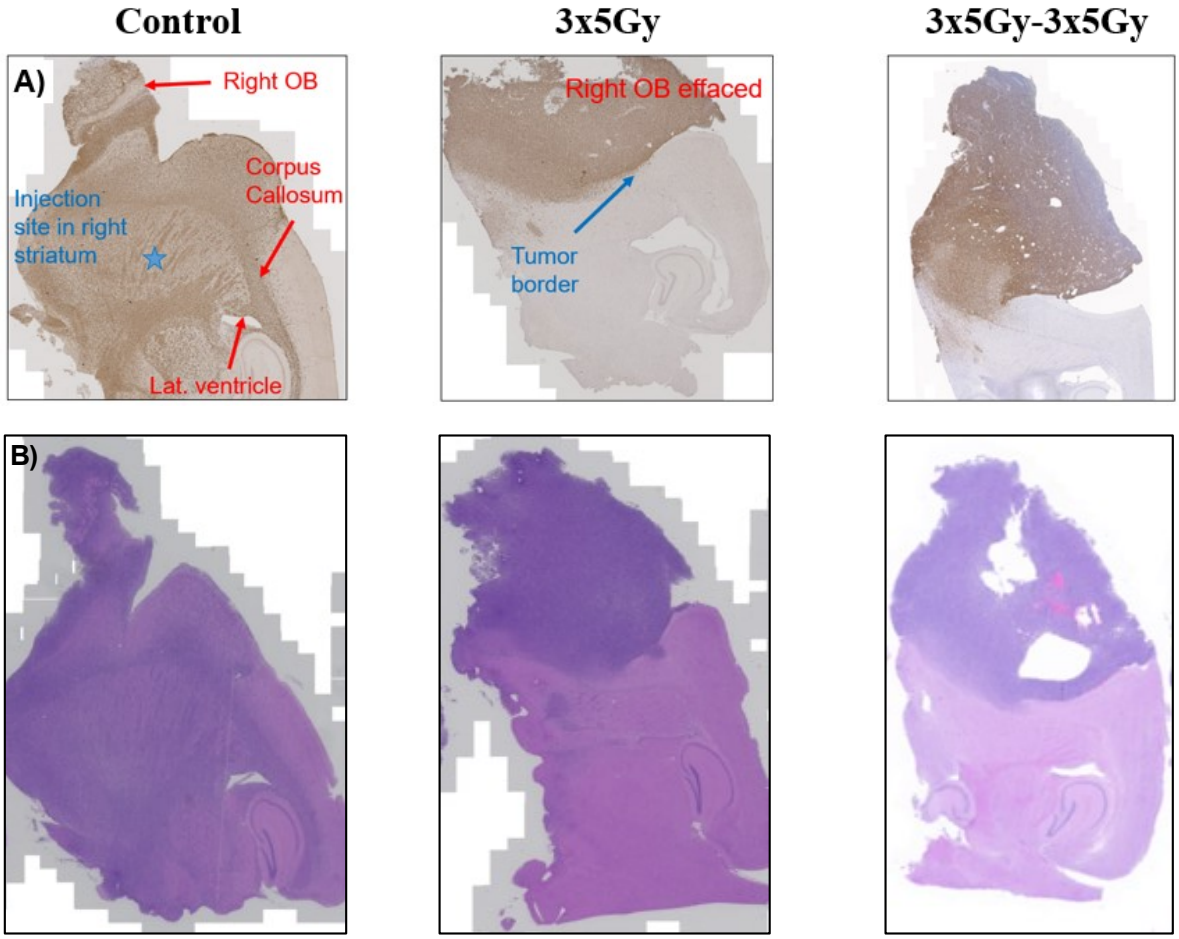

Figure 6.5 Morphology and histology of NSC11 and NSC20 tumours. Right hemisphere sagittal sections at plane of injection site stained with A) SOX2 or B) H&E (magnification 20x) from A) NSC11 or B) NSC20 control, irradiated (3x5Gy), and reirradiated (3x5Gy-3x5Gy) tumour-bearing brains at morbidity.

6.3 Discussion

The aim of this study was to test the hypothesis that radiation-induced evolution leads to the emergence of radioresistant clones. In vitro clonogenic survival and reimplantation studies of xenograft-derived cell lines were utilised as initial approaches for evaluating the functional implications of radiation-induced evolution. By returning control and irradiated xenograft tumour cells back to culture, we were able to test the hypothesis that in vivo irradiation leads to the emergence of radioresistance. The protocol we utilised for GB xenograft cell line derivation and subsequent in vitro maintenance potentially biased enrichment toward GSCs (241,267). Utilising serum-containing media may have allowed the retention of more diverse and differentiated tumour cell types. However, we ultimately required a population of clonogenic GSCs for successful reimplantation studies. In addition, GSCs cultures have been shown to be heterogeneous by the ability to populate heterogeneous tumours (252). Importantly, CSCs are considered to be an important cell type for mediating intrinsic radioresistance (245). Therefore, if irradiation of GSC-initiated xenografts led to a recurrent tumour repopulated with radioresistant GSCs, then the derivation of GSC lines from irradiated xenografts would be expected to enrich for more radioresistant GSCs compared to control xenograft-derived GSCs. If this is the case, then our results which showed no difference in in vitro clonogenic survival or in vivo survival after reimplantation suggest that radiation-induced evolution of GSC-initiated orthotopic xenografts does not lead to the emergence of radioresistant clones in recurrent GB xenografts. Instead of selecting for radioresistant clones, radiation may contribute to GB evolution by the selection of clones with different predilections for invasion versus proliferation and clones better able to benefit from microenvironmental interactions (migration to radioresistant niches, for example).

Despite aggressive first line treatment, glioblastoma inevitably recurs. Even though progression is expected, a consensus on the best treatment approach for recurrent glioblastoma does not currently exist. Many modalities have been employed with mostly palliative intent including re-resection, chemotherapy, and reirradiation. Certainly, clinicians must weight clinical benefits with apparent risks and make decisions based on a given patient's characteristics, but reirradiation seems to be a feasible retreatment strategy that may improve outcomes. However, early studies with reirradiation demonstrated limited survival benefit and relatively high side effect profiles with conventional RT (314,316). Fortunately, advances in imaging and radiation targeting, including conformal technology has improved tolerance and

survival (317). Indeed, with new techniques, the incidence of necrosis does not seem to increase significantly until a combined dose of at least 100 Gy (317). In a retrospective cohort study, Combs et al. demonstrated that fractionated stereotactic reirradiation with a median dose of 36Gy led to an 8-month median OS for reirradiated patients (5-month PFS) and was well tolerated with no major short- or long-term side effects (318). Survival results comparable to systemic recurrent treatment strategies (e.g. bevacizumab) have been reported in single institution retrospective studies for hypofractionated (319) and pulsed reduced-dose-rate protocols (198). Several retrospective studies have shown potential beneficial results for SRS with small volume recurrent tumours, but an increase in radionecrosis with larger volumes (320-322). Many other retrospective series and systematic literature reviews have further suggested that reirradiation is well tolerated and seems to yield survival times comparable or better than other treatment modalities (195,196,313,315,323-328). In addition to improved survival, studies have also observed the stabilisation and improvement of performance status (329,330). As with other recurrent treatment strategies, patient stratification seems to be important, as patients with higher performance status (KPS>60) and smaller lesions (<40mm) (325), longer intervals between radiation courses, and gross total reresection prior to reirradiation tended to have better outcomes (323). A few prognostic scoring mechanisms and expert survey data have been developed to delineate the patients who would best respond to reirradiation (197,331). While many retrospective observation studies and a few prospective studies suggest that reirradiation is well tolerated and may provide comparable or perhaps even favorable clinical benefit for recurrent GB, there is clearly a need for more prospective trials and randomized control trials to fully establish efficacy, better define optimal patient selection, to guide dose/fractionation decisions, to confirm safe dose limits, and to support addition of systemic therapies. While many reirradiation trials are currently ongoing, it seems likely that with continued improvements in radiation delivery and with the incorporation of targeted radiosensitisers to enhance radioresponse, reirradiation may eventually establish itself as a safe, effective recurrent GB treatment strategy.

Therefore, as an alternative approach to further assess the functional implications of radiation-induced evolution and to establish GSC-initiated xenografts as models for studying retreatment strategies, we added a reirradiation protocol to our previously described GSC-initiated xenograft model which involves a single course of irradiation (266). In the current study, after the initial course of irradiation, average tumour growth of irradiated tumours was monitored with bioluminescent imaging. Once the average tumour size began to increase, as

assessed by BLI ratio when compared to pre-treatment BLI values, the mice were re-randomised and half were reirradiated with the same fractionated radiation protocol (3x5Gy). The in vivo observations of initial response to treatment (delayed tumour growth assessed by differences in BLI), eventual progression of irradiated tumours (increase in BLI ratios above both pre-treatment and early post-treatment values), and response to a second course of irradiation (delayed tumour growth) seem to mimic standard GB clinical histories. After an initial response to treatment and a period of progression free survival, GB inevitably recurs. Depending on the performance status of the individual, retreatment may be provided which often leads to another, shorter treatment response. Unfortunately, the patient typically succumbs to the disease within 2 years of diagnosis. Because the addition of a reirradiation protocol to GSC xenografts mirrors GB clinical histories, allows for the retreatment of recurrent tumours that regrow after treatment, and yields the ability to investigate changes in tumours at different intervals after one or more courses of treatment, this model represents a useful evolutionary tool. This model of reirradiation and recurrent GB provides an opportunity to further interrogate the microenvironment-mediated mechanisms and implications of radiation-induced GB evolution, to more effectively study recurrent biology, and to test the preclinical efficacy of new retreatment protocols. A more thorough understanding of treatment-induced evolution and possible sensitisation strategies could have potential implications toward improving treatment for recurrent glioblastoma.

Chapter 7. Discussion

This work was performed to examine the impact of radiation on glioblastoma evolution. The intrinsic intratumoral heterogeneity of glioblastoma coupled with selective pressures imposed by standard treatment regimens can lead to therapy-induced evolution. This phenomenon has been demonstrated for chemotherapy (235,300). However, the ability of radiation alone to induce glioblastoma evolution has not previously been described. Therefore, this work presents novel findings on radiation-induced glioblastoma evolution and its potential implications for retreatment protocols and recurrent biology. Furthermore, the study of radiosensitivity in the context of intratumoral heterogeneity may provide insight on the applicability of such findings. Future work will seek to gain further understanding of the process of radiation-induced evolution in an effort to generate more effective treatment strategies for improving glioblastoma outcomes.

7.1 Summary of Key Findings

7.1.1 Impact of ITH on radiosensitivity

The hypothesis that there are differences in intrinsic radioresponse of glioblastoma cells isolated from spatially distinct regions of human tumours was tested by performing radiosensitivity studies and whole exome sequencing on patient-derived cell lines and corresponding tumour fragments. Comparison of Pearson's correlation coefficients and superFreq analysis of SNV and CNA data demonstrated that patient-derived cell lines were good models of their tumours of origin. In addition, the J14 cell lines were also found to be good models of their specific corresponding tumour fragments. SuperFreq-generated river plots allowed for the comparison of the presence and relative prevalence of defined clones between samples from a given tumour. These plots revealed that while samples shared clones, they also harboured unique clones and combinations of clones which supported the use of cell lines derived from spatially distinct tumour fragments as models of intratumoral heterogeneity.

Cell lines underwent radiosensitivity testing with γH2AX foci analysis and limiting dilution assays. The J7 cell lines displayed conflicting results in DSB foci induction (1-hour post RT) and repair (24 hours post RT). All other cell lines showed no significant differences in foci analysis. For limiting dilution assays, only the J14 cell lines displayed differences in proliferation capacity after irradiation. Because no cell lines displayed consistent differences across radiosensitivity studies, it seems that cell lines derived from spatially distinct tumour regions exhibit similar levels of radiosensitivity in spite of observed ITH. These results suggest that ITH does not produce differences in intrinsic radiosensitivity and that GB radioresponse may be conserved across heterogeneous clones within a tumour.

7.1.2 Radiation drives evolution of GSC-initiated orthotopic xenografts

Glioblastoma stem-like cell-initiated orthotopic xenografts were utilised to test whether radiation alone can drive the evolution of glioblastoma. The fractionated radiotherapy protocol (3x5Gy) provided a significant survival advantage and caused a tumour growth delay for irradiated mice, which mimics the clinical course of treated GB. Histological analysis revealed that control tumour-bearing brains demonstrated different growth patterns when compared to irradiated tumour-bearing brains. In particular, GB cells in control tumours were more diffusely scattered throughout the right hemisphere both anteriorly and posteriorly from the injection site in the striatum. In contrast, irradiated tumours demonstrated a clearly demarcated tumour border anterior to the right striatum. Such clear differences in growth patterns point towards a fundamental change in recurrent biology after irradiation.

We investigated the potential role of clonal selection in this process by performing Viral integration site analysis. VISA demonstrated a significant reduction in the number of unique integration sites when transitioning from an in vitro to an in vivo environment. Clonal diversity was even further reduced when implanted tumours were irradiated. This reduction in clonal diversity was detected in two different GSC lines, suggesting that radiation has the ability to drive evolution. To test whether radiation alone was sufficient to promote clonal selection, we irradiated NSC11 cells in vitro. However, there was no difference in the number of integration sites between control and irradiated cells in vitro. Furthermore, VISA of U251 xenografts demonstrated that while irradiation of subcutaneous xenografts did lead to a reduction in clonal diversity, the largest reduction in diversity occurred after irradiation of intracerebral xenografts.

This suggests that radiation-induced GB evolution is not specific to GSCs and that the brain microenvironment plays an important role in mediating the evolutionary process.

Whole exome sequencing of morbid control and irradiated tumours further supported the observed impact of radiation on GB evolution. COSMIC mutational signature profiles were found to be different between control and irradiated NSC11 and NSC20 tumours. Additionally, EXPANDS analysis demonstrated extensive subpopulation dynamics as many variants shifted into more or less prevalent subpopulations following irradiation. Similarly, patterns of GB driver genes differed between control and irradiated tumours and GB driver gene variants were also found to shift between defined subpopulations after irradiation. The WES results coupled with VISA, histology, and survival support the radiation-driven evolution of GSC-initiated orthotopic xenografts.

7.1.3 Glioblastoma reirradiation model

To test the hypothesis that radiation-driven evolution leads to the emergence of resistant clones, clonogenic assays of xenograft-derived cell lines as well as reimplantation studies were performed. Cells from control and irradiated NSC11 morbid tumours were put back into culture to establish xenograft-derived cell lines grown as neurospheres. These lines were subjected to clonogenic survival analysis which demonstrated no difference in radiosensitivity between the lines. Next, control and irradiated NSC11 xenograft-derived cell lines were reimplanted into the right striatum of nude mice and treated with fractionated irradiation. No differences in survival after irradiation were noted regardless of the prior treatment received by the xenograft-derived cell lines.

An alternative approach for testing the effects of radiation-driven evolution was the addition of a reirradiation protocol to the previously described GSC-initiated orthotopic xenograft model. Tumour bearing mice that received fractionated irradiation (3x5Gy) were followed by serial BLI imaging to monitor for tumour regrowth. Once an increase in BLI suggested regrowth (recurrence), an additional fractionated irradiation protocol (3x5Gy) was applied to half of the mice. Similar to a single course of irradiation, the second course of irradiation led to an observed tumour growth delay by BLI and mice that were reirradiated experienced a significant increase in median survival compared to mice that only received one course of irradiation. Because the GSC xenograft reirradiation protocol better mirrors the

clinical course of GB by retreating recurrent tumours, this model represents a useful method for studying recurrent GB biology and retreatment strategies. Furthermore, these reirradiation results coupled with clonogenic survival analysis and reimplantation results indicate that radiation-induced evolution does not lead to the emergence of radioresistant clones in GSC-initiated orthotopic xenografts.

7.2 Limitations

When comparing patient-derived cell lines to their tumours of origin, the cell lines were found to be good models of their parent tumours. However, in some cases the cell lines were good models of the originating tumour as a whole, but they were more similar to other cell lines from the same tumour than they were to their specific corresponding tumour fragments. Logistical and biological challenges could have contributed to this result. Care was taken in the operating room to cut a single, small tumour fragment in half to send one half for tissue processing and storage in the Tumour Bank and the other half for cell line derivation. While labelling was done in the operating room in an attempt to numerically define each tumour fragment, tissue frozen by the Tumour Bank was processed separately from tissue utilised for line derivation, which could have introduced unknown discrepancies in labelling. This could be rectified in the future by having both tasks performed in the same facility by the same personnel. Furthermore, as has been demonstrated with single cell analysis (281), even two halves of a small tumour fragment could possibly demonstrate ITH. While manual homogenisation of the entire tissue fragment prior to splitting for separate purposes would potentially lessen the amount of ITH present, homogenisation would also diminish tissue integrity which could have negative consequences for freezing, thawing, and eventual DNA extraction from tissue fragments. In this case, immediate DNA extraction from homogenized tissue would potentially be better than tissue bank storage and later extraction. In addition to improving derivation techniques to improve the accuracy of the models, in vivo radiosensitivity studies would provide further information on the impact of ITH on intrinsic radiosensitivity (discussed further in section 7.3).

As this study represents the first observation of the impact of radiation on glioblastoma evolution, WES was employed to examine differences in variant patterns, mutational

signatures, and subpopulation dynamics between untreated and irradiated tumours. WES of DNA extracted from bulk tumour samples has been a standard approach for studying cancer evolution and ITH. Despite its extensive use in studying cancer genomics, WES has been shown to be susceptible to sequencing artifacts particularly at low coverage and in low-mappability regions (332). In our analyses, we sought to improve likelihood of more accurate variant calling by only analyzing variants that were detected in 2 out of 3 replicates. While our sequencing had a depth >180x, ultra-deep sequencing could improve reliability of results (333). Also, single cell techniques could provide more detailed analysis of ITH and genomic/transcriptomic evolution (34,281). In addition, WGS would provide a more comprehensive picture of radiation-induced effects on the genome. Beyond just examining variants in protein-coding genes, WGS would describe the potential effects of radiation on genomic instability and the role that such instability may play in the evolutionary process (334-336). While many other genomic approaches could potentially be utilised in the future to more deeply investigate the impact of radiation on GB genomic evolution, WES is a reasonable first approach for studying and describing therapy-induced evolution.

The finding that in vitro irradiation of GSCs did not lead to a reduction in clonal diversity while irradiation of in vivo brain tumours led to a significant reduction in clonal diversity suggests a contributory role for the brain tumour microenvironment in radiation-induced glioblastoma evolution. As such, it seems likely that future studies on radiation-induced GB evolution will also need to be performed in vivo. Nude mice represent a commonly utilised immunocompromised mouse strain for studying glioblastoma orthotopic xenografts. Nude mice harbour a few functioning types of immune cells, unlike NOD-SCIDs which are even more immunocompromised. The use of nude mice is necessary when performing radioresponse studies due to SCID mice having a Prkdc mutation and deficiency in DNA-PK activity resulting in hypersensitivity to ionizing radiation (337). However, the lack of a functioning immune system may limit the ability to fully understand the interactions of the microenvironment and glioblastoma cells that result in treatment-induced evolution. For example, radiation-induced cell death is thought to release tumour neoantigens which in turn can be taken up by antigen presenting cells (dendritic cells) to generate and activate tumour-specific T cells. Radiation also has complex effects on the tumour microenvironment that can contribute to immune responses, such as increasing the production of cell adhesion molecules in irradiated vascular endothelium resulting in T cell recruitment (338). Therefore, various

trials are underway to enhance anti-tumour immunity by the complementary and potentially synergistic actions of targeted immunotherapies and radiation.

7.3 Future Work

To further confirm that ITH does not have a significant impact on radiosensitivity, a next step would be to compare in vivo growth patterns and in vivo radiosensitivities of patient-derived cell lines derived from spatially distinct tumour fragments. The brain microenvironment has been previously shown to influence radioresponse of GSCs and has even revealed differences in radiosensitivities of CD133+ and CD133- cell populations in vivo that were not found in vitro (254,266). Therefore, comparison of in vivo tumour growth and radiation treatment of multiple cell lines from the same tumour would be expected to provide a more clinically relevant picture of ITH. To date, J3 and J7 cells transduced to express GFP/Luciferase have been intracerebrally implanted into athymic nude mice. While these cells do produce tumours, untreated mice survive upwards of 100 days, making their utility for radiation-related studies difficult. The cell lines utilised in Appendix A, A25M and A25C, represent an attractive pair of lines to study due to observed differences in tumour growth patterns; A25M grows as a nodular tumour whereas A25C grows as a diffuse tumour. A25M has been successfully transduced and has already been incorporated into ongoing reirradiation studies. Unfortunately, while transduced A25C cells do generate tumours, the cells in culture and tumours in vivo seem to be growing more slowly than previously observed. Future studies will attempt to boost in vivo growth rates so that the two lines can be compared. However, many patient-derived cell lines are still available for future tumourigenicity studies. Ultimately, by generating a few workable models of in vivo ITH, the potential of ITH to yield differences in in vivo radiosensitivity could be assessed. In addition to the study of in vivo radiosensitivity, paired cell lines from the same tumour would provide the opportunity to study the impact of radiation and other treatments on clonal evolution of mixed cell populations in vivo.

As our results suggest, the microenvironment may play an important role in radiation-induced glioblastoma evolution. Therefore, future studies will seek to better delineate the role of the brain microenvironment, a unique and complex system, in guiding the evolutionary

process (339,340). Initial assessments could involve staining histological time course slides with various makers expressed in the brain microenvironment such as VEGF (angiogenesis), Tenascin C (ECM), and CD11b/CD68 (microglia) to assess potential differences in these microenvironmental components after irradiation. Future in vivo work could examine the potential role of protective niches in mediating cell survival and evolution after radiation. Additionally, examining the role of resident non-tumour brain cells in radioresponse could provide further insights on the ability of the microenvironment to guide evolution. For instance, astrocytes have been shown to both enhance the invasion of GSCs and to reduce their in vitro radiosensitivity (reduce DSBs and enhance foci dispersal) (229,230). Therefore, co-implantation of human GSCs with human astrocytes could potentially demonstrate the ability of an important resident brain cell to affect in vivo radioresponse. While utilizing in vivo methods arguably provide the most physiologically relevant microenvironmental model, such models can be difficult to manipulate. Therefore, new in vitro methods of 3D cell culturing including hyaluronic acid and hydrogel-based ECM 3D scaffolds, microfluidic systems, and brain and tumour organoids represent potential ways to mimic some of the features of the brain microenvironment while assessing the ability of radiation to impact the relationship of GB cells to those specific microenvironmental features (341).

The studied reirradiation protocol led to an increase in survival suggesting that radiation-driven evolution does not select for radioresistant clones. To further assess the functional implications of reirradiation and to study recurrent tumour biology and evolution (first recurrence to second recurrence), the studies described in this thesis (VISA, WES) could be extended to tumours that were reirradiated. Sequencing of recurrent tumours could provide valuable information on potential genomic divergence of tumours after reirradiation or other treatment exposures compared to primary tumours or earlier recurrent tumours. Many targeted therapies are selected based on GB driver mutations, so sequencing of recurrent tumours can assess the status of such driver mutations in order to inform whether previously utilized targeted therapies should be continued or stopped and whether new targeted therapies may be effective. While clinical tissue specimens are useful for sequencing if re-resection is completed as part of recurrent GB treatment regimens, liquid biopsies provide an important alternative when resection is not recommended to periodically (and less invasively) assess treatment effectiveness and to inform treatment decisions. In addition to sequencing recurrent tumours, histological time course studies could be done after reirradiation to examine differences in underlying phenotypes between control, once irradiated, and twice irradiated tumour-bearing

brains. To achieve a more comprehensive understanding of treatment-induced GB evolution, other treatment regimens should be assessed to compare to radiation-induced evolution. While it was necessary to study radiation-driven evolution and the subsequent reirradiation protocol by treating tumour-bearing mice with fractionated irradiation only, such treatment regimens do not mirror those typically utilised in clinic. First line treatment for most newly diagnosed and resected GB patients is the Stupp protocol consisting of radiotherapy with concomitant and adjuvant temozolomide (122). As such, future studies will interrogate the impact of combinatorial therapeutics on GSC-initiated xenograft evolution. In particular, it would be interesting to determine whether the addition of TMZ or a potent radiosensitiser to fractionated irradiation has any effect on the emergence of radioresistant clones. Such studies would pair well with additional retreatment protocols so that the treatment responses of recurrent tumours could be directly tested with various single modality retreatments in an effort to better understand resistance mechanisms and recurrent biology.

7.4 Conclusion

Glioblastoma is a heterogeneous, malignant brain tumour. Despite aggressive treatment with surgery, radiotherapy, and chemotherapy, patients have a median survival time from diagnosis of 15 months. Intratumoral heterogeneity and the ability of glioblastoma to rapidly evolve in response to selective pressures contribute to inevitable treatment failure and disease recurrence. Radiation is an integral component of most first line treatment regimens for glioblastoma. The results presented in this thesis demonstrate that radiation has the ability to drive glioblastoma evolution. In particular, radiation produced a reduction in clonal diversity. While the selection of subpopulations demonstrated in irradiated tumours may not lead to the emergence of radioresistant clones, as demonstrated by reirradiation protocols, the results do suggest changes in fundamental biology at tumour recurrence and an important role for the microenvironment in guiding the evolutionary process. Because intratumoral heterogeneity was not shown to yield differential radiosensitivities, future insights on radiation-induced glioblastoma evolution may contribute to improved therapies that enhance radioresponse for the entire tumour at both primary and recurrent stages.

Research Funding

Financial support for research described in Chapters 4-6 was provided by Division of Basic Sciences, Intramural Program, National Cancer Institute (Z1ABC011372, Z1ABC011373) to P.J. Tofilon. This project has also been funded in whole or in part with Federal funds from the National Cancer Institute, National Institutes of Health, under Contract No. HHSN261200800001E. The content of this thesis does not necessarily reflect the views or policies of the Department of Health and Human Services, nor does mention of trade names, commercial products, or organisations imply endorsement by the U.S. Government.

Financial support for research described in Appendix A was provided by Brain Tumour Charity (RG89672), the National Institute for Health Research Cambridge Biomedical Research Center, and the Higher Education Funding Council for England. Tissue was accessed through the Human Research Tissue Bank supported by the NIHR Cambridge Biomedical Research Centre and Addenbrooke's Hospital.

References

1. Institute NC. Cancer Statistics. **2019**
2. Hanahan D, Weinberg RA. Hallmarks of cancer: the next generation. Cell **2011**;144:646-74
3. Perona R. Cell signalling: growth factors and tyrosine kinase receptors. Clin Transl Oncol **2006**;8:77-82
4. Sherr CJ, McCormick F. The RB and p53 pathways in cancer. Cancer Cell **2002**;2:103-12
5. Lowe SW, Cepero E, Evan G. Intrinsic tumour suppression. Nature **2004**;432:307-15
6. White E, DiPaola RS. The double-edged sword of autophagy modulation in cancer. Clin Cancer Res **2009**;15:5308-16
7. Galluzzi L, Kroemer G. Necroptosis: a specialized pathway of programmed necrosis. Cell **2008**;135:1161-3
8. Blasco MA. Telomeres and human disease: ageing, cancer and beyond. Nat Rev Genet **2005**;6:611-22
9. Baeriswyl V, Christofori G. The angiogenic switch in carcinogenesis. Semin Cancer Biol **2009**;19:329-37
10. Ferrara N. Vascular endothelial growth factor. Arterioscler Thromb Vasc Biol **2009**;29:789-91
11. Thiery JP, Acloque H, Huang RY, Nieto MA. Epithelial-mesenchymal transitions in development and disease. Cell **2009**;139:871-90
12. Vinay DS, Ryan EP, Pawelec G, Talib WH, Stagg J, Elkord E*, et al.* Immune evasion in cancer: Mechanistic basis and therapeutic strategies. Semin Cancer Biol **2015**;35 Suppl:S185-S98
13. Beatty GL, Gladney WL. Immune escape mechanisms as a guide for cancer immunotherapy. Clin Cancer Res **2015**;21:687-92
14. Colotta F, Allavena P, Sica A, Garlanda C, Mantovani A. Cancer-related inflammation, the seventh hallmark of cancer: links to genetic instability. Carcinogenesis **2009**;30:1073-81
15. Ward PS, Thompson CB. Metabolic reprogramming: a cancer hallmark even warburg did not anticipate. Cancer Cell **2012**;21:297-308
16. DeBerardinis RJ, Lum JJ, Hatzivassiliou G, Thompson CB. The biology of cancer: metabolic reprogramming fuels cell growth and proliferation. Cell Metab **2008**;7:11-20
17. McGranahan N, Burrell RA, Endesfelder D, Novelli MR, Swanton C. Cancer chromosomal instability: therapeutic and diagnostic challenges. EMBO Rep **2012**;13:528-38
18. Negrini S, Gorgoulis VG, Halazonetis TD. Genomic instability--an evolving hallmark of cancer. Nat Rev Mol Cell Biol **2010**;11:220-8
19. Greaves M. Cancer stem cells: back to Darwin? Semin Cancer Biol **2010**;20:65-70
20. Greaves M. Cancer stem cells as 'units of selection'. Evol Appl **2013**;6:102-8

21. Greaves M. Cancer stem cells renew their impact. Nat Med **2011**;17:1046-8
22. Dick JE. Stem cell concepts renew cancer research. Blood **2008**;112:4793-807
23. Greaves M. Evolutionary determinants of cancer. Cancer discovery **2015**;5:806-20
24. Greaves M, Maley CC. Clonal evolution in cancer. Nature **2012**;481:306-13
25. Frank NY, Schatton T, Frank MH. The therapeutic promise of the cancer stem cell concept. J Clin Invest **2010**;120:41-50
26. Sosa MS, Bragado P, Aguirre-Ghiso JA. Mechanisms of disseminated cancer cell dormancy: an awakening field. Nat Rev Cancer **2014**;14:611-22
27. Liau BB, Sievers C, Donohue LK, Gillespie SM, Flavahan WA, Miller TE*, et al.* Adaptive Chromatin Remodeling Drives Glioblastoma Stem Cell Plasticity and Drug Tolerance. Cell Stem Cell **2017**;20:233-46 e7
28. Merlo LMF, Pepper JW, Reid BJ, Maley CC. Cancer as an evolutionary and ecological process. Nature reviews Cancer **2006**;6:924-35
29. Pepper JW, Scott Findlay C, Kassen R, Spencer SL, Maley CC. Cancer research meets evolutionary biology. Evol Appl **2009**;2:62-70
30. Nowell PC. The clonal evolution of tumor cell populations. Science **1976**;194:23-8
31. McGranahan N, Swanton C. Clonal Heterogeneity and Tumor Evolution: Past, Present, and the Future. Cell **2017**;168:613-28
32. Gatenby RA, Gillies RJ. A microenvironmental model of carcinogenesis. Nat Rev Cancer **2008**;8:56-61
33. Gilbert LA, Hemann MT. DNA damage-mediated induction of a chemoresistant niche. Cell **2010**;143:355-66
34. Neftel C, Laffy J, Filbin MG, Hara T, Shore ME, Rahme GJ*, et al.* An Integrative Model of Cellular States, Plasticity, and Genetics for Glioblastoma. Cell **2019**;178:835-49 e21
35. Maley CC, Aktipis A, Graham TA, Sottoriva A, Boddy AM, Janiszewska M*, et al.* Classifying the evolutionary and ecological features of neoplasms. Nature reviews Cancer **2017**;17:605-19
36. Hata AN, Niederst MJ, Archibald HL, Gomez-Caraballo M, Siddiqui FM, Mulvey HE*, et al.* Tumor cells can follow distinct evolutionary paths to become resistant to epidermal growth factor receptor inhibition. Nat Med **2016**;22:262-9
37. Bhang HE, Ruddy DA, Krishnamurthy Radhakrishna V, Caushi JX, Zhao R, Hims MM*, et al.* Studying clonal dynamics in response to cancer therapy using high-complexity barcoding. Nat Med **2015**;21:440-8
38. Su KY, Chen HY, Li KC, Kuo ML, Yang JC, Chan WK*, et al.* Pretreatment epidermal growth factor receptor (EGFR) T790M mutation predicts shorter EGFR tyrosine kinase inhibitor response duration in patients with non-small-cell lung cancer. J Clin Oncol **2012**;30:433-40
39. Turke AB, Zejnullahu K, Wu YL, Song Y, Dias-Santagata D, Lifshits E*, et al.* Preexistence and clonal selection of MET amplification in EGFR mutant NSCLC. Cancer Cell **2010**;17:77-88
40. Brastianos PK, Nayyar N, Rosebrock D, Leshchiner I, Gill CM, Livitz D*, et al.* Resolving the phylogenetic origin of glioblastoma via multifocal genomic analysis of pre-treatment and treatment-resistant autopsy specimens. NPJ Precis Oncol **2017**;1:33

41. Ostrom QT, Gittleman H, Liao P, Vecchione-Koval T, Wolinsky Y, Kruchko C*, et al.* Neuro-Oncology CBTRUS Statistical Report: Primary brain and other central nervous system tumors diagnosed in the United Introduction. **2017**:1-88
42. Ohgaki H, Kleihues P. The definition of primary and secondary glioblastoma. Clin Cancer Res **2013**;19:764-72
43. Ohgaki H, Kleihues P. Genetic pathways to primary and secondary glioblastoma. Am J Pathol **2007**;170:1445-53
44. Zong H, Parada LF, Baker SJ. Cell of origin for malignant gliomas and its implication in therapeutic development. Cold Spring Harb Perspect Biol **2015**;7
45. Ostrom QT, Gittleman H, Truitt G, Boscia A, Kruchko C, Barnholtz-Sloan JS. CBTRUS Statistical Report: Primary Brain and Other Central Nervous System Tumors Diagnosed in the United States in 2011-2015. Neuro-oncology **2018**;20:iv1-iv86
46. Brodbelt A, Greenberg D, Winters T, Williams M, Vernon S, Collins VP*, et al.* Glioblastoma in England: 2007-2011. Eur J Cancer **2015**;51:533-42
47. Burnet NG, Jefferies SJ, Benson RJ, Hunt DP, Treasure FP. Years of life lost (YLL) from cancer is an important measure of population burden--and should be considered when allocating research funds. British journal of cancer **2005**;92:241-5
48. Louis DN, Ohgaki H, Wiestler OD, Cavenee WK, Burger PC, Jouvet A*, et al.* The 2007 WHO classification of tumours of the central nervous system. Acta neuropathologica **2007**;114:97-109
49. Louis DN, Perry A, Reifenberger G, von Deimling A, Figarella-Branger D, Cavenee WK*, et al.* The 2016 World Health Organization Classification of Tumors of the Central Nervous System: a summary. Acta neuropathologica **2016**;131:803-20
50. Network CGAR. Comprehensive genomic characterization defines human glioblastoma genes and core pathways. Nature **2008**;455:1061-8
51. Frederick L, Wang XY, Eley G, James CD. Diversity and frequency of epidermal growth factor receptor mutations in human glioblastomas. Cancer Res **2000**;60:1383-7
52. Brennan CW, Verhaak RGW, McKenna A, Campos B, Noushmehr H, Salama SR*, et al.* The somatic genomic landscape of glioblastoma. Cell **2013**;155:462-77
53. Ekstrand AJ, Longo N, Hamid ML, Olson JJ, Liu L, Collins VP*, et al.* Functional characterization of an EGF receptor with a truncated extracellular domain expressed in glioblastomas with EGFR gene amplification. Oncogene **1994**;9:2313-20
54. Rajasekhar VK, Viale A, Socci ND, Wiedmann M, Hu X, Holland EC. Oncogenic Ras and Akt signaling contribute to glioblastoma formation by differential recruitment of existing mRNAs to polysomes. Mol Cell **2003**;12:889-901
55. Heimberger AB, Hlatky R, Suki D, Yang D, Weinberg J, Gilbert M*, et al.* Prognostic effect of epidermal growth factor receptor and EGFRvIII in glioblastoma multiforme patients. Clin Cancer Res **2005**;11:1462-6
56. Thorne AH, Zanca C, Furnari F. Epidermal growth factor receptor targeting and challenges in glioblastoma. Neuro Oncol **2016**;18:914-8

57. Ohgaki H, Dessen P, Jourde B, Horstmann S, Nishikawa T, Di Patre PL, *et al.* Genetic pathways to glioblastoma: a population-based study. Cancer Res **2004**;64:6892-9
58. Rasheed BK, McLendon RE, Friedman HS, Friedman AH, Fuchs HE, Bigner DD, *et al.* Chromosome 10 deletion mapping in human gliomas: a common deletion region in 10q25. Oncogene **1995**;10:2243-6
59. Cantley LC, Neel BG. New insights into tumor suppression: PTEN suppresses tumor formation by restraining the phosphoinositide 3-kinase/AKT pathway. Proc Natl Acad Sci U S A **1999**;96:4240-5
60. Stambolic V, Suzuki A, de la Pompa JL, Brothers GM, Mirtsos C, Sasaki T, *et al.* Negative regulation of PKB/Akt-dependent cell survival by the tumor suppressor PTEN. Cell **1998**;95:29-39
61. Schmidt MC, Antweiler S, Urban N, Mueller W, Kuklik A, Meyer-Puttlitz B, *et al.* Impact of genotype and morphology on the prognosis of glioblastoma. J Neuropathol Exp Neurol **2002**;61:321-8
62. Fujisawa H, Reis RM, Nakamura M, Colella S, Yonekawa Y, Kleihues P, *et al.* Loss of heterozygosity on chromosome 10 is more extensive in primary (de novo) than in secondary glioblastomas. Lab Invest **2000**;80:65-72
63. Bögler O, Huang HJ, Kleihues P, Cavenee WK. The p53 gene and its role in human brain tumors. Glia **1995**;15:308-27
64. Zhang Y, Xiong Y, Yarbrough WG. ARF promotes MDM2 degradation and stabilizes p53: ARF-INK4a locus deletion impairs both the Rb and p53 tumor suppression pathways. Cell **1998**;92:725-34
65. Ichimura K, Bolin MB, Goike HM, Schmidt EE, Moshref A, Collins VP. Deregulation of the p14ARF/MDM2/p53 pathway is a prerequisite for human astrocytic gliomas with G1-S transition control gene abnormalities. Cancer Res **2000**;60:417-24
66. Malkoun N, Chargari C, Forest F, Fotso MJ, Cartier L, Auberdiac P, *et al.* Prolonged temozolomide for treatment of glioblastoma: preliminary clinical results and prognostic value of p53 overexpression. J Neurooncol **2012**;106:127-33
67. Lee EY, Hu N, Yuan SS, Cox LA, Bradley A, Lee WH, *et al.* Dual roles of the retinoblastoma protein in cell cycle regulation and neuron differentiation. Genes Dev **1994**;8:2008-21
68. Lipinski MM, Jacks T. The retinoblastoma gene family in differentiation and development. Oncogene **1999**;18:7873-82
69. Serrano M, Lee H, Chin L, Cordon-Cardo C, Beach D, DePinho RA. Role of the INK4a locus in tumor suppression and cell mortality. Cell **1996**;85:27-37
70. Labuhn M, Jones G, Speel EJ, Maier D, Zweifel C, Gratzl O, *et al.* Quantitative real-time PCR does not show selective targeting of p14(ARF) but concomitant inactivation of both p16(INK4A) and p14(ARF) in 105 human primary gliomas. Oncogene **2001**;20:1103-9
71. Ichimura K, Schmidt EE, Goike HM, Collins VP. Human glioblastomas with no alterations of the CDKN2A (p16INK4A, MTS1) and CDK4 genes have frequent mutations of the retinoblastoma gene. Oncogene **1996**;13:1065-72

72. Ueki K, Ono Y, Henson JW, Efird JT, von Deimling A, Louis DN. CDKN2/p16 or RB alterations occur in the majority of glioblastomas and are inversely correlated. Cancer Res **1996**;56:150-3
73. Weller M, Wick W, von Deimling A. Isocitrate dehydrogenase mutations: a challenge to traditional views on the genesis and malignant progression of gliomas. Glia **2011**;59:1200-4
74. Parsons DW, Jones S, Zhang X, Lin JC-H, Leary RJ, Angenendt P*, et al.* An integrated genomic analysis of human glioblastoma multiforme. Science (New York, NY) **2008**;321:1807-12
75. Watanabe T, Nobusawa S, Kleihues P, Ohgaki H. IDH1 mutations are early events in the development of astrocytomas and oligodendrogliomas. Am J Pathol **2009**;174:1149-53
76. Hartmann C, Meyer J, Balss J, Capper D, Mueller W, Christians A*, et al.* Type and frequency of IDH1 and IDH2 mutations are related to astrocytic and oligodendroglial differentiation and age: a study of 1,010 diffuse gliomas. Acta Neuropathol **2009**;118:469-74
77. Yan H, Parsons DW, Jin G, McLendon R, Rasheed BA, Yuan W*, et al.* IDH1 and IDH2 mutations in gliomas. N Engl J Med **2009**;360:765-73
78. Lu C, Ward PS, Kapoor GS, Rohle D, Turcan S, Abdel-Wahab O*, et al.* IDH mutation impairs histone demethylation and results in a block to cell differentiation. Nature **2012**;483:474-8
79. Turcan S, Rohle D, Goenka A, Walsh LA, Fang F, Yilmaz E*, et al.* IDH1 mutation is sufficient to establish the glioma hypermethylator phenotype. Nature **2012**;483:479-83
80. Schaap FG, French PJ, Bovee JV. Mutations in the isocitrate dehydrogenase genes IDH1 and IDH2 in tumors. Adv Anat Pathol **2013**;20:32-8
81. Capper D, Weissert S, Balss J, Habel A, Meyer J, Jager D*, et al.* Characterization of R132H mutation-specific IDH1 antibody binding in brain tumors. Brain Pathol **2010**;20:245-54
82. SongTao Q, Lei Y, Si G, YanQing D, HuiXia H, XueLin Z*, et al.* IDH mutations predict longer survival and response to temozolomide in secondary glioblastoma. Cancer Sci **2012**;103:269-73
83. Beiko J, Suki D, Hess KR, Fox BD, Cheung V, Cabral M*, et al.* IDH1 mutant malignant astrocytomas are more amenable to surgical resection and have a survival benefit associated with maximal surgical resection. Neuro Oncol **2014**;16:81-91
84. Pope WB, Prins RM, Albert Thomas M, Nagarajan R, Yen KE, Bittinger MA*, et al.* Non-invasive detection of 2-hydroxyglutarate and other metabolites in IDH1 mutant glioma patients using magnetic resonance spectroscopy. Journal of neuro-oncology **2012**;107:197-205
85. Zhang J, Stevens MFG, Bradshaw TD. Temozolomide: mechanisms of action, repair and resistance. Current molecular pharmacology **2012**;5:102-14
86. Shiraishi A, Sakumi K, Sekiguchi M. Increased susceptibility to chemotherapeutic alkylating agents of mice deficient in DNA repair methyltransferase. Carcinogenesis **2000**;21:1879-83

87. Hegi ME, Diserens A-C, Gorlia T, Hamou M-F, de Tribolet N, Weller M, *et al.* MGMT gene silencing and benefit from temozolomide in glioblastoma. The New England journal of medicine **2005**;352:997-1003
88. Esteller M, Garcia-Foncillas J, Andion E, Goodman SN, Hidalgo OF, Vanaclocha V, *et al.* Inactivation of the DNA-repair gene MGMT and the clinical response of gliomas to alkylating agents. The New England journal of medicine **2000**;343:1350-4
89. Rivera AL, Pelloski CE, Gilbert MR, Colman H, De La Cruz C, Sulman EP, *et al.* MGMT promoter methylation is predictive of response to radiotherapy and prognostic in the absence of adjuvant alkylating chemotherapy for glioblastoma. Neuro-oncology **2010**;12:116-21
90. Yip S, Miao J, Cahill DP, Iafrate AJ, Aldape K, Nutt CL, *et al.* MSH6 mutations arise in glioblastomas during temozolomide therapy and mediate temozolomide resistance. Clinical cancer research : an official journal of the American Association for Cancer Research **2009**;15:4622-9
91. Cahill DP, Levine KK, Betensky RA, Codd PJ, Romany CA, Reavie LB, *et al.* Loss of the mismatch repair protein MSH6 in human glioblastomas is associated with tumor progression during temozolomide treatment. Clinical cancer research : an official journal of the American Association for Cancer Research **2007**;13:2038-45
92. Hunter C, Smith R, Cahill DP, Stephens P, Stevens C, Teague J, *et al.* A hypermutation phenotype and somatic MSH6 mutations in recurrent human malignant gliomas after alkylator chemotherapy. Cancer Res **2006**;66:3987-91
93. Hiyama E, Hiyama K. Telomere and telomerase in stem cells. Br J Cancer **2007**;96:1020-4
94. Killela PJ, Reitman ZJ, Jiao Y, Bettegowda C, Agrawal N, Diaz LA, *et al.* TERT promoter mutations occur frequently in gliomas and a subset of tumors derived from cells with low rates of self-renewal. Proceedings of the National Academy of Sciences of the United States of America **2013**;110:6021-6
95. Horn S, Figl A, Rachakonda PS, Fischer C, Sucker A, Gast A, *et al.* TERT promoter mutations in familial and sporadic melanoma. Science (New York, NY) **2013**;339:959-61
96. Lewis PW, Elsaesser SJ, Noh K-M, Stadler SC, Allis CD. Daxx is an H3.3-specific histone chaperone and cooperates with ATRX in replication-independent chromatin assembly at telomeres. Proceedings of the National Academy of Sciences of the United States of America **2010**;107:14075-80
97. Ramamoorthy M, Smith S. Loss of ATRX Suppresses Resolution of Telomere Cohesion to Control Recombination in ALT Cancer Cells. Cancer Cell **2015**;28:357-69
98. M C, FP B, TM M, TS S, SR S, BA M, *et al.* Molecular Profiling Reveals Biologically Discrete Subsets and Pathways of Progression in Diffuse Glioma. Cell **2016**;164:550-63
99. Jiao Y, Killela PJ, Reitman ZJ, Rasheed AB, Heaphy CM, de Wilde RF, *et al.* Frequent ATRX, CIC, FUBP1 and IDH1 mutations refine the classification of malignant gliomas. Oncotarget **2012**;3:709-22

100. Phillips HS, Kharbanda S, Chen R, Forrest WF, Soriano RH, Wu TD, *et al.* Molecular subclasses of high-grade glioma predict prognosis, delineate a pattern of disease progression, and resemble stages in neurogenesis. Cancer cell **2006**;9:157-73
101. Huse JT, Phillips HS, Brennan CW. Molecular subclassification of diffuse gliomas: seeing order in the chaos. Glia **2011**;59:1190-9
102. Verhaak RGW, Hoadley KA, Purdom E, Wang V, Qi Y, Wilkerson MD, *et al.* Integrated genomic analysis identifies clinically relevant subtypes of glioblastoma characterized by abnormalities in PDGFRA, IDH1, EGFR, and NF1. Cancer cell **2010**;17:98-110
103. Nigro JM, Misra A, Zhang L, Smirnov I, Colman H, Griffin C, *et al.* Integrated array-comparative genomic hybridization and expression array profiles identify clinically relevant molecular subtypes of glioblastoma. Cancer Res **2005**;65:1678-86
104. Eckel-Passow JE, Lachance DH, Molinaro AM, Walsh KM, Decker PA, Sicotte H, *et al.* Glioma Groups Based on 1p/19q, IDH, and TERT Promoter Mutations in Tumors. The New England journal of medicine **2015**;372:2499-508
105. Noushmehr H, Weisenberger DJ, Diefes K, Phillips HS, Pujara K, Berman BP, *et al.* Identification of a CpG island methylator phenotype that defines a distinct subgroup of glioma. Cancer Cell **2010**;17:510-22
106. Christensen BC, Smith AA, Zheng S, Koestler DC, Houseman EA, Marsit CJ, *et al.* DNA methylation, isocitrate dehydrogenase mutation, and survival in glioma. J Natl Cancer Inst **2011**;103:143-53
107. Li T, Cox CD, Ozer BH, Nguyen NT, Nguyen HN, Lai TJ, *et al.* D-2-Hydroxyglutarate Is Necessary and Sufficient for Isocitrate Dehydrogenase 1 Mutant-Induced MIR148A Promoter Methylation. Mol Cancer Res **2018**;16:947-60
108. Olar A, Aldape KD. Using the molecular classification of glioblastoma to inform personalized treatment. The Journal of pathology **2014**;232:165-77
109. Weller M, Stupp R, Hegi ME, van den Bent M, Tonn JC, Sanson M, *et al.* Personalized care in neuro-oncology coming of age: why we need MGMT and 1p/19q testing for malignant glioma patients in clinical practice. Neuro-oncology **2012**;14 Suppl 4:iv100-8
110. Sottoriva A, Spiteri I, Piccirillo SGM, Touloumis A, Collins VP, Marioni JC, *et al.* Intratumor heterogeneity in human glioblastoma reflects cancer evolutionary dynamics. Proceedings of the National Academy of Sciences of the United States of America **2013**;110:4009-14
111. Sottoriva A, Spiteri I, Shibata D, Curtis C, Tavaré S. Single-molecule genomic data delineate patient-specific tumor profiles and cancer stem cell organization. Cancer research **2013**;73:41-9
112. Mahlokozera T, Vellimana AK, Li T, Mao DD, Zohny ZS, Kim DH, *et al.* Biological and therapeutic implications of multisector sequencing in newly diagnosed glioblastoma. Neuro-oncology **2018**;20:472-83
113. Parker NR, Hudson AL, Khong P, Parkinson JF, Dwight T, Ikin RJ, *et al.* Intratumoral heterogeneity identified at the epigenetic, genetic and transcriptional level in glioblastoma. Scientific Reports **2016**;6:22477

114. Mazor T, Pankov A, Johnson Brett E, Hong C, Hamilton Emily G, Bell Robert JA, *et al.* DNA Methylation and Somatic Mutations Converge on the Cell Cycle and Define Similar Evolutionary Histories in Brain Tumors. Cancer Cell **2015**;28:307-17
115. Lee JK, Wang J, Sa JK, Ladewig E, Lee HO, Lee IH, *et al.* Spatiotemporal genomic architecture informs precision oncology in glioblastoma. Nat Genet **2017**;49:594-9
116. Eder K, Kalman B. Molecular heterogeneity of glioblastoma and its clinical relevance. Pathology oncology research : POR **2014**;20:777-87
117. Gillies RJ, Verduzco D, Gatenby RA. Evolutionary dynamics of carcinogenesis and why targeted therapy does not work. Nature reviews Cancer **2012**;12:487-93
118. McGranahan N, Swanton C. Biological and therapeutic impact of intratumor heterogeneity in cancer evolution. Cancer cell **2015**;27:15-26
119. Watts C, Piccirillo SGM. Clonal diversity in glioblastoma: is it clinically relevant? Future oncology (London, England) **2015**;11:1703-6
120. Snuderl M, Fazlollahi L, Le LP, Nitta M, Zhelyazkova BH, Davidson CJ, *et al.* Mosaic amplification of multiple receptor tyrosine kinase genes in glioblastoma. Cancer cell **2011**;20:810-7
121. Szerlip NJ, Pedraza A, Chakravarty D, Azim M, McGuire J, Fang Y, *et al.* Intratumoral heterogeneity of receptor tyrosine kinases EGFR and PDGFRA amplification in glioblastoma defines subpopulations with distinct growth factor response. Proceedings of the National Academy of Sciences of the United States of America **2012**;109:3041-6
122. Stupp R, Mason WP, van den Bent MJ, Weller M, Fisher B, Taphoorn MJB, *et al.* Radiotherapy plus concomitant and adjuvant temozolomide for glioblastoma. The New England journal of medicine **2005**;352:987-96
123. Ciric I, Ammirati M, Vick N, Mikhael M. Supratentorial gliomas: surgical considerations and immediate postoperative results. Gross total resection versus partial resection. Neurosurgery **1987**;21:21-6
124. Thumma SR, Fairbanks RK, Lamoreaux WT, Mackay AR, Demakas JJ, Cooke BS, *et al.* Effect of pretreatment clinical factors on overall survival in glioblastoma multiforme: a Surveillance Epidemiology and End Results (SEER) population analysis. World journal of surgical oncology **2012**;10:75
125. McGirt MJ, Chaichana KL, Gathinji M, Attenello FJ, Than K, Olivi A, *et al.* Independent association of extent of resection with survival in patients with malignant brain astrocytoma. Journal of neurosurgery **2009**;110:156-62
126. Sanai N, Polley MY, McDermott MW, Parsa AT, Berger MS. An extent of resection threshold for newly diagnosed glioblastomas. J Neurosurg **2011**;115:3-8
127. Fadul C, Wood J, Thaler H, Galicich J, Patterson RH, Jr., Posner JB. Morbidity and mortality of craniotomy for excision of supratentorial gliomas. Neurology **1988**;38:1374-9
128. Vuorinen V, Hinkka S, Färkkilä M, Jääskeläinen J. Debulking or biopsy of malignant glioma in elderly people - a randomised study. Acta neurochirurgica **2003**;145:5-10
129. McAbee JH, Golahmadi A, Watts C. Age: A Criterion to Offer Surgical Treatment as a Cytoreductive Tool for Malignant Primary Brain Tumour? In: Bartels RHMA, editor. Evidence for Neurosurgery. Switzerland: Springer Nature; 2019.

130. Kubben PL, ter Meulen KJ, Schijns OE, ter Laak-Poort MP, van Overbeeke JJ, van Santbrink H. Intraoperative MRI-guided resection of glioblastoma multiforme: a systematic review. Lancet Oncol **2011**;12:1062-70
131. Stummer W, Pichlmeier U, Meinel T, Wiestler OD, Zanella F, Reulen H-J*, et al.* Fluorescence-guided surgery with 5-aminolevulinic acid for resection of malignant glioma: a randomised controlled multicentre phase III trial. The Lancet Oncology **2006**;7:392-401
132. Stummer W, Reulen H-J, Meinel T, Pichlmeier U, Schumacher W, Tonn J-C*, et al.* Extent of resection and survival in glioblastoma multiforme: identification of and adjustment for bias. Neurosurgery **2008**;62:564-76
133. Stummer W, Stocker S, Wagner S, Stepp H, Fritsch C, Goetz C*, et al.* Intraoperative detection of malignant gliomas by 5-aminolevulinic acid-induced porphyrin fluorescence. Neurosurgery **1998**;42:518-25; discussion 25-6
134. Batlle AM. Porphyrins, porphyrias, cancer and photodynamic therapy--a model for carcinogenesis. J Photochem Photobiol B **1993**;20:5-22
135. Iinuma S, Farshi SS, Ortel B, Hasan T. A mechanistic study of cellular photodestruction with 5-aminolaevulinic acid-induced porphyrin. Br J Cancer **1994**;70:21-8
136. Piccirillo SGM, Dietz S, Madhu B, Griffiths J, Price SJ, Collins VP*, et al.* Fluorescence-guided surgical sampling of glioblastoma identifies phenotypically distinct tumour-initiating cell populations in the tumour mass and margin. British journal of cancer **2012**;107:462-8
137. Stummer W, van den Bent MJ, Westphal M. Cytoreductive surgery of glioblastoma as the key to successful adjuvant therapies: new arguments in an old discussion. Acta neurochirurgica **2011**;153:1211-8
138. LA S. Chemotherapy in adult high-grade glioma: a systematic review and meta-analysis of individual patient data from 12 randomised trials. Lancet **2002**;359:1011-8
139. Stupp R, Hegi ME, Mason WP, van den Bent MJ, Taphoorn MJ, Janzer RC*, et al.* Effects of radiotherapy with concomitant and adjuvant temozolomide versus radiotherapy alone on survival in glioblastoma in a randomised phase III study: 5-year analysis of the EORTC-NCIC trial. Lancet Oncol **2009**;10:459-66
140. Kim KJ, Li B, Winer J, Armanini M, Gillett N, Phillips HS*, et al.* Inhibition of vascular endothelial growth factor-induced angiogenesis suppresses tumour growth in vivo. Nature **1993**;362:841-4
141. Vredenburgh JJ, Desjardins A, Herndon JE, 2nd, Dowell JM, Reardon DA, Quinn JA*, et al.* Phase II trial of bevacizumab and irinotecan in recurrent malignant glioma. Clin Cancer Res **2007**;13:1253-9
142. Kreisl TN, Kim L, Moore K, Duic P, Royce C, Stroud I*, et al.* Phase II trial of single-agent bevacizumab followed by bevacizumab plus irinotecan at tumor progression in recurrent glioblastoma. J Clin Oncol **2009**;27:740-5
143. Friedman HS, Prados MD, Wen PY, Mikkelsen T, Schiff D, Abrey LE*, et al.* Bevacizumab alone and in combination with irinotecan in recurrent glioblastoma. J Clin Oncol **2009**;27:4733-40

144. Gilbert MR, Dignam JJ, Armstrong TS, Wefel JS, Blumenthal DT, Vogelbaum MA, *et al.* A randomized trial of bevacizumab for newly diagnosed glioblastoma. The New England journal of medicine **2014**;370:699-708
145. Chinot OL, Wick W, Mason W, Henriksson R, Saran F, Nishikawa R, *et al.* Bevacizumab plus radiotherapy-temozolomide for newly diagnosed glioblastoma. The New England journal of medicine **2014**;370:709-22
146. McGranahan T, Therkelsen KE, Ahmad S, Nagpal S. Current State of Immunotherapy for Treatment of Glioblastoma. Curr Treat Options Oncol **2019**;20:24
147. Neagu MR, Reardon DA. An Update on the Role of Immunotherapy and Vaccine Strategies for Primary Brain Tumors. Curr Treat Options Oncol **2015**;16:54
148. Louveau A, Harris TH, Kipnis J. Revisiting the Mechanisms of CNS Immune Privilege. Trends Immunol **2015**;36:569-77
149. Weiss N, Miller F, Cazaubon S, Couraud PO. The blood-brain barrier in brain homeostasis and neurological diseases. Biochim Biophys Acta **2009**;1788:842-57
150. Wu A, Wei J, Kong LY, Wang Y, Priebe W, Qiao W, *et al.* Glioma cancer stem cells induce immunosuppressive macrophages/microglia. Neuro Oncol **2010**;12:1113-25
151. Keir ME, Liang SC, Guleria I, Latchman YE, Qipo A, Albacker LA, *et al.* Tissue expression of PD-L1 mediates peripheral T cell tolerance. J Exp Med **2006**;203:883-95
152. Reardon DA, Omuro AMP, Brandes AA, Rieger J, Wick A, Sepulveda J, *et al.* OS10.3 Randomized Phase 3 Study Evaluating the Efficacy and Safety of Nivolumab vs Bevacizumab in Patients With Recurrent Glioblastoma: CheckMate 143. Neuro Oncol **2017**;19:iii21
153. Reardon D, Nayak L, Peters KB, Clarke JL, Jordan JT, De Groot JF, *et al.* Phase II study of pembrolizumab or pembrolizumab plus bevacizumab for recurrent glioblastoma (rGBM) patients. J Clin Oncol **2018**;36:2006
154. Swartz AM, Li QJ, Sampson JH. Rindopepimut: a promising immunotherapeutic for the treatment of glioblastoma multiforme. Immunotherapy **2014**;6:679-90
155. Celldex Therapeutics I. Data Safety and Monitoring Board Recommends Celldex's Phase 3 Study of RINTEGA® (rindopepimut) in Newly Diagnosed Glioblastoma be Discontinued as it is Unlikely to Meet Primary Overall Survival Endpoint in Patients with Minimal Residual Disease. **2016**
156. Wheeler CJ, Black KL, Liu G, Mazer M, Zhang X-x, Pepkowitz S, *et al.* Vaccination elicits correlated immune and clinical responses in glioblastoma multiforme patients. Cancer research **2008**;68:5955-64
157. Eagles ME, Nassiri F, Badhiwala JH, Suppiah S, Almenawer SA, Zadeh G, *et al.* Dendritic cell vaccines for high-grade gliomas. Ther Clin Risk Manag **2018**;14:1299-313
158. Oldfield EH, Ram Z, Culver KW, Blaese RM, DeVroom HL, Anderson WF. Gene therapy for the treatment of brain tumors using intra-tumoral transduction with the thymidine kinase gene and intravenous ganciclovir. Hum Gene Ther **1993**;4:39-69
159. Sandmair AM, Loimas S, Puranen P, Immonen A, Kossila M, Puranen M, *et al.* Thymidine kinase gene therapy for human malignant glioma, using replication-deficient retroviruses or adenoviruses. Hum Gene Ther **2000**;11:2197-205

160. Desjardins A, Gromeier M, Herndon JE, 2nd, Beaubier N, Bolognesi DP, Friedman AH, *et al.* Recurrent Glioblastoma Treated with Recombinant Poliovirus. N Engl J Med **2018**;379:150-61
161. Rodriguez A, Brown C, Badie B. Chimeric antigen receptor T-cell therapy for glioblastoma. Transl Res **2017**;187:93-102
162. Neelapu SS, Tummala S, Kebriaei P, Wierda W, Gutierrez C, Locke FL, *et al.* Chimeric antigen receptor T-cell therapy - assessment and management of toxicities. Nat Rev Clin Oncol **2018**;15:47-62
163. Basso J, Miranda A, Sousa J, Pais A, Vitorino C. Repurposing drugs for glioblastoma: From bench to bedside. Cancer Lett **2018**;428:173-83
164. Brem H, Piantadosi S, Burger PC, Walker M, Selker R, Vick NA, *et al.* Placebo-controlled trial of safety and efficacy of intraoperative controlled delivery by biodegradable polymers of chemotherapy for recurrent gliomas. The Polymer-brain Tumor Treatment Group. Lancet (London, England) **1995**;345:1008-12
165. Westphal M, Hilt DC, Bortey E, Delavault P, Olivares R, Warnke PC, *et al.* A phase 3 trial of local chemotherapy with biodegradable carmustine (BCNU) wafers (Gliadel wafers) in patients with primary malignant glioma. Neuro-oncology **2003**;5:79-88
166. Sage W, Guilfoyle M, Luney C, Young A, Sinha R, Sgubin D, *et al.* Local alkylating chemotherapy applied immediately after 5-ALA guided resection of glioblastoma does not provide additional benefit. J Neurooncol **2018**;136:273-80
167. FJ A, D M, G D, MJ M, E B, JD W, *et al.* Attenello FJ1, Mukherjee D, Datoo G, McGirt MJ, Bohan E, Weingart JD, Olivi A, Quinones-Hinojosa A, Brem H. Ann Surg Oncol **2008**;15:2887-93
168. S N. The role of BCNU polymer wafers (Gliadel) in the treatment of malignant glioma. Neurosurg Clin N Am **2012**;23:289-95
169. Rowland MJ, Atgie M, Hoogland D, Scherman OA. Preparation and Supramolecular Recognition of Multivalent Peptide-Polysaccharide Conjugates by Cucurbit[8]uril in Hydrogel Formation. Biomacromolecules **2015**;16:2436-43
170. Tabet A, Jensen MP, Parkins CC, Patil PG, Watts C, Scherman OA. Designing Next-Generation Local Drug Delivery Vehicles for Glioblastoma Adjuvant Chemotherapy: Lessons from the Clinic. Adv Healthc Mater **2019**;8:e1801391
171. Yamahara T, Numa Y, Oishi T, Kawaguchi T, Seno T, Asai A, *et al.* Morphological and flow cytometric analysis of cell infiltration in glioblastoma: a comparison of autopsy brain and neuroimaging. Brain tumor pathology **2010**;27:81-7
172. Lee SW, Fraass BA, Marsh LH, Herbort K, Gebarski SS, Martel MK, *et al.* Patterns of failure following high-dose 3-D conformal radiotherapy for high-grade astrocytomas: a quantitative dosimetric study. Int J Radiat Oncol Biol Phys **1999**;43:79-88
173. Oppitz U, Maessen D, Zunterer H, Richter S, Flentje M. 3D-recurrence-patterns of glioblastomas after CT-planned postoperative irradiation. Radiother Oncol **1999**;53:53-7
174. Chang CH, Horton J, Schoenfeld D, Salazer O, Perez-Tamayo R, Kramer S, *et al.* Comparison of postoperative radiotherapy and combined postoperative radiotherapy and chemotherapy in the multidisciplinary management of malignant gliomas. A joint

Radiation Therapy Oncology Group and Eastern Cooperative Oncology Group study. Cancer **1983**;52:997-1007

175. Walker MD, Green SB, Byar DP, Alexander E, Jr., Batzdorf U, Brooks WH, *et al.* Randomized comparisons of radiotherapy and nitrosoureas for the treatment of malignant glioma after surgery. N Engl J Med **1980**;303:1323-9
176. Chalmers AJ, Ruff EM, Martindale C, Lovegrove N, Short SC. Cytotoxic effects of temozolomide and radiation are additive- and schedule-dependent. Int J Radiat Oncol Biol Phys **2009**;75:1511-9
177. Niyazi M, Brada M, Chalmers AJ, Combs SE, Erridge SC, Fiorentino A, *et al.* ESTRO-ACROP guideline "target delineation of glioblastomas". Radiother Oncol **2016**;118:35-42
178. Gilbert MR, Wang M, Aldape KD, Stupp R, Hegi ME, Jaeckle KA, *et al.* Dose-dense temozolomide for newly diagnosed glioblastoma: a randomized phase III clinical trial. Journal of clinical oncology : official journal of the American Society of Clinical Oncology **2013**;31:4085-91
179. Gilbert MR, Wang M, Aldape KD, Stupp R, Hegi M, Jaeckle KA, *et al.* RTOG 0525: A randomized phase III trial comparing standard adjuvant temozolomide (TMZ) with a dose-dense (dd) schedule in newly diagnosed glioblastoma (GBM). **2011**;29:2006-
180. Minniti G, Amelio D, Amichetti M, Salvati M, Muni R, Bozzao A, *et al.* Patterns of failure and comparison of different target volume delineations in patients with glioblastoma treated with conformal radiotherapy plus concomitant and adjuvant temozolomide. Radiother Oncol **2010**;97:377-81
181. Amelio D, Lorentini S, Schwarz M, Amichetti M. Intensity-modulated radiation therapy in newly diagnosed glioblastoma: a systematic review on clinical and technical issues. Radiother Oncol **2010**;97:361-9
182. Narayana A, Yamada J, Berry S, Shah P, Hunt M, Gutin PH, *et al.* Intensity-modulated radiotherapy in high-grade gliomas: clinical and dosimetric results. Int J Radiat Oncol Biol Phys **2006**;64:892-7
183. Khoo VS, Oldham M, Adams EJ, Bedford JL, Webb S, Brada M. Comparison of intensity-modulated tomotherapy with stereotactically guided conformal radiotherapy for brain tumors. Int J Radiat Oncol Biol Phys **1999**;45:415-25
184. Curran WJ, Jr., Scott C, Yung WK. No survival benefit of hyperfractionated radiotherapy (RT) to 72.0 Gy and carmustine versus standard RT and carmustine for malignant glioma patients: preliminary results of RTOG 90-06. J Clin Oncol **1996**;15:15
185. Laperriere N, Zuraw L, Cairncross G, Cancer Care Ontario Practice Guidelines Initiative Neuro-Oncology Disease Site G. Radiotherapy for newly diagnosed malignant glioma in adults: a systematic review. Radiother Oncol **2002**;64:259-73
186. Horiot JC, van den Bogaert W, Ang KK, Van der Schueren E, Bartelink H, Gonzalez D, *et al.* European Organization for Research on Treatment of Cancer trials using radiotherapy with multiple fractions per day. A 1978-1987 survey. Front Radiat Ther Oncol **1988**;22:149-61
187. Minniti G, Scaringi C, Lanzetta G, Terrenato I, Esposito V, Arcella A, *et al.* Standard (60 Gy) or Short-Course (40 Gy) Irradiation Plus Concomitant and Adjuvant

Temozolomide for Elderly Patients With Glioblastoma: A Propensity-Matched Analysis. International Journal of Radiation Oncology*Biology*Physics **2015**;91:109-15

188. Roa W, Brasher PM, Bauman G, Anthes M, Bruera E, Chan A*, et al.* Abbreviated course of radiation therapy in older patients with glioblastoma multiforme: a prospective randomized clinical trial. J Clin Oncol **2004**;22:1583-8
189. Selker RG, Shapiro WR, Burger P, Blackwood MS, Arena VC, Gilder JC*, et al.* The Brain Tumor Cooperative Group NIH Trial 87-01: a randomized comparison of surgery, external radiotherapy, and carmustine versus surgery, interstitial radiotherapy boost, external radiation therapy, and carmustine. Neurosurgery **2002**;51:343-55; discussion 55-7
190. Laperriere NJ, Leung PM, McKenzie S, Milosevic M, Wong S, Glen J*, et al.* Randomized study of brachytherapy in the initial management of patients with malignant astrocytoma. Int J Radiat Oncol Biol Phys **1998**;41:1005-11
191. Souhami L, Seiferheld W, Brachman D, Podgorsak EB, Werner-Wasik M, Lustig R*, et al.* Randomized comparison of stereotactic radiosurgery followed by conventional radiotherapy with carmustine to conventional radiotherapy with carmustine for patients with glioblastoma multiforme: report of Radiation Therapy Oncology Group 93-05 protocol. Int J Radiat Oncol Biol Phys **2004**;60:853-60
192. Cardinale R, Won M, Choucair A, Gillin M, Chakravarti A, Schultz C*, et al.* A phase II trial of accelerated radiotherapy using weekly stereotactic conformal boost for supratentorial glioblastoma multiforme: RTOG 0023. Int J Radiat Oncol Biol Phys **2006**;65:1422-8
193. Baumert BG, Brada M, Bernier J, Kortmann RD, Dehing-Oberije C, Collette L*, et al.* EORTC 22972-26991/MRC BR10 trial: fractionated stereotactic boost following conventional radiotherapy of high grade gliomas. Clinical and quality-assurance results of the stereotactic boost arm. Radiother Oncol **2008**;88:163-72
194. Cuneo KC, Vredenburgh JJ, Sampson JH, Reardon DA, Desjardins A, Peters KB*, et al.* Safety and efficacy of stereotactic radiosurgery and adjuvant bevacizumab in patients with recurrent malignant gliomas. Int J Radiat Oncol Biol Phys **2012**;82:2018-24
195. Kazmi F, Soon YY, Leong YH, Koh WY, Vellayappan B. Re-irradiation for recurrent glioblastoma (GBM): a systematic review and meta-analysis. J Neurooncol **2019**;142:79-90
196. Navarria P, Minniti G, Clerici E, Tomatis S, Pinzi V, Ciammella P*, et al.* Re-irradiation for recurrent glioma: outcome evaluation, toxicity and prognostic factors assessment. A multicenter study of the Radiation Oncology Italian Association (AIRO). J Neurooncol **2019**;142:59-67
197. Krauze AV, Attia A, Braunstein S, Chan M, Combs SE, Fietkau R*, et al.* Expert consensus on re-irradiation for recurrent glioma. Radiat Oncol **2017**;12:194
198. Adkison JB, Tome W, Seo S, Richards GM, Robins HI, Rassmussen K*, et al.* Reirradiation of large-volume recurrent glioma with pulsed reduced-dose-rate radiotherapy. Int J Radiat Oncol Biol Phys **2011**;79:835-41

199. Harasaki Y, Waziri A. Potential usefulness of radiosensitizers in glioblastoma. Neurosurgery clinics of North America **2012**;23:429-37
200. Krauze AV, Myrehaug SD, Chang MG, Holdford DJ, Smith S, Shih J*, et al.* A Phase 2 Study of Concurrent Radiation Therapy, Temozolomide, and the Histone Deacetylase Inhibitor Valproic Acid for Patients With Glioblastoma. International journal of radiation oncology, biology, physics **2015**;92:986-92
201. Kahn J, Hayman TJ, Jamal M, Rath BH, Kramp T, Camphausen K*, et al.* The mTORC1/mTORC2 inhibitor AZD2014 enhances the radiosensitivity of glioblastoma stem-like cells. Neuro-oncology **2014**;16:29-37
202. Carruthers R, Ahmed SU, Strathdee K, Gomez-Roman N, Amoah-Buahin E, Watts C*, et al.* Abrogation of radioresistance in glioblastoma stem-like cells by inhibition of ATM kinase. Molecular oncology **2015**;9:192-203
203. Dungey FA, Loser DA, Chalmers AJ. Replication-dependent radiosensitization of human glioma cells by inhibition of poly(ADP-Ribose) polymerase: mechanisms and therapeutic potential. Int J Radiat Oncol Biol Phys **2008**;72:1188-97
204. Loser DA, Shibata A, Shibata AK, Woodbine LJ, Jeggo PA, Chalmers AJ. Sensitization to radiation and alkylating agents by inhibitors of poly(ADP-ribose) polymerase is enhanced in cells deficient in DNA double-strand break repair. Mol Cancer Ther **2010**;9:1775-87
205. Ahmed SU, Carruthers R, Gilmour L, Yildirim S, Watts C, Chalmers AJ. Selective Inhibition of Parallel DNA Damage Response Pathways Optimizes Radiosensitization of Glioblastoma Stem-like Cells. Cancer research **2015**;75:4416-28
206. Carruthers RD, Ahmed SU, Ramachandran S, Strathdee K, Kurian KM, Hedley A*, et al.* Replication Stress Drives Constitutive Activation of the DNA Damage Response and Radioresistance in Glioblastoma Stem-like Cells. Cancer Res **2018**;78:5060-71
207. Setua S, Ouberai M, Piccirillo SG, Watts C, Welland M. Cisplatin-tethered gold nanospheres for multimodal chemo-radiotherapy of glioblastoma. Nanoscale **2014**;6:10865-73
208. Tofilon PJ, Camphausen K. Molecular targets for tumor radiosensitization. Chemical Reviews **2009**;109
209. Kim H, Zheng S, Amini SS, Virk SM, Mikkelsen T, Brat DJ*, et al.* Whole-genome and multisector exome sequencing of primary and post-treatment glioblastoma reveals patterns of tumor evolution. Genome research **2015**;25:316-27
210. Kim J, Lee IH, Cho HJ, Park CK, Jung YS, Kim Y*, et al.* Spatiotemporal Evolution of the Primary Glioblastoma Genome. Cancer Cell **2015**;28:318-28
211. Alexandrov LB, Kim J, Haradhvala NJ, Huang MN, Ng AW, Boot A*, et al.* The Repertoire of Mutational Signatures in Human Cancer. bioRxiv **2018**:322859
212. Alexandrov LB, Nik-Zainal S, Wedge DC, Aparicio SAJR, Behjati S, Biankin AV*, et al.* Signatures of mutational processes in human cancer. Nature **2013**;500:415-21
213. Neilsen BK, Sleightholm R, McComb R, Ramkissoon SH, Ross JS, Corona RJ*, et al.* Comprehensive genetic alteration profiling in primary and recurrent glioblastoma. Journal of neuro-oncology **2018**

214. Aldape K, Amin SB, Ashley DM, Barnholtz-Sloan JS, Bates AJ, Beroukhim R, *et al.* Glioma through the looking GLASS: molecular evolution of diffuse gliomas and the Glioma Longitudinal Analysis Consortium. Neuro-Oncology **2018**;20:873-84
215. Mair R, Mouliere F, Smith CG, Chandrananda D, Gale D, Marass F, *et al.* Measurement of Plasma Cell-Free Mitochondrial Tumor DNA Improves Detection of Glioblastoma in Patient-Derived Orthotopic Xenograft Models. Cancer Research **2019**;79:220-30
216. Mouliere F, Mair R, Chandrananda D, Marass F, Smith CG, Su J, *et al.* Detection of cell-free DNA fragmentation and copy number alterations in cerebrospinal fluid from glioma patients. EMBO Mol Med **2018**;10
217. Miller AM, Shah RH, Pentsova EI, Pourmaleki M, Briggs S, Distefano N, *et al.* Tracking tumour evolution in glioma through liquid biopsies of cerebrospinal fluid. Nature **2019**;565:654-8
218. Shankar GM, Balaj L, Stott SL, Nahed B, Carter BS. Liquid biopsy for brain tumors. Expert Review of Molecular Diagnostics **2017**;17:943-7
219. Hambardzumyan D, Gutmann DH, Kettenmann H. The role of microglia and macrophages in glioma maintenance and progression. Nat Neurosci **2016**;19:20-7
220. Markovic DS, Glass R, Synowitz M, Rooijen N, Kettenmann H. Microglia stimulate the invasiveness of glioma cells by increasing the activity of metalloprotease-2. J Neuropathol Exp Neurol **2005**;64:754-62
221. Markovic DS, Vinnakota K, Chirasani S, Synowitz M, Raguet H, Stock K, *et al.* Gliomas induce and exploit microglial MT1-MMP expression for tumor expansion. Proc Natl Acad Sci U S A **2009**;106:12530-5
222. Coniglio SJ, Eugenin E, Dobrenis K, Stanley ER, West BL, Symons MH, *et al.* Microglial stimulation of glioblastoma invasion involves epidermal growth factor receptor (EGFR) and colony stimulating factor 1 receptor (CSF-1R) signaling. Mol Med **2012**;18:519-27
223. Carvalho da Fonseca AC, Wang H, Fan H, Chen X, Zhang I, Zhang L, *et al.* Increased expression of stress inducible protein 1 in glioma-associated microglia/macrophages. J Neuroimmunol **2014**;274:71-7
224. Saederup N, Cardona AE, Croft K, Mizutani M, Cotleur AC, Tsou CL, *et al.* Selective chemokine receptor usage by central nervous system myeloid cells in CCR2-red fluorescent protein knock-in mice. PLoS One **2010**;5:e13693
225. Wick W, Platten M, Weller M. Glioma cell invasion: regulation of metalloproteinase activity by TGF-beta. J Neurooncol **2001**;53:177-85
226. Chen X, Zhang L, Zhang IY, Liang J, Wang H, Ouyang M, *et al.* RAGE expression in tumor-associated macrophages promotes angiogenesis in glioma. Cancer Res **2014**;74:7285-97
227. Bhat KPL, Balasubramaniyan V, Vaillant B, Ezhilarasan R, Hummelink K, Hollingsworth F, *et al.* Mesenchymal differentiation mediated by NF-kappaB promotes radiation resistance in glioblastoma. Cancer Cell **2013**;24:331-46
228. Wang Q, Hu B, Hu X, Kim H, Squatrito M, Scarpace L, *et al.* Tumor Evolution of Glioma-Intrinsic Gene Expression Subtypes Associates with Immunological Changes in the Microenvironment. Cancer Cell **2017**;32:42-56.e6

229. Rath BH, Fair JM, Jamal M, Camphausen K, Tofilon PJ. Astrocytes enhance the invasion potential of glioblastoma stem-like cells. PloS one **2013**;8:e54752
230. Rath BH, Wahba A, Camphausen K, Tofilon PJ. Coculture with astrocytes reduces the radiosensitivity of glioblastoma stem-like cells and identifies additional targets for radiosensitization. Cancer medicine **2015**;4:1705-16
231. Henrik Heiland D, Ravi VM, Behringer SP, Frenking JH, Wurm J, Joseph K*, et al.* Tumor-associated reactive astrocytes aid the evolution of immunosuppressive environment in glioblastoma. Nat Commun **2019**;10:2541
232. Hambardzumyan D, Bergers G. Glioblastoma: Defining Tumor Niches. Trends Cancer **2015**;1:252-65
233. Daniel P, Sabri S, Chaddad A, Meehan B, Jean-Claude B, Rak J*, et al.* Temozolomide Induced Hypermutation in Glioma: Evolutionary Mechanisms and Therapeutic Opportunities. Front Oncol **2019**;9:41
234. Finocchiaro G, Langella T, Corbetta C, Pellegatta S. Hypermutations in gliomas: a potential immunotherapy target. Discov Med **2017**;23:113-20
235. Lan X, Jorg DJ, Cavalli FMG, Richards LM, Nguyen LV, Vanner RJ*, et al.* Fate mapping of human glioblastoma reveals an invariant stem cell hierarchy. Nature **2017**;549:227-32
236. Muscat AM, Wong NC, Drummond KJ, Algar EM, Khasraw M, Verhaak R*, et al.* The evolutionary pattern of mutations in glioblastoma reveals therapy-mediated selection. Oncotarget **2018**;9:7844-58
237. Wang J, Cazzato E, Ladewig E, Frattini V, Rosenbloom DI, Zairis S*, et al.* Clonal evolution of glioblastoma under therapy. Nat Genet **2016**;48:768-76
238. Schäfer N, Gielen GH, Rauschenbach L, Kebir S, Till A, Reinartz R*, et al.* Longitudinal heterogeneity in glioblastoma: moving targets in recurrent versus primary tumors. Journal of translational medicine **2019**;17:96
239. Draaisma K, Chatzipli A, Taphoorn M, Kerkhof M, Weyerbrock A, Sanson M*, et al.* The molecular evolution of IDH-wildtype glioblastomas treated with standard of care impacts survival and design of precision medicine trials. A report from the EORTC 1542 study. J Clin Oncol **2019**;Accepted for Publication
240. van den Bent MJ, Gao Y, Kerkhof M, Kros JM, Gorlia T, van Zwieten K*, et al.* Changes in the EGFR amplification and EGFRvIII expression between paired primary and recurrent glioblastomas. Neuro Oncol **2015**;17:935-41
241. Galli R, Binda E, Orfanelli U, Cipelletti B, Gritti A, De Vitis S*, et al.* Isolation and characterization of tumorigenic, stem-like neural precursors from human glioblastoma. Cancer research **2004**;64:7011-21
242. Singh SK, Hawkins C, Clarke ID, Squire JA, Bayani J, Hide T*, et al.* Identification of human brain tumour initiating cells. Nature **2004**;432:396-401
243. Liebelt BD, Shingu T, Zhou X, Ren J, Shin SA, Hu J. Glioma Stem Cells: Signaling, Microenvironment, and Therapy. Stem Cells Int **2016**;2016:7849890
244. Lathia JD, Mack SC, Mulkearns-Hubert EE, Valentim CL, Rich JN. Cancer stem cells in glioblastoma. Genes Dev **2015**;29:1203-17

245. Bao S, Wu Q, McLendon RE, Hao Y, Shi Q, Hjelmeland AB, *et al.* Glioma stem cells promote radioresistance by preferential activation of the DNA damage response. Nature **2006**;444:756-60
246. Liu G, Yuan X, Zeng Z, Tunici P, Ng H, Abdulkadir IR, *et al.* Analysis of gene expression and chemoresistance of CD133+ cancer stem cells in glioblastoma. Mol Cancer **2006**;5:67
247. Kenney-Herbert EM, Ball SLR, Al-Mayhani TMF, Watts C. Glioblastoma cell lines derived under serum-free conditions can be used as an in vitro model system to evaluate therapeutic response. Cancer Lett **2011**;305:50-7
248. Chen R, Nishimura MC, Bumbaca SM, Kharbanda S, Forrest WF, Kasman IM, *et al.* A hierarchy of self-renewing tumor-initiating cell types in glioblastoma. Cancer Cell **2010**;17:362-75
249. Al-Mayhani TF, Heywood RM, Vemireddy V, Lathia JD, Piccirillo SGM, Watts C. A non-hierarchical organization of tumorigenic NG2 cells in glioblastoma promoted by EGFR. Neuro Oncol **2019**;21:719-29
250. Piccirillo SGM, Colman S, Potter NE, van Delft FW, Lillis S, Carnicer M-J, *et al.* Genetic and functional diversity of propagating cells in glioblastoma. Stem cell reports **2015**;4:7-15
251. Piccirillo SG, Combi R, Cajola L, Patrizi A, Redaelli S, Bentivegna A, *et al.* Distinct pools of cancer stem-like cells coexist within human glioblastomas and display different tumorigenicity and independent genomic evolution. Oncogene **2009**;28:1807-11
252. Lee J, Kotliarova S, Kotliarov Y, Li A, Su Q, Donin NM, *et al.* Tumor stem cells derived from glioblastomas cultured in bFGF and EGF more closely mirror the phenotype and genotype of primary tumors than do serum-cultured cell lines. Cancer cell **2006**;9:391-403
253. Wakimoto H, Mohapatra G, Kanai R, Curry WT, Yip S, Nitta M, *et al.* Maintenance of primary tumor phenotype and genotype in glioblastoma stem cells. Neuro-oncology **2012**;14:132-44
254. Jamal M, Rath BH, Williams ES, Camphausen K, Tofilon PJ. Microenvironmental regulation of glioblastoma radioresponse. Clinical cancer research : an official journal of the American Association for Cancer Research **2010**;16:6049-59
255. Orzan F, De Bacco F, Crisafulli G, Pellegatta S, Mussolin B, Siravegna G, *et al.* Genetic Evolution of Glioblastoma Stem-Like Cells From Primary to Recurrent Tumor. Stem cells (Dayton, Ohio) **2017**;35:2218-28
256. Tanaka S, Luk S, Kiyokawa J, Onozato ML, Iafrate AJ, Shah K, *et al.* Genetically distinct glioma stem-like cell xenografts established from paired glioblastoma samples harvested before and after molecularly targeted therapy. Scientific Reports **2019**;9:139
257. Chen J, Li Y, Yu T-S, McKay RM, Burns DK, Kernie SG, *et al.* A restricted cell population propagates glioblastoma growth after chemotherapy. Nature **2012**;488:522-6
258. Bond AM, Ming GL, Song H. Adult Mammalian Neural Stem Cells and Neurogenesis: Five Decades Later. Cell Stem Cell **2015**;17:385-95

259. Spiteri I, Caravagna G, Cresswell GD, Vatsiou A, Nichol D, Acar A, *et al.* Evolutionary dynamics of residual disease in human glioblastoma. Annals of oncology : official journal of the European Society for Medical Oncology **2018**
260. Abdullah KG, Adamson C, Brem S. The Molecular Pathogenesis of Glioblastoma. In: Brem S, Abdullah KG, editors. Glioblastoma. Philadelphia, PA: Elsevier; 2017. p 21-31.
261. Lathia JD, Gallagher J, Heddleston JM, Wang J, Eyler CE, Macswords J, *et al.* Integrin alpha 6 regulates glioblastoma stem cells. Cell Stem Cell **2010**;6:421-32
262. Bao S, Wu Q, Sathornsumetee S, Hao Y, Li Z, Hjelmeland AB, *et al.* Stem cell-like glioma cells promote tumor angiogenesis through vascular endothelial growth factor. Cancer Res **2006**;66:7843-8
263. Wang R, Chadalavada K, Wilshire J, Kowalik U, Hovinga KE, Geber A, *et al.* Glioblastoma stem-like cells give rise to tumour endothelium. Nature **2010**;468:829-33
264. Ricci-Vitiani L, Pallini R, Biffoni M, Todaro M, Invernici G, Cenci T, *et al.* Tumour vascularization via endothelial differentiation of glioblastoma stem-like cells. Nature **2010**;468:824-8
265. Soda Y, Marumoto T, Friedmann-Morvinski D, Soda M, Liu F, Michiue H, *et al.* Transdifferentiation of glioblastoma cells into vascular endothelial cells. Proc Natl Acad Sci U S A **2011**;108:4274-80
266. Jamal M, Rath BH, Tsang PS, Camphausen K, Tofilon PJ. The brain microenvironment preferentially enhances the radioresistance of CD133(+) glioblastoma stem-like cells. Neoplasia (New York, NY) **2012**;14:150-8
267. McCord AM, Jamal M, Shankavaram UT, Shankavarum UT, Lang FF, Camphausen K, *et al.* Physiologic oxygen concentration enhances the stem-like properties of CD133+ human glioblastoma cells in vitro. Molecular cancer research : MCR **2009**;7:489-97
268. McCord AM, Jamal M, Williams ES, Camphausen K, Tofilon PJ. CD133+ glioblastoma stem-like cells are radiosensitive with a defective DNA damage response compared with established cell lines. Clinical cancer research : an official journal of the American Association for Cancer Research **2009**;15:5145-53
269. Pollard SM, Yoshikawa K, Clarke ID, Danovi D, Stricker S, Russell R, *et al.* Glioma Stem Cell Lines Expanded in Adherent Culture Have Tumor-Specific Phenotypes and Are Suitable for Chemical and Genetic Screens. Cell Stem Cell **2009**;4:568-80
270. Khandelwal G, Girotti MR, Smowton C, Taylor S, Wirth C, Dynowski M, *et al.* Next-Generation Sequencing Analysis and Algorithms for PDX and CDX Models. Molecular Cancer Research **2017**;15:1012-6
271. Bolger AM, Lohse M, Usadel B. Trimmomatic: a flexible trimmer for Illumina sequence data. Bioinformatics **2014**;30:2114-20
272. Li H. Aligning sequence reads, clone sequences and assembly contigs with BWA-MEM. arXiv:13033997v2 [q-bioGN] **2013**
273. Li H, Handsaker B, Wysoker A, Fennell T, Ruan J, Homer N, *et al.* The Sequence Alignment/Map format and SAMtools. Bioinformatics **2009**;25:2078-9

274. McKenna A, Hanna M, Banks E, Sivachenko A, Cibulskis K, Kernytsky A, *et al.* The Genome Analysis Toolkit: a MapReduce framework for analyzing next-generation DNA sequencing data. Genome research **2010**;20:1297-303
275. Van der Auwera GA, Carneiro MO, Hartl C, Poplin R, Del Angel G, Levy-Moonshine A, *et al.* From FastQ data to high confidence variant calls: the Genome Analysis Toolkit best practices pipeline. Current protocols in bioinformatics **2013**;43:11.0.1-33
276. Ewels P, Magnusson M, Lundin S, Kaller M. MultiQC: summarize analysis results for multiple tools and samples in a single report. Bioinformatics **2016**;32:3047-8
277. Barnett DW, Garrison EK, Quinlan AR, Stromberg MP, Marth GT. BamTools: a C++ API and toolkit for analyzing and managing BAM files. Bioinformatics **2011**;27:1691-2
278. Cibulskis K, Lawrence MS, Carter SL, Sivachenko A, Jaffe D, Sougnez C, *et al.* Sensitive detection of somatic point mutations in impure and heterogeneous cancer samples. Nature biotechnology **2013**;31:213-9
279. Lek M, Karczewski KJ, Minikel EV, Samocha KE, Banks E, Fennell T, *et al.* Analysis of protein-coding genetic variation in 60,706 humans. Nature **2016**;536:285-91
280. Bamshad MJ, Ng SB, Bigham AW, Tabor HK, Emond MJ, Nickerson DA, *et al.* Exome sequencing as a tool for Mendelian disease gene discovery. Nat Rev Genet **2011**;12:745-55
281. Patel AP, Tirosh I, Trombetta JJ, Shalek AK, Gillespie SM, Wakimoto H, *et al.* Single-cell RNA-seq highlights intratumoral heterogeneity in primary glioblastoma. Science (New York, NY) **2014**;344:1396-401
282. Hu Y, Smyth GK. ELDA: Extreme limiting dilution analysis for comparing depleted and enriched populations in stem cell and other assays. Journal of Immunological Methods **2009**;347:70-8
283. Flensburg C, Sargeant T, Oshlack A, Majewski I. SuperFreq: Integrated mutation detection and clonal tracking in cancer. bioRxiv **2018**
284. Rogakou EP, Pilch DR, Orr AH, Ivanova VS, Bonner WM. DNA Double-stranded Breaks Induce Histone H2AX Phosphorylation on Serine 139. Journal of Biological Chemistry **1998**;273:5858-68
285. Sedelnikova OA, Rogakou EP, Panyutin IG, Bonner WM. Quantitative detection of (125)IdU-induced DNA double-strand breaks with gamma-H2AX antibody. Radiation research **2002**;158:486-92
286. Banáth JP, MacPhail SH, Olive PL. Radiation Sensitivity, H2AX Phosphorylation, and Kinetics of Repair of DNA Strand Breaks in Irradiated Cervical Cancer Cell Lines. Cancer Research **2004**;64:7144-9
287. Olive PL, Banáth JP. Phosphorylation of histone H2AX as a measure of radiosensitivity. International journal of radiation oncology, biology, physics **2004**;58:331-5
288. Hall EJ, Giaccia AJ. Radiobiology for the Radiologist. **2012**
289. Goodspeed A, Heiser LM, Gray JW, Costello JC. Tumor-Derived Cell Lines as Molecular Models of Cancer Pharmacogenomics. Mol Cancer Res **2016**;14:3-13

290. Barretina J, Caponigro G, Stransky N, Venkatesan K, Margolin AA, Kim S*, et al.* The Cancer Cell Line Encyclopedia enables predictive modelling of anticancer drug sensitivity. Nature **2012**;483:603-7
291. Daniel VC, Marchionni L, Hierman JS, Rhodes JT, Devereux WL, Rudin CM*, et al.* A primary xenograft model of small-cell lung cancer reveals irreversible changes in gene expression imposed by culture in vitro. Cancer Res **2009**;69:3364-73
292. Domcke S, Sinha R, Levine DA, Sander C, Schultz N. Evaluating cell lines as tumour models by comparison of genomic profiles. Nat Commun **2013**;4:2126
293. Li H, Wawrose JS, Gooding WE, Garraway LA, Lui VW, Peyser ND*, et al.* Genomic analysis of head and neck squamous cell carcinoma cell lines and human tumors: a rational approach to preclinical model selection. Mol Cancer Res **2014**;12:571-82
294. Shoemaker RH. The NCI60 human tumour cell line anticancer drug screen. Nat Rev Cancer **2006**;6:813-23
295. Shankavaram UT, Varma S, Kane D, Sunshine M, Chary KK, Reinhold WC*, et al.* CellMiner: a relational database and query tool for the NCI-60 cancer cell lines. BMC Genomics **2009**;10:277
296. Nagai Y, Miyazawa H, Huqun, Tanaka T, Udagawa K, Kato M*, et al.* Genetic heterogeneity of the epidermal growth factor receptor in non-small cell lung cancer cell lines revealed by a rapid and sensitive detection system, the peptide nucleic acid-locked nucleic acid PCR clamp. Cancer Res **2005**;65:7276-82
297. Eskilsson E, Rosland GV, Talasila KM, Knappskog S, Keunen O, Sottoriva A*, et al.* EGFRvIII mutations can emerge as late and heterogenous events in glioblastoma development and promote angiogenesis through Src activation. Neuro Oncol **2016**;18:1644-55
298. Schuster J, Lai RK, Recht LD, Reardon DA, Paleologos NA, Groves MD*, et al.* A phase II, multicenter trial of rindopepimut (CDX-110) in newly diagnosed glioblastoma: the ACT III study. Neuro Oncol **2015**;17:854-61
299. Meyer M, Reimand J, Lan X, Head R, Zhu X, Kushida M*, et al.* Single cell-derived clonal analysis of human glioblastoma links functional and genomic heterogeneity. Proc Natl Acad Sci U S A **2015**;112:851-6
300. Johnson BE, Mazor T, Hong C, Barnes M, Aihara K, McLean CY*, et al.* Mutational analysis reveals the origin and therapy-driven evolution of recurrent glioma. Science (New York, NY) **2014**;343
301. Wu X, Li Y, Crise B, Burgess SM. Transcription start regions in the human genome are favored targets for MLV integration. Science **2003**;300:1749-51
302. De Ravin SS, Wu X, Moir S, Anaya-O'Brien S, Kwatemaa N, Littel P*, et al.* Lentiviral hematopoietic stem cell gene therapy for X-linked severe combined immunodeficiency. Sci Transl Med **2016**;8:335ra57
303. D H, Gu Z, Schlesner M. YAPSA: Yet Another Package for Signature Analysis. 2019.
304. Gröschel S, Hübschmann D, Raimondi F, Horak P, Warsow G, Fröhlich M*, et al.* Defective homologous recombination DNA repair as therapeutic target in advanced chordoma. Nature communications **2019**;10:1635

305. Andor N, Harness JV, Müller S, Mewes HW, Petritsch C. EXPANDS: expanding ploidy and allele frequency on nested subpopulations. Bioinformatics **2014**;30:50-60
306. Körber V, Yang J, Barah P, Wu Y, Stichel D, Gu Z*, et al.* Evolutionary Trajectories of IDHWT Glioblastomas Reveal a Common Path of Early Tumorigenesis Instigated Years ahead of Initial Diagnosis. Cancer Cell **2019**;35:692-704.e12
307. Bailey MH, Tokheim C, Porta-Pardo E, Sengupta S, Bertrand D, Weerasinghe A*, et al.* Comprehensive Characterization of Cancer Driver Genes and Mutations. Cell **2018**;174:1034-5
308. Martincorena I, Raine KM, Gerstung M, Dawson KJ, Haase K, Van Loo P*, et al.* Universal Patterns of Selection in Cancer and Somatic Tissues. Cell **2017**;171:1029-41 e21
309. Stieber D, Golebiewska A, Evers L, Lenkiewicz E, Brons NH, Nicot N*, et al.* Glioblastomas are composed of genetically divergent clones with distinct tumourigenic potential and variable stem cell-associated phenotypes. Acta Neuropathol **2014**;127:203-19
310. Wild-Bode C, Weller M, Rimner A, Dichgans J, Wick W. Sublethal irradiation promotes migration and invasiveness of glioma cells: implications for radiotherapy of human glioblastoma. Cancer Res **2001**;61:2744-50
311. Goetze K, Scholz M, Taucher-Scholz G, Mueller-Klieser W. The impact of conventional and heavy ion irradiation on tumor cell migration in vitro. Int J Radiat Biol **2007**;83:889-96
312. Campos B, Olsen LR, Urup T, Poulsen HS. A comprehensive profile of recurrent glioblastoma. Oncogene **2016**;35:5819-25
313. Combs SE, Debus J, Schulz-Ertner D. Radiotherapeutic alternatives for previously irradiated recurrent gliomas. BMC Cancer **2007**;7:167
314. Amelio D, Amichetti M. Radiation therapy for the treatment of recurrent glioblastoma: an overview. Cancers (Basel) **2012**;4:257-80
315. Howard SP, Krauze A, Chan MD, Tsien C, Tome WA. The evolving role for re-irradiation in the management of recurrent grade 4 glioma. J Neurooncol **2017**;134:523-30
316. Bauman GS, Sneed PK, Wara WM, Stalpers LJ, Chang SM, McDermott MW*, et al.* Reirradiation of primary CNS tumors. Int J Radiat Oncol Biol Phys **1996**;36:433-41
317. Mayer R, Sminia P. Reirradiation tolerance of the human brain. Int J Radiat Oncol Biol Phys **2008**;70:1350-60
318. Combs SE, Thilmann C, Edler L, Debus J, Schulz-Ertner D. Efficacy of fractionated stereotactic reirradiation in recurrent gliomas: long-term results in 172 patients treated in a single institution. J Clin Oncol **2005**;23:8863-9
319. Fogh SE, Andrews DW, Glass J, Curran W, Glass C, Champ C*, et al.* Hypofractionated stereotactic radiation therapy: an effective therapy for recurrent high-grade gliomas. J Clin Oncol **2010**;28:3048-53
320. Combs SE, Widmer V, Thilmann C, Hof H, Debus J, Schulz-Ertner D. Stereotactic radiosurgery (SRS): treatment option for recurrent glioblastoma multiforme (GBM). Cancer **2005**;104:2168-73

321. Shrieve DC, Alexander E, 3rd, Wen PY, Fine HA, Kooy HM, Black PM*, et al.* Comparison of stereotactic radiosurgery and brachytherapy in the treatment of recurrent glioblastoma multiforme. Neurosurgery **1995**;36:275-82; discussion 82-4
322. Hall WA, Djalilian HR, Sperduto PW, Cho KH, Gerbi BJ, Gibbons JP*, et al.* Stereotactic radiosurgery for recurrent malignant gliomas. J Clin Oncol **1995**;13:1642-8
323. Shen CJ, Kummerlowe MN, Redmond KJ, Martinez-Gutierrez JC, Usama SM, Holdhoff M*, et al.* Re-irradiation for malignant glioma: Toward patient selection and defining treatment parameters for salvage. Adv Radiat Oncol **2018**;3:582-90
324. Veninga T, Langendijk HA, Slotman BJ, Rutten EH, van der Kogel AJ, Prick MJ*, et al.* Reirradiation of primary brain tumours: survival, clinical response and prognostic factors. Radiother Oncol **2001**;59:127-37
325. Shanker M, Chua B, Bettington C, Foote MC, Pinkham MB. Re-irradiation for recurrent high-grade gliomas: a systematic review and analysis of treatment technique with respect to survival and risk of radionecrosis. Neurooncol Pract **2019**;6:144-55
326. Muller K, Henke G, Pietschmann S, van Gool S, De Vleeschouwer S, von Bueren AO*, et al.* Re-irradiation or re-operation followed by dendritic cell vaccination? Comparison of two different salvage strategies for relapsed high-grade gliomas by means of a new prognostic model. J Neurooncol **2015**;124:325-32
327. Huncharek M, Muscat J. Treatment of recurrent high grade astrocytoma; results of a systematic review of 1,415 patients. Anticancer Res **1998**;18:1303-11
328. Nieder C, Andratschke NH, Grosu AL. Re-irradiation for Recurrent Primary Brain Tumors. Anticancer Res **2016**;36:4985-95
329. Nieder C, Nestle U, Ketter R, Kolles H, Gentner SJ, Steudel WI*, et al.* Hyperfractionated and accelerated-hyperfractionated radiotherapy for glioblastoma multiforme. Radiat Oncol Investig **1999**;7:36-41
330. Cho KH, Hall WA, Gerbi BJ, Higgins PD, McGuire WA, Clark HB. Single dose versus fractionated stereotactic radiotherapy for recurrent high-grade gliomas. Int J Radiat Oncol Biol Phys **1999**;45:1133-41
331. Combs SE, Edler L, Rausch R, Welzel T, Wick W, Debus J. Generation and validation of a prognostic score to predict outcome after re-irradiation of recurrent glioma. Acta Oncol **2013**;52:147-52
332. Shi W, Ng CKY, Lim RS, Jiang T, Kumar S, Li X*, et al.* Reliability of Whole-Exome Sequencing for Assessing Intratumor Genetic Heterogeneity. Cell reports **2018**;25:1446-57
333. Yoshida K, Sanada M, Ogawa S. Deep sequencing in cancer research. Jpn J Clin Oncol **2013**;43:110-5
334. Nakagawa H, Fujita M. Whole genome sequencing analysis for cancer genomics and precision medicine. Cancer science **2018**;109:513-22
335. Rausch T, Jones DT, Zapatka M, Stutz AM, Zichner T, Weischenfeldt J*, et al.* Genome sequencing of pediatric medulloblastoma links catastrophic DNA rearrangements with TP53 mutations. Cell **2012**;148:59-71
336. Korbel JO, Campbell PJ. Criteria for inference of chromothripsis in cancer genomes. Cell **2013**;152:1226-36

337. Biedermann KA, Sun JR, Giaccia AJ, Tosto LM, Brown JM. scid mutation in mice confers hypersensitivity to ionizing radiation and a deficiency in DNA double-strand break repair. Proc Natl Acad Sci U S A **1991**;88:1394-7
338. Carvalho HA, Villar RC. Radiotherapy and immune response: the systemic effects of a local treatment. Clinics (Sao Paulo) **2018**;73:e557s
339. Quail DF, Joyce JA. Microenvironmental regulation of tumor progression and metastasis. Nature medicine **2013**;19:1423-37
340. Quail DF, Joyce JA. The Microenvironmental Landscape of Brain Tumors. Cancer Cell **2017**;31:326-41
341. Caragher S, Chalmers AJ, Gomez-Roman N. Glioblastoma's Next Top Model: Novel Culture Systems for Brain Cancer Radiotherapy Research. Cancers (Basel) **2019**;11

List of Abbreviations

2-HG	2-hydroxy glutarate
5-ALA	5-Aminolevulinic acid
ALT	Alternative lengthening of telomeres
ATRX	Alpha thalassemia/mental retardation syndrome X-linked
BBB	Blood brain barrier
BCNU	Bis-chloroethylnitrosourea (carmustine)
BLI	Bioluminescent imaging
CCBR	Cancer Research Collaborative Bioinformatics Resource
CNA/CNV	Copy number alteration/Copy number variation
COSMIC	Catalogue of Somatic Mutations in Cancer
CSC	Cancer stem cell
DC	Dendritic cell
DCTD	Division of Cancer Treatment and Diagnosis Tumour Repository
DSB	Double strand break
ECM	Extracellular matrix
EGFR	Epidermal growth factor receptor
EMT	Epithelial-mesenchymal transition
EORTC	European Organisation for Research and Treatment of Cancer
GATK	Genome Analysis Toolkit
GB	Glioblastoma
G-CIMP	Glioma-CpG island methylator phenotype
GEM	Genetically engineered mouse model
GFP	Green fluorescent protein
GLASS	Glioma Longitudinal Analysis Consortium
GSC	Glioblastoma stem-like cells
IC	Intracranial/intracerebral
IDH	Isocitrate dehydrogenase
ITH	Intratumoral heterogeneity
LDA	Limiting dilution assay
LOH	Loss of heterozygosity
MGMT	Methylguanine DNA methyltransferase

NCI	National Cancer Institute
OS	Overall survival
PBS	Phosphate-buffered saline
PE	Plating efficiency
PFS	Progression free survival
PI3K	Phosphatidylinositol 3-kinase
PLL	Poly-L-lysine
PO	Poly-L-ornithine
PTEN	Tyrosine phosphatase/tensin homolog protein
RAGE	Receptor for advanced glycation end product
Rb	Retinoblastoma
RT	Radiotherapy
RTK	Receptor Tyrosine Kinase
RTOG	Radiation Therapy Oncology Group
SC	Subcutaneous
SF	Surviving fraction
SFM	Serum-free media
SNV	Single nucleotide variant
SRS	Stereotactic radiosurgery
TAM	Tumour-associated macrophages
TCGA	The Cancer Genome Atlas
TERT	Telomerase reverse transcriptase
TET	Ten-eleven translocation methylcytosine dioxygenase
TME	Tumour microenvironment
TMZ	Temozolomide
TP53/P53	Tumour suppressor protein 53
VAF	Variant allele frequency
VEGF	Vascular endothelial growth factor
VISA	Viral integration site analysis
WES/WGS	Whole exome sequencing/Whole genome sequencing
WHO	World Health Organisation